An Evaluation of the Organic Geochemical Potential to Reconstruct Mid-Pleistocene Paleoclimate Adjacent to an Established Hominin Site: Lake Magadi, Kenya

by

Troy M. Ferland

B.S. Chemistry, University of Pittsburgh, 2015

Submitted to the Graduate Faculty of

the Kenneth P. Dietrich School of Arts & Sciences in partial fulfillment

of the requirements for the degree of

Master of Science

University of Pittsburgh

2017

UNIVERSITY OF PITTSBURGH

DIETRICH SCHOOL OF ARTS & SCIENCES

This thesis was presented

by

Troy M. Ferland

It was defended on

July 7th, 2017

and approved by

Emily M. Elliott, Associate Professor, Geology & Environmental Science

Daniel J. Bain, Assistant Professor, Geology & Environmental Science

Thesis Director: Josef P. Werne, Professor, Geology & Environmental Science

An Evaluation of the Organic Geochemical Potential to Reconstruct Mid-Pleistocene Paleoclimate Adjacent to an Established Hominin Site: Lake Magadi, Kenya

Troy M. Ferland, M.S.

University of Pittsburgh, 2017

The paleo-Lake Magadi was one of five sites selected by the Hominin Sites and Paleolakes Drilling Project (HSPDP), with the goal of establishing high resolution, multi-proxy reconstructions of climate and environmental change adjacent to established hominin sites. The overall goal of the HSPDP is to provide a context of climate and environmental change for many of the milestones in hominin adaptation and evolution, spatially adjacent to where hominins lived, and temporally resolved to evolutionary (orbital to sub-millennial) timescales. The core recovered from Lake Magadi is estimated to represent the past 1.08 Ma, during which several significant hominin adaptation and evolutionary events occurred. Based on initial chronology efforts by HSPDP collaborators, the Magadi core can be separated into four sections: 0-26 kyr, 26-165 kyr, 165-242.8 kyr, and 242.8 kyr to 1.08 Ma. We estimate the future biomarker potential for the four sections, and determine Lake Magadi to have particularly exciting promise for the 0-26 kyr and 26-165 kyr sections.

To that end, 68 pilot samples were analyzed for leaf waxes (n-alkanes and fatty acids) and glycerol dialkyl glycerol tetraethers (GDGTs), to evaluate the potential to reconstruct vegetation regime, precipitation, and temperature from Magadi. The n-alkanes were determined to have a better potential to yield compound specific carbon and hydrogen isotope data than fatty acids due to better chemical separation, and approximately 70% of samples analyzed for n-alkanes recorded a robust terrestrial signal. The TetraEther indeX with 86 carbon atoms (TEX_{86})

temperature proxy was established for ~90% of samples analyzed for isoprenoid GDGTs, however the Methane Index and Ring Index suggest that the TEX_{86} is not applicable to temperature reconstruction at Magadi. Additionally, no samples contained the complete suite of branched GDGTs necessary to construct the Methylation of Branched Tetraethers and Cyclisation of Branched Tetraethers (MBT/CBT) temperature proxy.

Initial reconstruction of Lake Magadi paleoclimate shows an oscillating vegetation regime from mid-Pleistocene to present, but a directional trend towards a cooler and drier climate. Plotted alongside $\delta^{18}O$ data from the GRIP-2 ice core, our climate data demonstrate a potentially interesting correlation between climate at Lake Magadi and ice volume in the Arctic.

TABLE OF CONTENTS

LIST OF TABLES

LIST OF FIGURES

LIST OF EQUATIONS

ACKNOWLEDGEMENTS

I would like to take this section to thank the numerous people without whom this thesis would not have been possible. No man is an island, and I am certainly no exception - nor would I want to be. More now than ever, both science and life are collaborative efforts, where triumphs as well as failures are shared, and made all the sweeter (or less bitter) for it. I am fortunate to have a great many collaborators, scientific and otherwise, to help me along my way. To all those mentioned, and those not, thank you.

Firstly, I'd like to thank my family. They've supported me, and my involvement in science not only during my Master's but for my entire life - especially my mother, Amy, and my sisters, Paige and Grace. I know I haven't always been the best son and brother, but you guys have never given up on me.

Thank you to Alan Reed, Mallory Hudson, Marc Khouzami, Rachel Orlando, Daniel Rinkus, and of course, Joseph DeShane, for being my Pittsburgh (and abroad) family. You've all been the stalwarts of my personal life, and a support system that has provided me the strength to get back up again after being knocked down. You all are amazing friends, and though I'll be moving on to the next chapter in my life, I can't wait to have you with me along the way.

To my fellow graduate students at Pitt, notably Robert Rossi, Justin Coughlin, Nick, Weidhass, Angela Mullins, Marja Copeland, Irene Wallrich, Angela Chung, and James Thompson - thank you for always being a shoulder to lean on, a friend to celebrate with, an ear

for frustrations, and encouragement on rainy days. I know I'll keep in touch with all of you, and I hope the best for your futures.

To Joe Werne, thank you for being an advisor but also a friend. Your open door has led to so many good discussions, and you even bought me a drink every now and then. To Dervla Kumar, my ever-smiling commiserate, I cherish our friendship and I earnestly hope you find yourself back in academia one day. To Arielle Woods, wry compatriot and friend – thank you for the long lab nights, struggling through classes, and access to your back scratcher. You've all made this experience unforgettable for me.

To Isla Castañeda, my academic sibling, thank you for being like a secondary advisor to me. I hope the future holds opportunities for us to continue to work together. To Jim Russell, Anders Noren, Anne Billingsley, and Chris Campisano, along with the other HSPDP folk, thank you for supporting my work on Lake Magadi – see you at the next workshop.

Finally, thank you to Molly O'Beirne. If there could only be one person acknowledged here, it would be you. Over the past two years, no one has been more of a mentor, teacher, or friend than you have. I truly feel indebted to you for believing in me, though along the way I've given you every reason not to. Thank you for the tough love, and for helping me get hard, but also for knowing when I need patience and a hug. Thank you for teaching me how to be a scientist, and for making me a more critically-thinking and self-assured person. I look forward to writing our book, to getting punched by you every time I try to hug you at a conference, and to all the spoils that our friendship is bound to yield in the years to come. Thank you again and again.

This research was supported by NSF grant EAR-1338553.

1.0 INTRODUCTION

Homo sapiens is a unique species in Earth's history – a species that has expanded globally, and has the innovative capacity to develop tools and technologies, rendering it capable of intelligently modifying its environment. To the extent of current knowledge, *Homo sapiens* is the most intelligent, dominant, and intentionally world-altering species to have existed on Earth. However, there is still much debate about what led to the evolution of the species. Due to the density and dating of both hominin fossils and artifacts in the region, East Africa is considered the birthplace of the species, as many of the milestones in hominin evolution, both evolutionary and technological, originated in the region and proceeded to disperse outward. For this reason, the East African region has been the focus of much research on hominins, their environment, and evolutionary events related to the origins and dispersal of Homo sapiens.

1.1 CLIMATE AND HOMININ EVOLUTION

The role of climate variability on the evolution and dispersal of hominins in East Africa has been a subject of much research, and though the extent and mechanisms of the relationship are still debated, the assumption that environmental parameters impacted hominin evolution is long-standing (Maslin and Christensen, 2007). Potts (2013) and Maslin et al. (2014) summarize

several hypotheses put forward (see specific citations below) regarding the relationship between climate and hominin evolution. These hypotheses (Table 1), developed over the past several decades, encompass several combinations of climate histories of East Africa and hominin evolutionary mechanisms.

EVOLUTIONARY FORM		CLIMATE STRESS: None	Long-term state change	Threshold event	Variability
Phyletic Gradualism	constant	Red Queen (Van Valen 1973)	*Allopatic speciation*		
	variable	Red Queen (Van Valen 1973)	Turnover-pulse hypothesis (Vrba 1985) Savannah hypothesis	*Allopatic speciation*	Variability selection hypothesis (Potts 1998) Pulsed-climate variability hypothesis (Maslin & Trauth 2009)
Puncuated Equilibrium		Court Jester (e.g. Impact event) (Bamosky 2001)	Aridity hypothesis (de Menocal 1995)	Court Jester (Bamosky 2001) *Allopatic speciation*	Pulsed-climate variability hypothesis (Maslin & Trauth 2009)

Table 1 – A table adapted from Maslin et al. (2014) showing various climate-evolution hypotheses involving hominins. The hypotheses are separated by their type of climate stress and evolutionary mechanism.

The *Red Queen* hypothesis (Van Valen, 1973) was a null hypothesis and stated that climate has no influence on evolution. Instead, evolution is impacted exclusively by biotic events, such as competition for resources. The *Court Jester* hypothesis (Bamosky, 2001) refuted the *Red Queen* hypothesis, stating abiotic factors (e.g. climate) can influence evolution. However, the *Court Jester* is not specific to climate, including abiotic events such as bolide impact, and provides no mechanism for the interaction between abiotic influences and evolution.

Initially, Washburn (1960) established the iconic *savannah hypothesis*, positing that the onset of the savannah grassland fragmented what had previously been a tropical rainforest-dominated central and East Africa. This initial fragmentation, followed by the gradual takeover of the savannah grassland, caused a group apes to abandon their arboreal lifestyle, stand upright, and traverse this new habitat via bipedal locomotion. Subsequently, Vrba (1988) developed the *turnover pulse hypothesis*, suggesting that abrupt, intense shifts in climate were responsible for speciation, extinction, and adaptation in ungulate (and other large mammalian) species. A key observation of the *turnover pulse hypothesis* was that acute climate shifts caused more extinctions in specialist species (leading to more rapid allopatric speciation) than generalist species (leading to greater geographic ranges). These initial two hypotheses laid the framework for many subsequent hominin evolution theories.

Refining the initial *savannah hypothesis* was the *aridity hypothesis* (deMenocal 1995, 2004), which asserted that regional tectonic uplift caused long-term climate to trend towards a drier East Africa. The *aridity hypothesis* states that this directional increase in aridity allowed for the propagation of the savannah biome, and had a significant impact on hominin evolution. The *variability selection hypothesis* (Potts 1998, 2013) was a refinement of the *turnover pulse hypothesis*, and suggested that over time, environmental variability played a role in selecting for adaptive, flexible behavioral and ecological traits. The *variability selection hypothesis* posits that a species' evolutionary success is correlated to its potential to adapt to an increasingly variable environment (with the overall trend of East African climate aridification towards the present day). However, the *variability selection hypothesis* could not adequately justify the seemingly pulsed pattern of hominin evolutionary events suggested by recent paleoanthropological evidence.

Maslin and Trauth (2009) further refined the *variability selection hypothesis* to form the *pulsed climate variability hypothesis*, which emphasizes the impact of short periods of intense climate variability (not necessarily with a directionality) in East Africa on the evolution, extinction, and adaptation of hominins. The *pulsed climate variability hypothesis* is currently one of the more popular theories, as many lines of paleoclimatic and paleoanthropological evidence fit well into its framework (Maslin et al., 2014).

1.2 PLIO-PLEISTOCENE CLIMATE IN EAST AFRICA

Understanding the effects of climate on hominin evolution is complex, as many climatic processes and events (from millennial- to tectonic-scale), have the potential to force evolutionary pressures (Figure 1). A comprehensive overview of climatic processes and events important to hominin evolution is laid out below.

The climate in East Africa has changed significantly over the last 40 Ma, and much of this climate change has been tectonically controlled. The continual development of the East African Rift System (EARS) caused regional elevation changes that in turn resulted in changes in precipitation, aridity, and vegetation, as well as the formation and propagation of fault graben basins along the rift. These basins functioned as catchments for lakes, many of which remain.

Trauth et al. (2005, 2007) estimate that volcanism first began in the EARS between 45-33 Ma in the Ethiopian section of the rift, with the initial uplift beginning between 38-35 Ma (Underwood et al., 2013). Though the central and southern sections of the EARS lagged the northern section, with magmatic activity commencing in southern Kenya and Tanzania between 15-8 Ma (George et al., 1998; Ebinger et al., 2000), progressive uplift established the relief of

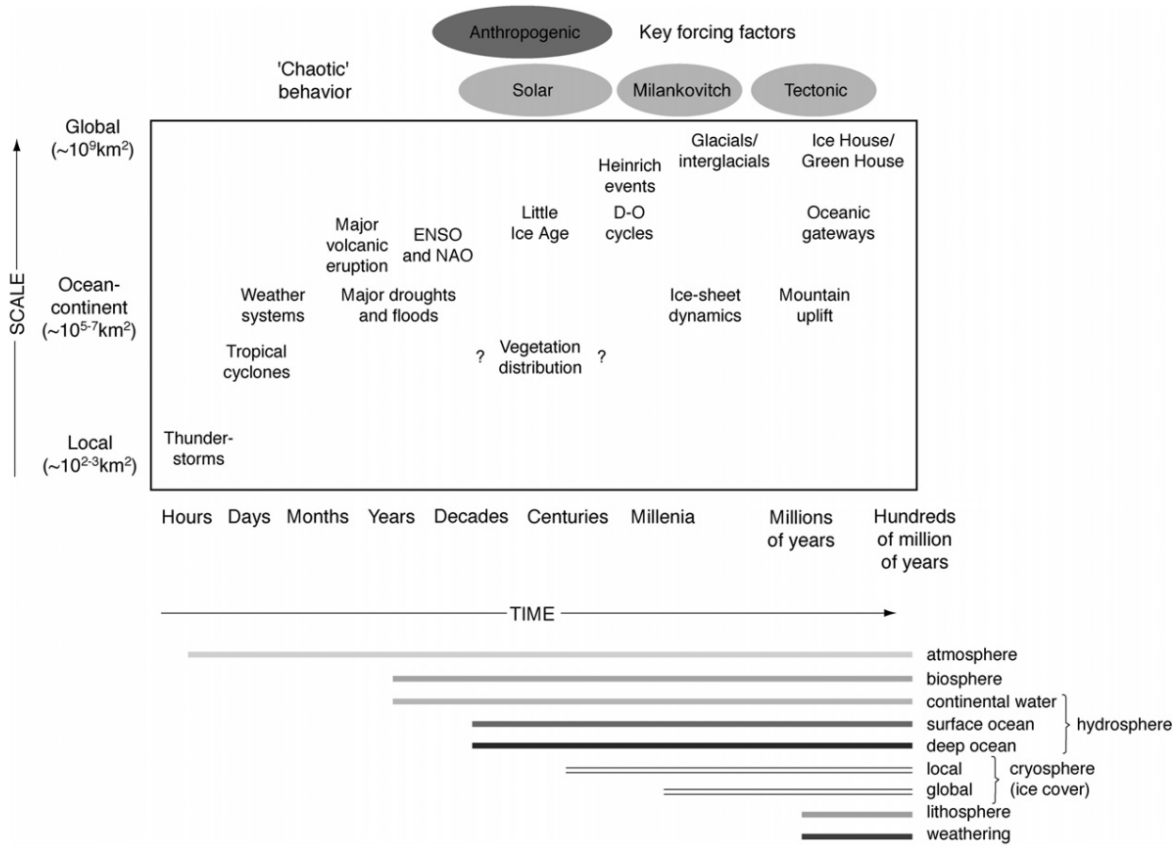

Figure 1 – A figure from Maslin and Christensen (2007) showing the relative temporal and spatial scales of climate factors that may have impacted hominin evolution.

much of the EARS beginning between 18-13 Ma (Wichura et al., 2010). East-dipping faults formed in the northern Kenya section of the rift between 12 and 7 Ma, followed by normal faulting in the central and southern Kenya rift between 9 and 6 Ma (Ebinger et al., 2000). Continual faulting in central and southern Kenya formed, and later segmented, the full-graben morphology (Strecker et al., 1990) through the Pliocene. Fragmentation of the lake basins in Kenya continued throughout the Pleistocene due to ongoing volcanism (McDougall et al., 2012).

This tectonic activity resulted in significant biological changes as well. Evidence from Couvreur et al. (2008) suggests that waves of endemic species emerged at 33, 16, and 8 Ma, due to fragmentation of the pan-African rainforest (previously connecting East Africa and the Congo)

following periods of major tectonic activity. The progressive uplift-induced increase in aridity along the EARS also caused a vegetation shift from a C_3 to C_4 plant dominated environment during the Pliocene and Pleistocene, as indicated by paleorecords of soil carbonates (Levin et al., 2004; Levin, 2013), marine sediment n-alkane carbon isotopes (Feakins et al., 2013), and fossil mammal teeth (Brachert et al., 2010). The association between increased aridity and increased uplift has also been demonstrated with climate models of the EARS (Sepulchre et al., 2006; Prömmel et al., 2013) and indicates that increased elevation induces a rain shadow effect on the Rift Valley. This generally agrees with the aridification trend identified in many paleorecords from the EARS, however Maslin et al. (2012) suggest that soil carbonate isotope records indicate an intensification of seasonality – increased aridity during dry periods, but similar levels of precipitation during wet periods. Elsewhere, the cessation of constant El Niño-like conditions in East Africa due to the closing of the Indonesian Seaway and associated decrease in the sea-surface temperatures in the Indian Ocean around 4 Ma may have additionally led to increased aridification (Cane and Molnar 2001, Molnar and Cane 2007) on tectonic timescales.

On shorter timescales (i.e. 1 Ma – 100 kyr, Figure 1), other potential controls on climate in East Africa exist. Currently, it is thought that the onset of high-latitude glaciations (~2.7-2.5 Ma; Haug et al., 1998), intensification of Walker circulation (1.9-1.7 Ma; Ravelo et al., 2004), and variability in El Niño-Southern Oscillation (ENSO)/Indian Ocean Dipole (IOD) (Berger et al., 1994) have played a role in East African aridity, affecting lake levels and seasonality. Trauth et al. (2005, 2007, 2009) argue that variations in insolation have driven periods of wetter climate, expanded lakes, and greater seasonality at approximately ~2.8, 1.7 and 1.0 Ma (coinciding with the aforementioned climate events, see Figure 1), whereas deMenocal (2004) suggest that these intervals experienced step-like increases in regional aridity and climate variability in East Africa.

On even shorter timescales (i.e. Milankovich: ~100, 40, and 20 kyr), the relationships among climatic parameters and evolutionary pressures become more tangible, but the number of potentially influential climatic pressures increase - including the effects of orbital forcing (Magill et al., 2013b), air-mass boundary positions (Tierney et al., 2011), and other high-latitude events (Kingston et al. 2007; Joordens et al. 2011). These environmental cycles are thought to have impacted ecological parameters such as the distribution of resources (food, water, shelter, etc.) that would have affected early hominins (Armitage et al. 2011; Reed 1997).

Paleoclimate records from East Africa have been established to elucidate Milankovich-scale climate effects on the region. Early studies of Mediterranean sapropels (Rossignol-Strick 1985; Kroon et al., 1998) and the Gulf of Aden (deMenocal et al., 1995) suggested a strong cyclical relationship between monsoonal precipitation/aridity and insolation/global ice volume. More recent records show that the expansion and contraction of many East African lakes oscillates on precessional cycles, with some influence from eccentricity as well (Magill et al., 2013b; Joordens et al., 2011). The influence of eccentricity on an otherwise precession-driven precipitation cycle causes some unpredictability, which both Trauth et al. (2007) and deMenocal et al. (2000) suggested may be due to an established insolation threshold that must be reached before significant precipitation changes occur. Trauth et al. (2009) argues however, that discrepancies between marine and terrestrial records highlight the ineffectiveness of continental-scale records to track regional or local responses to insolation forcings, and thus consequently, fail to record the environmental variability actually experienced by hominins in East Africa.

1.3 HOMININ SITES AND PALEOLAKES DRILLING PROJECT

Hominin evolution, and particularly the role climate may have played in it, is challenging to study for several reasons. Climate records must be established near sites where hominins lived – localities and outcrops where fossils have been found and studied. However, many of the climate records of East Africa come from much further away, such as marine cores from the Gulf of Aden (deMenocal et al., 1995; and others previously mentioned). These records, though important, may record too broad a signal of regional or continental climate to correlate to basin-scale evolutionary events (Trauth et al., 2009). Establishing paleorecords from the same sites, or sites adjacent to hominin fossils, can clarify climate forcings and move the field forward.

The second challenge is achieving sufficient resolution in paleoclimate data reconstructed from outcrop samples. Though much more adjacent to hominin sites than other types of records (e.g. marine cores), paleorecords taken from local outcrops are often highly weathered, resulting in low temporal resolution that limits the precise application of outcrop records to hominin evolution questions. Paleorecords resolved on sub-millennial timescales are necessary to reveal changes in climate that potentially impact the biologic factors influencing hominin evolution (such as food and water availability, shelter, etc.). Lake bed outcrops are subject to significant and unpredictable degradation of organic matter (Petsch et al., 2000). In contrast, lake sediments can remain relatively undisturbed, a necessary condition for recovering paleorecords from organic matter (especially biomarkers) at temporal resolutions useful for advancing climate-hominin evolution research.

The Hominin Sites and Paleolakes Drilling Project (HSPDP) was established to address these two issues. In 2013 and 2014, five paleolake sites (Figure 2) were selected for their proximity to hominin sites and drilled to recover the lake sediment. The goal of the HSPDP is to

use these lake sediments to reconstruct high-resolution, multi-proxy records of climate from these paleolake sites. Proxies for the initial project funding include pollen, carbonates, elemental analyses (XRF/XRD), diatoms, phytoliths, and organic biomarkers – leaf waxes and archaeal/bacterial membrane lipids. Together, this collection of proxies may provide a robust reconstruction of the past climate and environment adjacent to hominin sites, providing unprecedented ability to test climate-evolution hypotheses.

1.4 STUDY SITE

Lake Magadi is a present-day saline/alkaline pan located ~20 km northwest of the Koora Plain (the sister project, the Olorgesailie Drilling Project, is located 25 km north of the Koora Plain, Figures 3 and 4) along the southern Kenya Rift in East Africa. Lake Magadi has existed as a series of paleolakes back through the early Pleistocene (Cohen et al. 2016). The paleolake Magadi was a regional sump for water and sediment in the Magadi/Natron Basin (Figure 5), making it a potentially promising site for the preservation of the proxies identified by the HSPDP. Magadi is known to have relatively thick underlying sequences of lake sediments based on cores recovered decades ago (Surdam and Eugster 1976) and more recent geophysical probing (Simiyu and Keller 2001). The oldest sediments from these previous studies are thought to be ~0.8 Ma, deposited in a large lake setting, after which Lake Magadi went through a series of drying and rewetting events, becoming progressively more saline (Cohen et al., 2016).

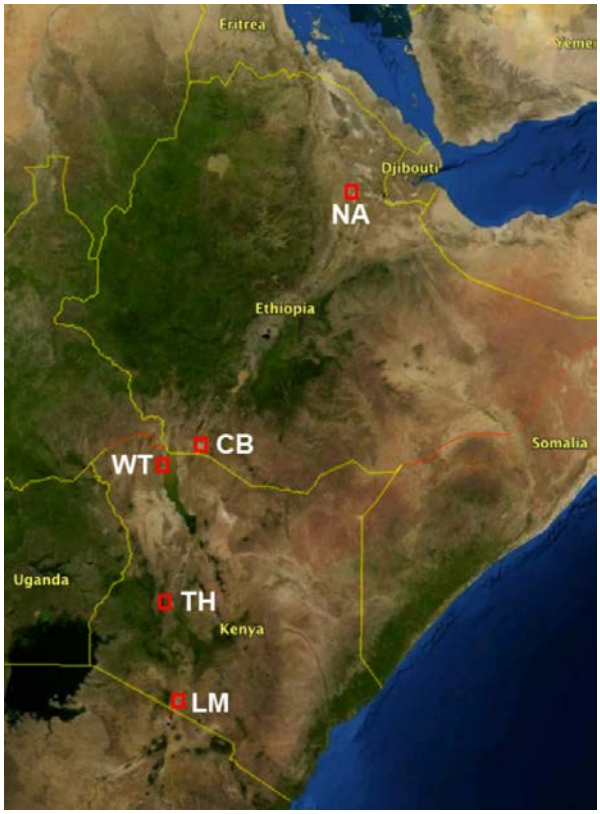

Figure 2 – A figure from Cohen et al. (2016) showing the five sites chosen and drilled by the Hominin Sites and Paleolakes Drilling Project. Lake Magadi (site LM) is the southernmost of the sites, located just north of the Kenya-Tanzania border.

Lake Magadi was initially targeted by the HSPDP not only because of its early characterization as a Pleistocene-modern depocenter, but also because of the decades of archaeological work that has been done nearby. From the Olorgesailie Formation there are abundant artifacts detailing the transition from Acheulean (large cutting tools, from local sources) to Middle Stone Age technology (more diverse tools, often from more distant rock sources) (Potts et al., 1999, Behrensmeyer et al., 2002). This transition is a major behavioral event in hominin evolution. Paleoenvironmental reconstruction during this transition may begin to elucidate some evolutionary pressures that resulted in the emergence of this new behavior.

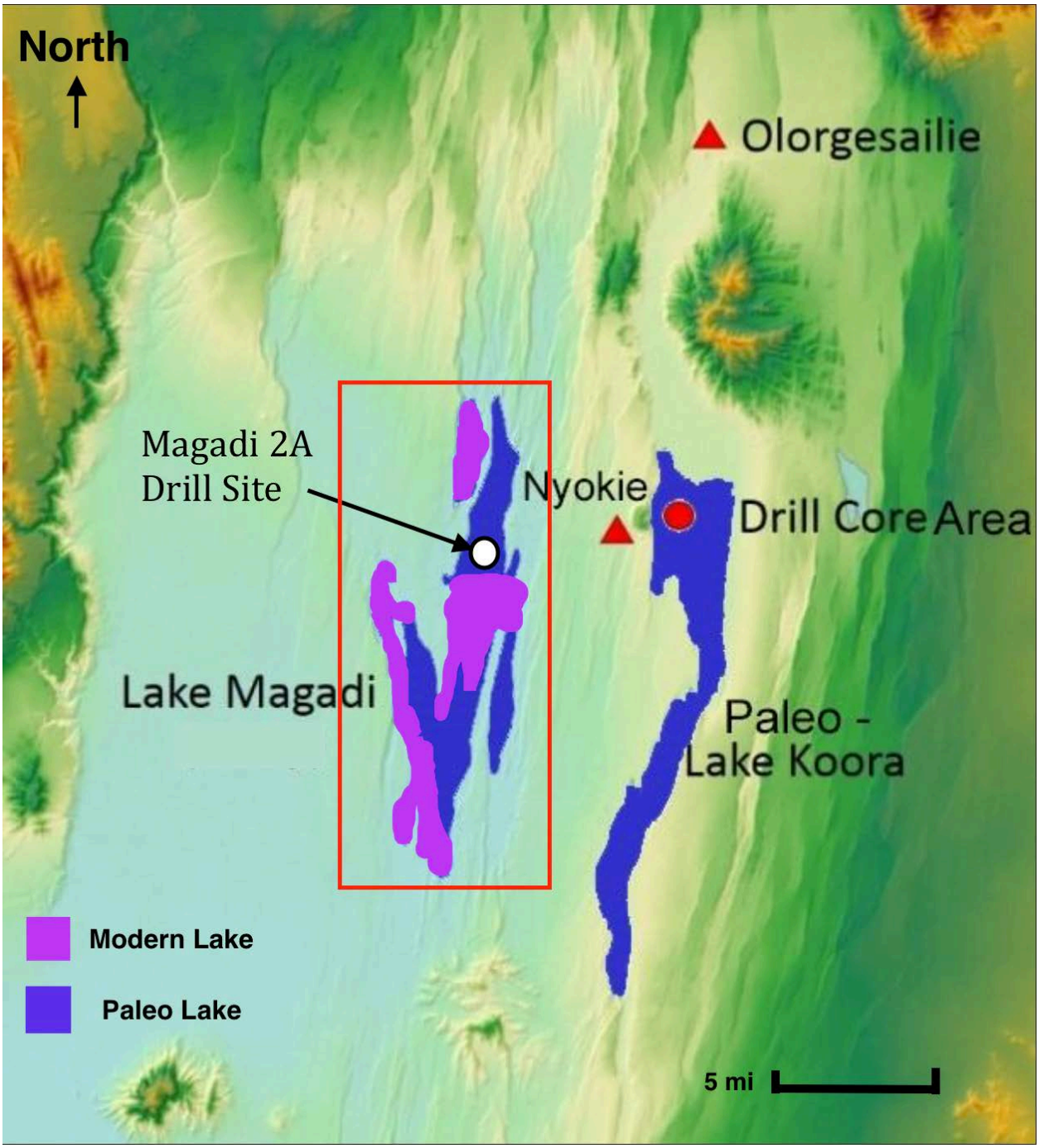

Figure 3 – A map adapted from *http://humanorigins.si.edu/research/east-african-research-projects/olorgesailie-drilling-project*, the Smithsonian page for the Olorgesailie Drilling Project. The Magadi 2A Drill site is shown with a white dot, and the red square outlines the spatial extent of Figure 4. The core used in the Olorgesailie Drilling Project was obtained from the red dot labeled "Drill Core Area". Map scale is approximate.

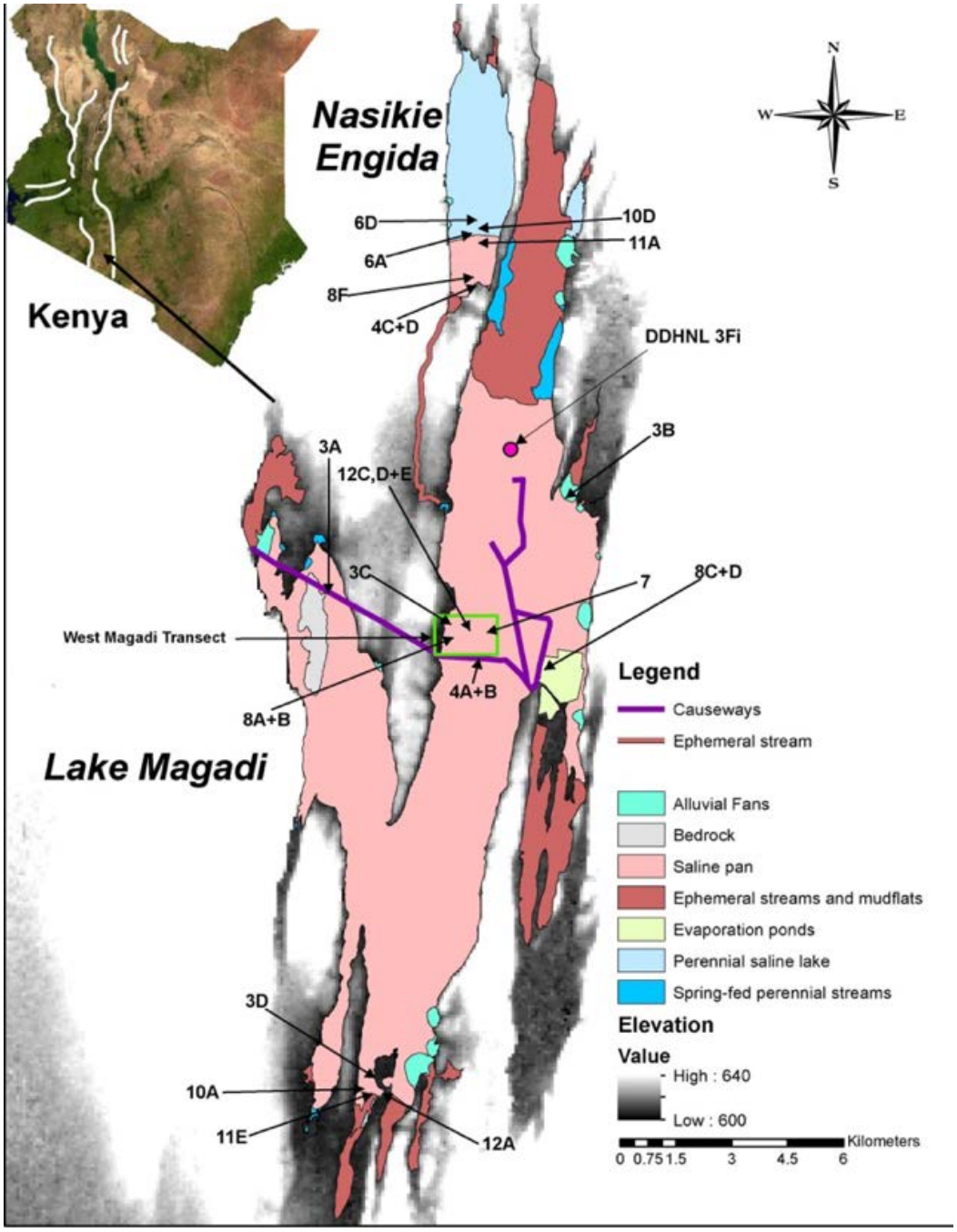

Figure 4 – A figure from McNulty et al. (2016) showing the modern layout of paleolake Magadi. The drilling area for cores 1A, 1B, and 1C are shown by the green box, and the drill site for core 2A is represented by the magenta dot.

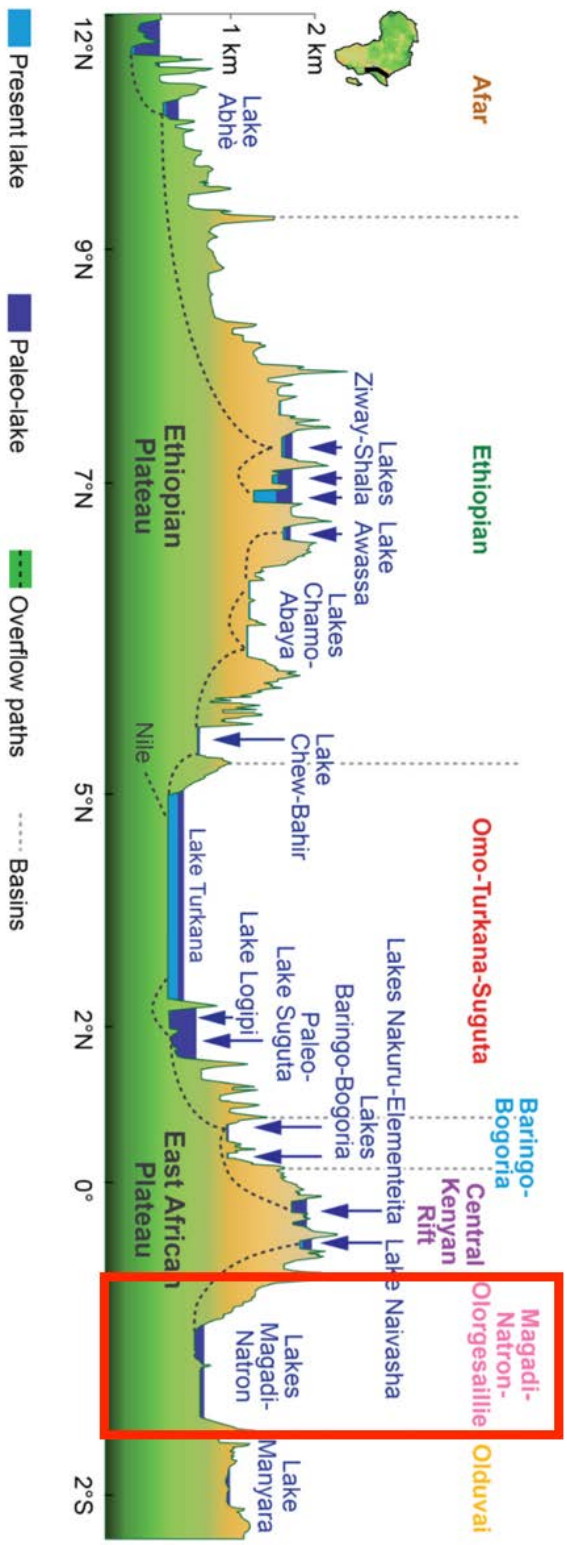

Figure 5 – A figure adapted from Maslin et al. (2014) showing a side view of the EARS. Lake Magadi sits in the Magadi-Natron Basin, in the south section of the rift.

1.5 PALEOCLIMATE PROXIES

1.5.1 Leaf Waxes

Leaf waxes, the n-alkyl compounds that are a major component of the cuticle of vascular plants (Eglinton et al., 1962), can be excellent recorders of climatic variables such as precipitation and vegetation regime in lacustrine environments (e.g. Castañeda et al., 2009a). This class of compounds includes n-alkanes, n-alkanols, n-alkanoic acids, and wax esters, whose structures are shown in Figure 6. Leaf waxes have been the focus of many terrestrial climate paleoreconstructions because they generally resist degradation and preserve well in sediments (Cranwell, 1981).

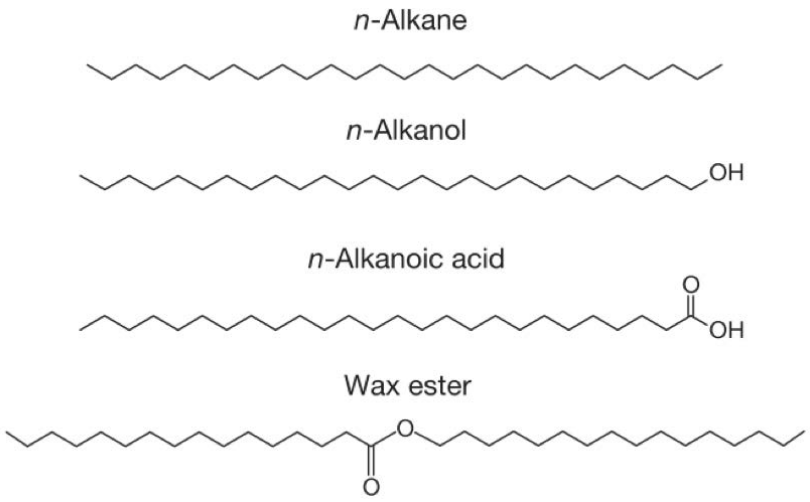

Figure 6 – A figure from Freeman and Pancost (2014) showing examples of the various molecule types that are identified in the cuticle of vascular plants. This study focused on the n-alkanes and the fatty acids, which includes alkanols and alkanoic acids.

Leaf waxes are useful two-fold – their abundances can provide information on the relative proportion of terrestrial plant to aquatic plant to bacterial input to the sedimentary

record, as well as an estimate of contributions of C_3 and C_4 plants to the record. Generally, n-alkanes with carbon chain length from C_{27} to C_{35} are considered to be terrestrially sourced. Mid-length (C_{21}-C_{25}) n-alkanes are considered to be produced by aquatic macrophytes, and the P_{aq} ratio (Ficken et al., 2000; Appendix A, Equation 2) can be used to determine relative input. The P_{aq} ratio ranges from zero to one, with higher values representing increased aquatic macrophyte input (e.g. Magill et al., 2013b). Short-length (C_{15}-C_{19}) n-alkanes, whose relative input is expressed by the terrestrial and aquatic hydrocarbon ratio (TAR_{HC}, Meyers et al., 1997; Appendix A, Equation 3), are indicative of algae (Cranwell et al., 1987) or thermal/biotic degradation. The TAR_{HC} ranges from zero to one, where a value of zero represents purely aquatic input and a value of one is purely terrestrial (Meyers et al., 1997). The carbon preference index (CPI, Marzi et al., 1993; Appendix A, Equation 1) is a measure of odd- or even-chain length predominance in n-alkanes. The CPI is not bound between zero and one – the higher the value, the more robustly it resembles a terrestrial plant wax distribution (predominance of odd-chain length n-alkanes; CPI>4), whereas a CPI<3 suggests microbial/algal input, degradation, or both (Marzi et al., 1993; Freeman and Pancost, 2014). These indices are summarized below in Table 2.

Leaf wax production in higher plants is affected by phylogeny (Diefendorf et al., 2011), ontogeny (the development and growth of an organism; Sachse et al., 2009), environmental variables and stresses (Shepherd and Griffiths, 2006). Diefendorf et al. (2011) demonstrated that angiosperms produce far greater quantities of n-alkanes than gymnosperms, with evergreen angiosperms producing the largest quantities on average. Paleoenvironmental reconstructions using n-alkanes therefore have a tendency to bias towards angiosperms (specifically evergreen angiosperms), a problem that can arise when using leaf wax abundances to make environmental

inferences. Measuring the isotopic composition of hydrogen (δD) and carbon ($\delta^{13}C$) of leaf waxes can lead to a more robust paleo-reconstruction than just using leaf wax abundances as discussed below. However, due to the effect photosynthetic pathway has on leaf wax distributions (C_4 plants generally produce longer [i.e. more C_{33} and C_{35}] than C_3), some studies (Castañeda et al., 2009a) have shown a strong correlation between n-alkane average chain length (ACL; Appendix A, Equation 4) and paleotemperature, as C_4 grasses tend to outcompete C_3 woody plants (e.g. deciduous trees) in warmer environments.

As previously mentioned, compound specific isotope measurements are a useful, complementary tool to the abundances of leaf waxes for paleoenvironmental studies. The isotopic composition of hydrogen and carbon in n-alkanes and fatty acids is sensitive to changes in the source and amount of past precipitation (Sachse et al., 2009) and plant metabolic pathway (Hayes et al., 1990), respectively. The H isotope composition (δD) of leaf waxes are first and foremost controlled by the H isotope composition of the water used by plants for biosynthesis, and is typically driven by regional precipitation H isotope composition, but is also subject to further isotopic fractionation. Isotopic fractionation is any process (physical or chemical) that alters the isotopic composition between reactant pool and product pool, and is apparent only when the chemical reaction or physical transport is incomplete. There are many fractionations that occur during the pathway from hydrogen in precipitation to hydrogen in leaf wax, including evaporation, transport of rain water into the soil, from the soil to plant roots, from the roots up through the xylem of plants, transpiration, and the biosynthetic incorporation of water into the leaf waxes (acetyl Co-A biosynthetic pathway is utilized for leaf wax compounds; Appendix B, Figures 21 and 22) (Ehleringer and Dawson 1992, Tipple and Pagani, 2007). The total apparent fractionation (ε) from precipitation to leaf wax has been studied extensively, but can't be applied

universally, due to phylogenetic differences in plant-water utilization. Near Lake Magadi (i.e. Olduvai Gorge), modern plants have been used to calibrate paleorecords (Magill et al., 2013a) and establish a framework for quantitatively estimating past precipitation amount in the region.

The C isotope composition ($\delta^{13}C$) of leaf waxes can be used to estimate plant community composition (C_3 woody plants versus C_4 grasses) in an environment over time (e.g. Castañeda et al., 2009b). For reconstructions, the C_{29}-C_{33} n-alkanes are often used because they are in relatively high abundance, and have a primarily terrestrial higher plant source. Though the carbon in leaf waxes is sourced from atmospheric CO_2, the $\delta^{13}C$ composition of individual leaf waxes is poorly correlated (r^2=0.34) with past atmospheric $\delta^{13}C$-CO_2 (and paleo-pCO_2) measurements (Pancost and Boot, 2004, and references therein). The ε between atmospheric CO_2 and leaf wax carbon is susceptible to multiple fractionations, including photosynthetic pathway, plant water availability/stress, stomatal conductance, pCO_2, and leaf height (e.g. the canopy effect, Baldocchi et al., 1993) (Hayes et al., 1990; Bowling et al., 2001; Prentice et al., 2011; Farquhar et al., 1989). Despite these competing factors to consider, the application of $\delta^{13}C$ to sedimentary leaf waxes has worked well in East Africa, where measured leaf wax $\delta^{13}C$ values have been used to reconstruct a paleo-vegetation (Magill et al., 2013b, Cerling et al., 2011). Although beyond the scope of this thesis, measuring both δD and $\delta^{13}C$ from sedimentary leaf waxes in Lake Magadi will allow a more robust interpretation of paleoclimate and environment, and provide a point of comparison between Magadi and nearby sites (e.g. Olorgesailie [Potts et al., unpublished] and Olduvai [Magill et al., 2013a, 2013b]).

1.5.2 Glycerol Dialkyl Glycerol Tetraethers

Glycerol dialkyl glycerol tetraethers (GDGTs) are microbial membrane lipids that have been used as a proxy for paleotemperature (Schouten et al., 2002; Castañeda and Schouten, 2011). These compounds are separated into two categories, isoprenoid GDGTs (isoGDGTs) and branched GDGTs (brGDGTs), by both their source organisms and their skeleton unit structure. The isoGDGTs have a backbone comprised of isoprenoid units and are Archaeal (Karner et al., 2001; Lipp et al., 2008) whereas brGDGTs have a straight-chained alkyl backbone and are thought to be produced primarily by anaerobic soil bacteria (for structures see Figure 7) (Weijers et al., 2006a).

The isoGDGTs are found ubiquitously in marine sediments, and in many lacustrine sediments as well. These compounds contain anywhere from zero to three cyclopentane rings (GDGTs 0-3, Figure 7) and are of interest in paleo studies (mainly the TetraEther indeX with 86 carbon atoms [TEX_{86}]; Appendix C, Equation 8) as cyclization is thought to increase with temperature (Schouten et al., 2002). Currently, it is understood that several groups within the domain Archaea produce isoGDGTs (Schouten et al., 2007). 16S rRNA data from marine waters have identified *Thaumarchaeota* and Group 2 *Euryarchaeota* as potentially large contributors to isoGDGT production (Delong, 1992). "Crenarchaeol" (GDGT 4, consisting of four cyclopentane rings and one cyclohexane ring, see Figure 7) is often abundant in marine sediments, and is thought to be produced exclusively by *Thaumarchaeota* (Pitcher et al., 2011). The isoGDGTs and crenarchaeol are present in lake waters and sediments (Sinninghe-Damsté et al., 2009) and 16S rRNA data suggests that the same *Thaumarchaeota* present in marine environments may also be producing isoGDGTs in lakes (Keough et al., 2003; Sinninghe-Damsté et al., 2009).

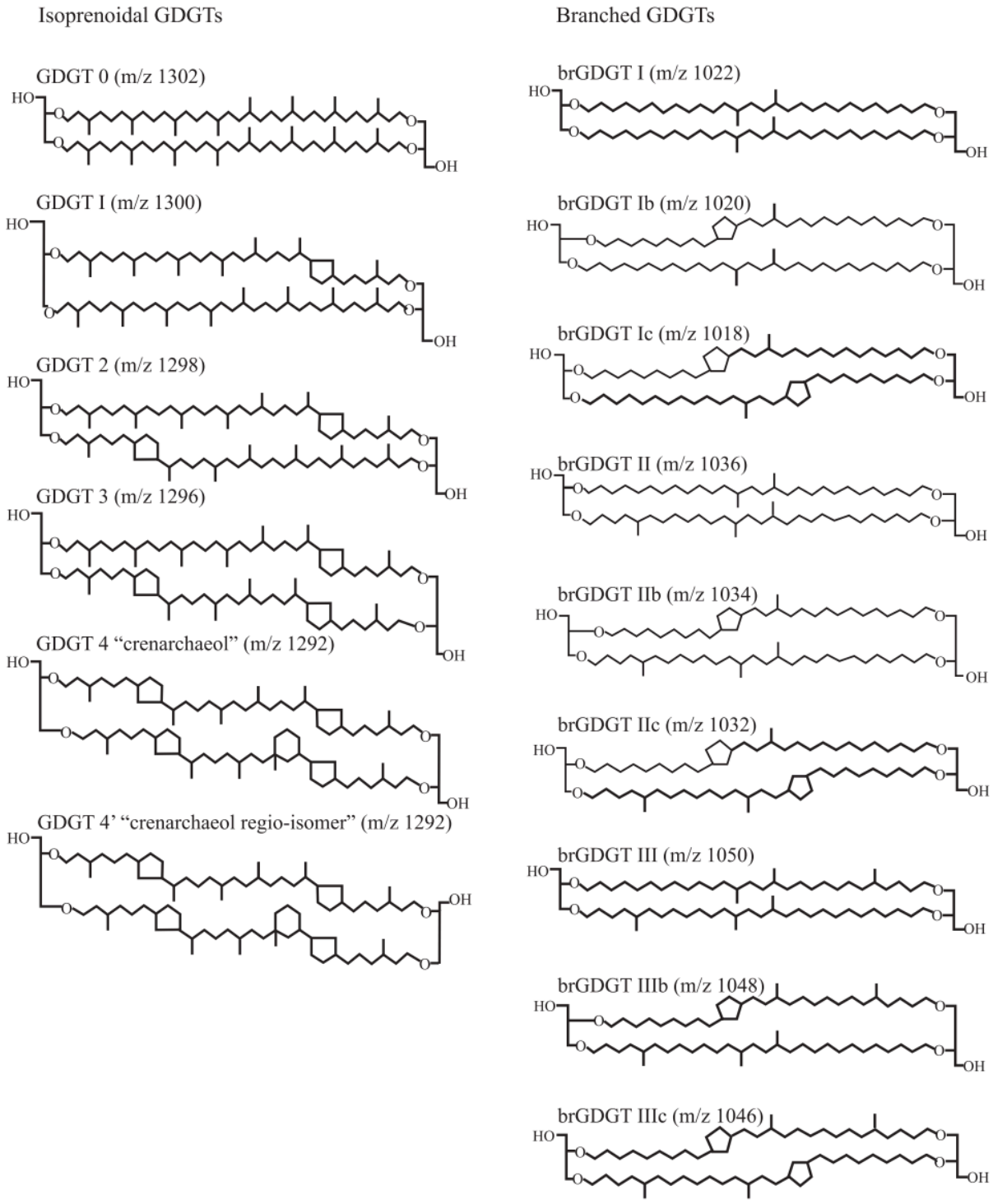

Figure 7 – A figure from Castañeda and Schouten (2011) showing the structures of common isoprenoid and branched glycerol dialkyl glycerol tetraethers.

The brGDGTs are comprised of a C_{28} n-alkyl skeleton that additionally has 4, 5, or 6 methyl groups (brGDGTs I, II, and III, respectively) incorporated along the skeleton (see Figure 7). Like the isoGDGTs, these compounds are also of interest as a paleotemperature proxy (the Methylation of Branched Tetraethers [MBT] and Cyclisation of Branched Tetraethers [CBT] proxies; Appendix C, Equations 6 and 7), potentially recording the mean annual soil temperature from their growing environment, as well as soil pH (Weijers et al., 2007). Though the source organisms are still unknown, it is suggested that brGDGTs are mainly produced by anaerobic soil bacteria (Weijers et al., 2006a), as they are both ubiquitous and abundant in soils (Weijers et al., 2006b).

The Branched and Isoprenoid Tetraether (BIT) index is a ratio (Appendix C, Equation 5) established by Hopmans et al. (2004) to estimate the relative abundance of soil-derived GDGTs (i.e. brGDGTs I, II and III) to those produced in the water column (isoGDGTs), of which crenarchaeol is assumed to be representative. BIT values can range from 0 to 1, with low values indicating greater input from aquatic sources, and high values indicating greater soil organic matter input (Hopmans et al., 2004). Crenarchaeol has been found in some soils, so while BIT values of 0 are taken to represent purely aquatic input, BIT values of >0.9 are generally seen as solely soil input (Weijers et al., 2006b). The BIT index is relatively easy to construct (i.e. the GDGTs involved are usually present in sediments) and can provide useful information on soil organic matter input into aquatic systems.

The MBT and CBT proxies are the two most commonly utilized proxies based on brGDGTs, serving as proxies for mean annual soil temperature (which is similar to mean annual air temperature [MAAT] in many cases) and soil pH, respectively (Weijers et al., 2007). As the MBT proxy also weakly correlates to soil pH, CBT can be used to correct MBT for soil pH

influence, yielding the MBT/CBT temperature proxy that better correlates to MAAT (Weijers et al. 2007). Weijers et al. (2007) established global soil calibrations for the MBT and CBT proxies, with uncertainties of ~±1 pH unit from CBT and ~5°C for absolute MAAT from MBT/CBT, though local and regional calibrations have yielded better correlations to absolute MAAT than the global calibrations (Sinninghe Damsté et al., 2008; e.g. Loomis et al. 2012, Tierney et al., 2010). These indices are summarized below in Table 2.

The TEX_{86} (Schouten et al., 2002) is a paleothermometer based on the relative abundances of isoGDGTs produced by *Thaumarchaeota* (excluding GDGT-0 and crenarchaeol, the two most abundant GDGTs) and reflects the number of cyclopentane rings incorporated into the lipids increases with growth temperature. The exclusion of GDGT-0 and crenarchaeol in TEX_{86} is to avoid their potentially overwhelming influence on the ratio due to their high relative abundances, but also because GDGT-0 is produced by methanogenic and methanotrophic *Euryarchaeota* (in addition to *Thaumarchaeota*) living in sedimentary environments (Schouten et al., 2007) that could obfuscate the TEX_{86} temperature signal.

The Methane Index and Ring Index (Appendix C, Equations 9-12) have both been established to validate the TEX_{86} for temperature reconstructions (Zhang et al., 2011; Zhang et al., 2016). The Methane Index (Zhang et al., 2011) ranges from 0-1 and quantifies the relative contributions of methanotrophic *Euryarchaeota* versus non-methanotrophic marine *Crenarchaeota*. Values closer to zero correspond to abundant crenarchaeol and its regioisomer, and represent a predominance of *Crenarchaeota*. A dominance of GDGT-1, -2 and -3 over crenarchaeol is indicative of greater influence from methanotrophic *Euryarchaeota*. Samples with a Methane Index value of >0.5 are unsuitable for paleoclimate reconstruction with TEX_{86} (Zhang et al., 2011). The Ring Index (Zhang et al., 2016) was developed to determine if TEX_{86}

values are influenced by environmental parameters other than temperature or deviate from modern calibration studies. The Ring Index (Appendix C, Equation 10) incorporates contributions of isoGDGTs weighted by their number of rings, and is significantly correlated with the TEX_{86} indices from published global core top data sets (Zhang et al., 2016; Appendix C, Equation 11). The ΔRI (Appendix C, Equation 12) evaluates the extent that a given sample's RI value deviates from the established RI-TEX_{86} relationship (Appendix C, Equation 11). Samples with ΔRI of <|0.3| have TEX_{86} values that robustly record temperature.

Several temperature calibrations have been applied to the TEX_{86} (Castañeda and Schouten, 2011) (Appendix C, Equations 14-16). Kim et al. (2010) established a marine calibration incorporating 426 core top samples. As crenarchaeol is unresponsive to temperature variability in polar waters, two equations were established to differentiate between polar and temperate/tropical waters, referred to as TEX^{L}_{86} (surface water temperatures <15 °C) and TEX^{H}_{86} (surface water temperatures >15 °C) (Appendix C, Equation 13). Additionally, several lacustrine calibrations for TEX_{86} have been constructed (e.g. Powers et al., 2010; Tierney et al., 2008). The Powers et al. (2010) calibration incorporated a small number of samples (n=12) from medium to large lakes (with BIT<0.5). The Tierney et al. (2010) calibration added five additional samples (all with temperatures >23°C) to the Powers et al. (2010) calibration, and removed lake samples with temperatures <10°C to create a temperate/tropical lacustrine calibration. It should be noted that combing the Powers et al. (2010) and Tierney et al. (2010) calibrations together also yields a calibration with a good correlation to temperature. More calibrations exist, but the three highlighted above were described because they were applied to the Lake Magadi TEX_{86} record to attempt to reconstruct paleotemperature.

INDEX	RANGE OF VALUES	LOWER VALUES MEAN	HIGHER VALUES MEAN
P_{AQ}	0 – 1	**terrestrial input**	aquatic macrophyte input
TAR_{HC}	0 – 1	algal input	**terrestrial input**
CPI	0 – ~40	thermal/biotic degradation; petroleum contamination	**terrestrial input**
ACL	27 – 33	greater C_3 input	greater C_4 input
BIT	0 – 1	aquatic input	soil input
MBT	0 – 1	cooler soil temperature	warmer soil temperature
CBT	0 – 1	lower pH	higher pH
TEX_{86}	0 – 1	cooler water temperature	warmer water temperature
MI	0 – 1	*Crenarchaeota* source	methanotrophic *Euryarchaeota* source
ΔRI	|0 – 3|	TEX_{86} influenced by temperature	non-temperature influences on TEX_{86}

Table 2 – A summary of the indices for n-alkanes (upper section) and GDGTs (lower section) that are used in this thesis.

1.6 THESIS OBJECTIVES

The aim of this thesis is to determine the potential to produce a climate record from leaf waxes and GDGTs at Lake Magadi. This involves the identification of n-alkyl and GDGT compounds and data assessment to determine how robustly these proxies represent the past precipitation/vegetation regime and temperature, respectively. Additionally this thesis outlines the potential future sample yield from the core and evaluates whether the achievable temporal resolution for organic proxies in Magadi matches the goals of the HSPDP.

2.0 MATERIALS AND METHODS

2.1 CORE STRATIGRAPHY AND CORE DATA

Lake Magadi was drilled in 2014 by the HSPDP, recovering four cores (1A, 1B, 1C, and 2A) from Lake Magadi. Core recovery was poor, as interbedded hard and soft layers throughout the sediment proved difficult for drilling (Cohen et al., 2016; Appendix D, Table 7). The four cores were transported to and stored at the National Lacustrine Core Repository (LacCore) at the University of Minnesota, in Minneapolis, MN.

The Lake Magadi core stratigraphy (Appendix D, Figure 24) was mapped and detailed by HSPDP collaborators Emma McNulty and Dr. Tim Lowenstein at the State University of New York – Binghamton (McNulty et al., 2016). Due to poor recovery during drilling (Appendix D, Table 7), there are significant gaps throughout the core. However, the sedimentological core description, along with initial loss on ignition (LOI [at 550°C]) data, allowed us to target potential biomarker-rich sediments.

Within the HSPDP project, other proxy work is being done on the Lake Magadi cores, including pollen analysis, inorganic geochemical analyses, phytolith analysis, and diatom assays, as well as various dating methods. Pollen and diatom assemblages are being constructed by Dr. Bernie Owen and Veronica Mwihaki at Hong Kong Baptist University. Core mineralogy was established by Nate Rabideaux at Georgia State University (Rabideaux et al., unpublished) and

sulfur isotopes are being analyzed by Dr. Jonathan Wynn at the University of South Florida. At the University of Arizona, phytolith data is being processed by Chad Yost; charcoal is being analyzed by Chenyu Wang and Brant Davis; loss on ignition data has been completed by Julia Richter; and Shangde Luo and Dr. Andrew Cohen are working on uranium series and ^{14}C dating. Additionally, Dr. Mark Sier from Utrecht University is working on paleomagnetism data. Though these data sets are not the focus of this thesis, this complementary work demonstrates the rich, multi-proxy environmental reconstruction from the Lake Magadi core site.

2.2 EXTRACTION AND SEPARATION

Samples for biomarker analysis were selected from facies determined by McNulty et al. (2016) to be high in organic content and relatively undisturbed. Sampling protocol at LacCore included the use of gloves and acetone-washed tools for sample collection. Each sample was collected from the center of the core to avoid potential contamination from drilling fluids.

Sediment samples were freeze-dried and homogenized, then extracted sonically with 2:1 DCM/MeOH to generate the total lipid extract (TLE). Activated copper shot was added to the TLE to remove elemental sulfur. For the initial 21 samples, the TLE was separated by solid phase extraction (SPE) using an aminopropyl stationary phase, collecting three fractions: a neutral/polar fraction (2:1 DCM/IPA), a free fatty acid fraction (4% glacial acetic acid in ethyl ether), and a phospholipid fatty acid fraction (MeOH). The n-alkanes and GDGTs eluted first in the neutral/polar fraction, and the fatty acids eluted in the free fatty acid fraction. No compounds of interest to this study eluted in the phospholipid fatty acid fraction. The TLE from the second set of 47 samples did not go through SPE aminopropyl stationary phase, instead going straight to

the alumina column chromatography separation (Figure 9). This decision was made to attempt to isolate lacustrine alkenones (another biomarker, thought to record surface water temperature in oceans and some lakes) that could be present in Lake Magadi due to its saline nature (e.g. D'Andrea and Huang, 2005; Pearson E.J. et al., 2008).

After running the TLE (from the first 21 samples; Figure 8) through the aminopropyl SPE columns, the free fatty acid fractions (and a palmitic acid standard) were methylated with BF_3-methanol to convert the fatty acids to fatty acid methyl esters (FAMEs) and prevent adsorption to the gas chromatograph column during analysis.

The neutral/polar fractions from the aminopropyl SPE (containing the n-alkanes and GDGTs) from the first 21 samples were separated by alumina column chromatography into another three fractions: apolar (9:1 hexane/DCM), polar 1 (1:1 DCM/MeOH), and polar 2 (MeOH). The n-alkanes eluted in the apolar fraction, and the GDGTs eluted in the polar 1 fraction (Figure 8). The TLE from the second set of samples was split into apolar 1 (9:1 hexane/DCM), apolar 2 (1:1 hexane/DCM), and polar 1 (1:1 DCM/MeOH) fractions. In this separation, the apolar fraction was split into apolar 1 (containing n-alkanes) and apolar 2 (lacustrine alkenones would elute in this fraction, if present), while the GDGTs still eluted in the polar 1 fraction (Figure 9). The apolar (and apolar 1) fractions were passed through a silver silica column to remove unsaturated compounds (e.g. n-alkenes), separating into a saturated fraction (pure hexane solvent) and an unsaturated fraction (pure ethyl acetate solvent).

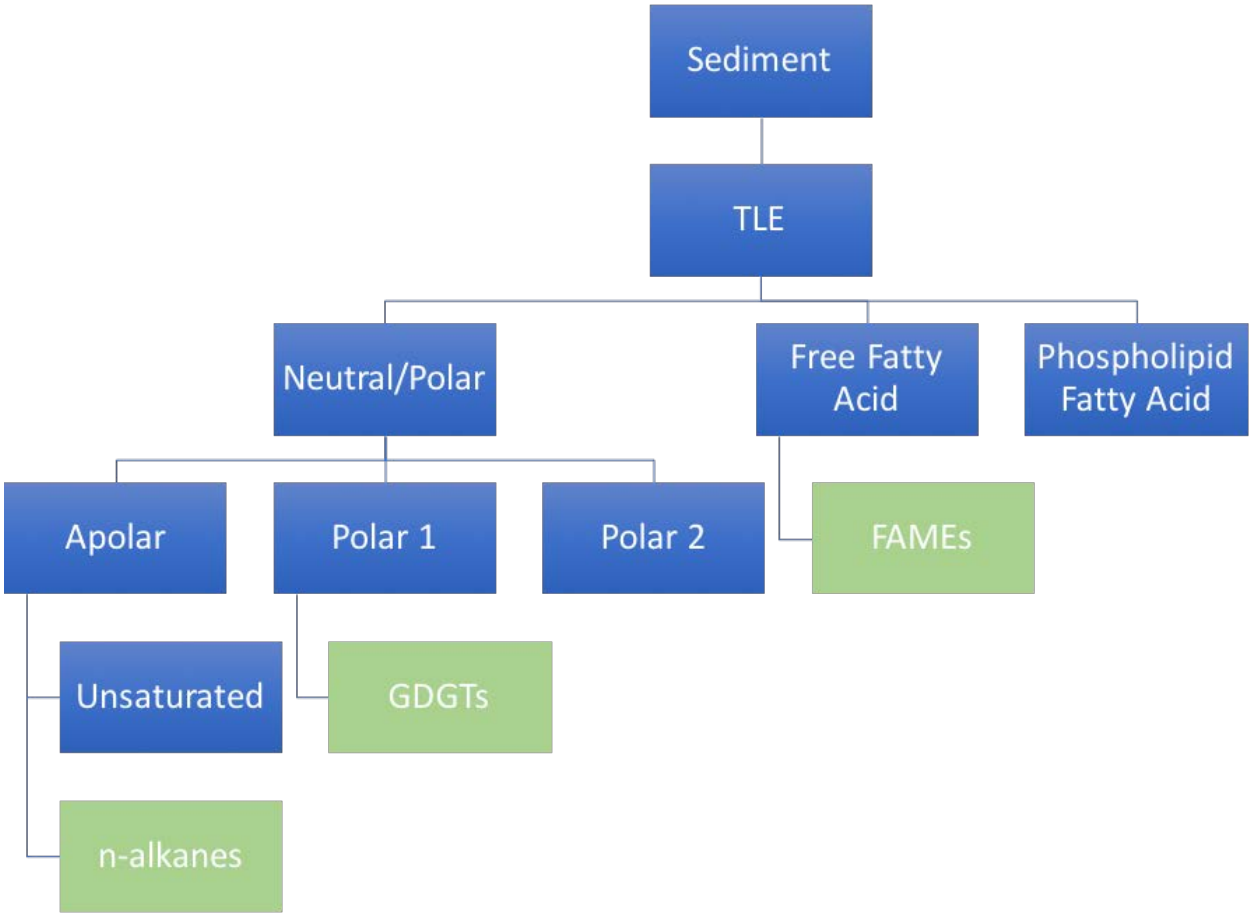

Figure 8 – The extraction and separation scheme for the first set (21) of pilot samples. Compounds of interest are in fractions designated by green coloring.

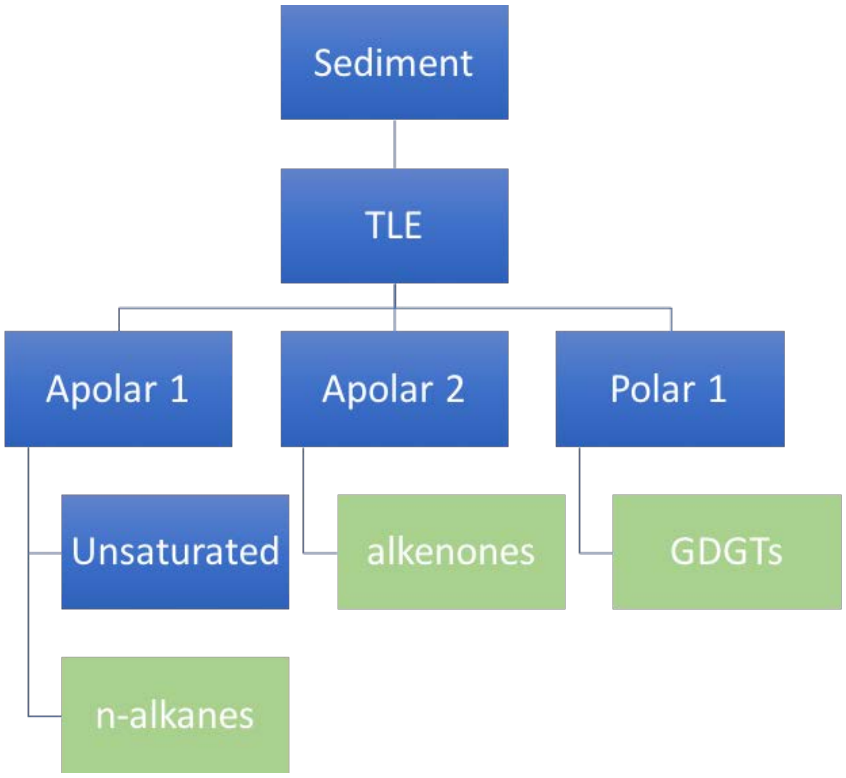

Figure 9 – The extraction and separation scheme for the second set (47) of pilot samples. FAMEs were not collected and a new fraction potentially containing alkenones, another organic temperature proxy, was collected.

2.3 INSTRUMENTAL ANALYSES

None of the samples analyzed in this thesis were run in duplicate. Leaf wax abundances are consistently reproducible (e.g. Castañeda et al., 2009a), and other studies have reported uncertainties in isoGDGT-derived TEX_{86} of ~0.0076 corresponding to a 2σ temperature range of 0.8°C (e.g. Johnson et al, 2016).

2.3.1 Leaf waxes

The BF_3-methylated free fatty acid fractions (from the first 21 samples; Figure 8) were analyzed by gas chromatography (GC) coupled with flame ionization detection (FID) and mass spectrometry (MS) for abundances and identification of FAMEs (same settings as described below) in the Werne Organic Geochemistry Lab at the University of Pittsburgh. Due to crowded chromatograms from the first set of pilot samples, FAMEs were not analyzed from the second set of samples.

The apolar fraction (from the first 21 samples) and the apolar 1 fraction (from the second set of 47 samples) were then analyzed by GC-FID and GC-MS for quantification and identification of the n-alkanes (Figures 8 and 9). Samples were analyzed on a Thermo Scientific Trace 1310 GC, equipped with an Agilent DB-5 column (30m x 0.320 mm, 0.25 μm film) with an FID detector, and a Thermo Scientific ISQ QD Single Quadrupole Mass Spectrometer (separate runs necessary due to loss of sample from FID). The GC injector temperature was set to 250°C, and the column oven held at 70°C for 1 min, ramped to 130°C over 6 min at a rate of 10°C/min, and then ramped again to 320°C over 57.5 minutes at a rate of 4°C/min. The column carrier gas used was helium (He), and the gas flow to the FID was a mixture of 350 mL/min air, 20 mL/min He, and 35 mL/min hydrogen. The MS transfer line temperature was maintained at 300°C, the ion source temperature was 275°C, and the MS method followed the "acquisition-general" setting. These same samples will be run through GC-coupled isotope ratio mass spectrometry (IRMS) for isotopic analysis of the n-alkanes.

2.3.2 GDGTs

From both sample sets, the polar 1 fraction after alumina column chromatography was filtered using a 0.47 μm syringe filter. The samples were then analyzed for isoprenoid and branched GDGTs using liquid chromatography coupled with mass spectrometry (LC-MS) on an Agilent 1260 series Single Quad LC (with an autoinjector) and an Agilent 6120 series Mass Selective Detector (MSD) by collaborator Dr. Isla Castañeda at the University of Massachusetts – Amherst. The instrument conditions follow those outlined in Hopmans et al. (2016), such that a 2.1 x 5 mm pre-column (BEH HILIC columns, 2.1 x 5 mm, 1.7 μm; Waters) was followed by two UHPLC silica columns (BEH HILIC columns, 2.1 x 150 mm, 1.7 μm; Waters) in series. These columns were kept at 30°C, and used to separate GDGT compounds. At a flow rate of 0.2 mL/min, the compounds were eluted for 25 min with 18% B, then linearly increased to 35% B over 25 min, followed by another linear increase to 100% B over 30 min, where A is pure hexane and B is hexane:isopropanol (9:1, v/v). Due to relatively low concentrations of GDGTs in many of the samples, very large injection sizes (generally 15-20 μL, but up to 25 μL for some samples) were necessary to achieve a large enough instrument response to quantify the compounds.

3.0 RESULTS

3.1 LEAF WAXES

3.1.1 n-alkanes abundances and distributions

Of the 68 samples analyzed for leaf waxes, 57 of them (83.8%) yielded measurable data for n-alkanes. A sample chromatogram of the n-alkanes can be found in Appendix E (Figure 25). The n-alkane concentrations spanned a wide range, from 0.06 μg/g to 143.46 μg/g sediment. The samples have an average of 19.63 μg n-alkanes/g sediment, with a standard deviation of ±15.82 μg/g sediment. Raw abundance data can be found in Appendix F (Table 8).

The n-alkane indices previously mentioned (section 1.5.1) are plotted as a function of core depth in Figure 10. The TAR_{HC} shows predominantly terrestrial input throughout the core, with all but one sample lying above a value of 0.8. Ten samples, representing 17.5% of the 57 samples yielding n-alkane data, produced CPI values of less than 3 and indicate potentially extensive degradation (three samples from ~130-165 m depth, four samples from core top to ~35 m depth), and were subsequently discarded (Figure 11). All samples produced P_{aq} values of <0.5, though many of the samples with the highest P_{aq} values also had CPI values of <3. Five samples with P_{aq} values >0.2 and CPI values from 3-4, though not omitted, were marked (as shown in Figure 12) and are less certain than the remaining data points. Average chain length

was plotted alongside the other proxies in Figures 10, 11, and 12 to show the effect of removing bad or questionable data points from the n-alkane record.

3.1.2 Fatty acid methyl esters (FAMEs) abundances and distributions

All 20 of the samples analyzed for FAMEs contained the fatty acid compounds of interest (sample chromatogram in Appendix E, Figure 26). FAMEs were only examined in the first set of pilot samples (20 samples), as the chromatography of the n-alkanes was cleaner and had better peak separation, and thus had a greater chance of producing compound specific isotope measurements. The FAMEs chromatograms exhibit the expected even over odd predominance (the opposite of the n-alkane samples), indicating a primarily terrestrial source with minimal degradation. The FAMEs had high abundances, ranging from 0.012-31.05 μg total FAMEs/g sediment, with an average of 6.80 μg/g sediment and a standard deviation of 8.46 μg/g sediment. After further chemical separation (to clean up the chromatograms and better isolate compounds of interest), the FAMEs have the potential to be useful for future environmental reconstruction, but are not pursued further in the present study.

3.1.3 n-alkane $\delta^{13}C$ and δD

Isotopic measurements have not yet been completed on the pilot n-alkane samples from Lake Magadi. However, many environmental reconstructions from compound specific analysis of δD and $\delta^{13}C$ focus on the C_{29} (e.g. Tierney et al., 2017) and C_{31} (e.g. Magill et al., 2013b) n-alkanes. In Appendix F (Table 8), the abundances of the C_{29} and C_{31} n-alkanes are presented and indicate their potential to provide good isotopic data in the future.

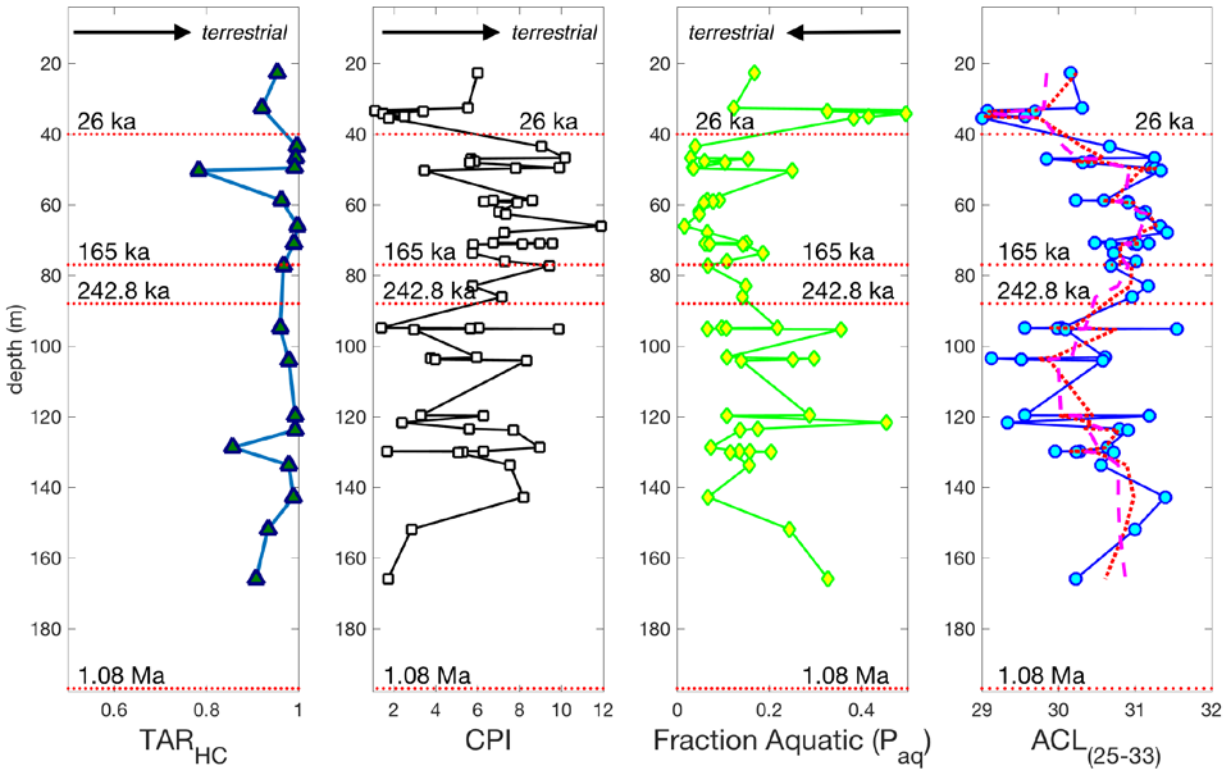

Figure 10 – The four n-alkane indices (from the left: TAR_{HC}, CPI, P_{aq}, and ACL) plotted against depth, including all possible data points. The TAR_{HC} has only 19 points as many of the lower chain (C_{15}-C_{19}) n-alkanes were difficult to identify and quantify due to the presence of a hump in the chromatogram caused by unresolved complex mixture (UCM; see Discussion below). In the ACL plot (and for all plots of ACL in this thesis) the red dotted line represents a three-point moving average, and the magenta dashed line represents a five-point moving average. Four ages along the core have been identified by Alan Deino at the Berkeley Geochronology Center, and those four dates are included on all plots in this thesis, though no age model has been completed to date.

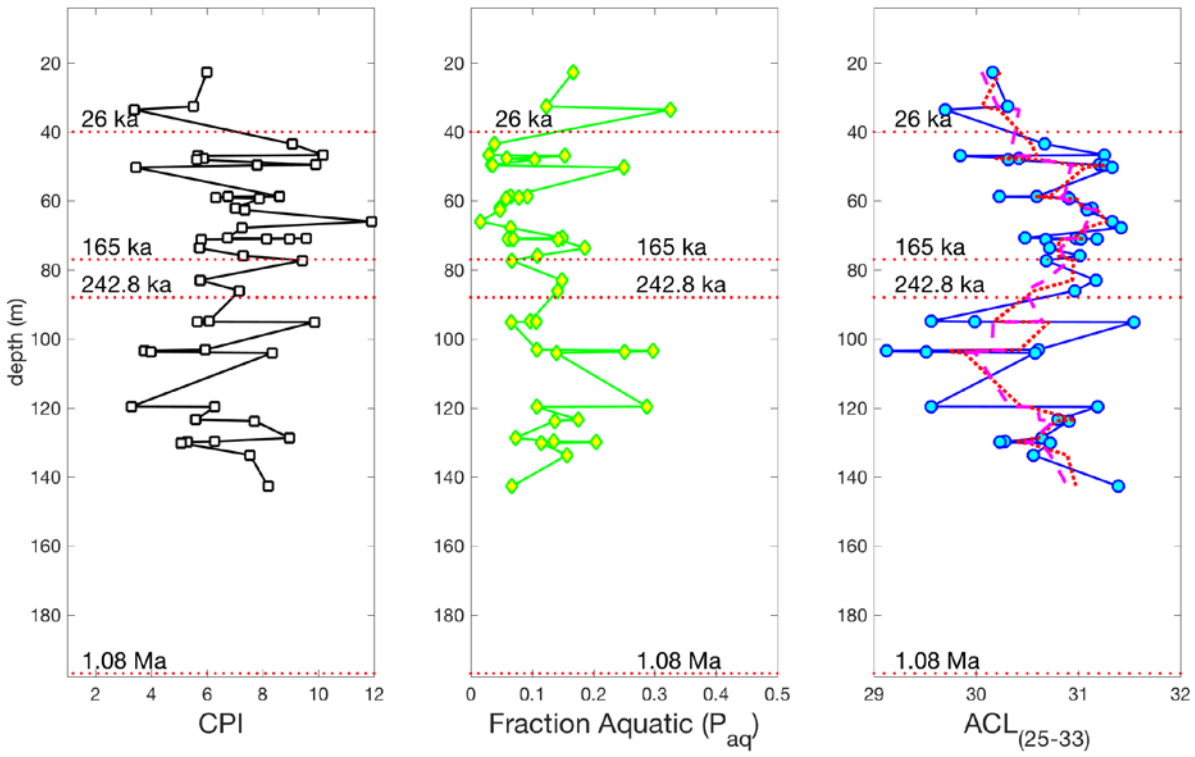

Figure 11 – The CPI, P_{aq}, and ACL plotted with all data points where CPI<3 (10 in total) removed. Though somewhat interspersed throughout the core, seven of the ten samples removed came from depths of ~130-165 m and core top to ~35 m. Both of those sections had poor core recovery (Appendix D, Figure 24) with increased chances of contamination from drilling fluid, which may have contributed to the low CPI values.

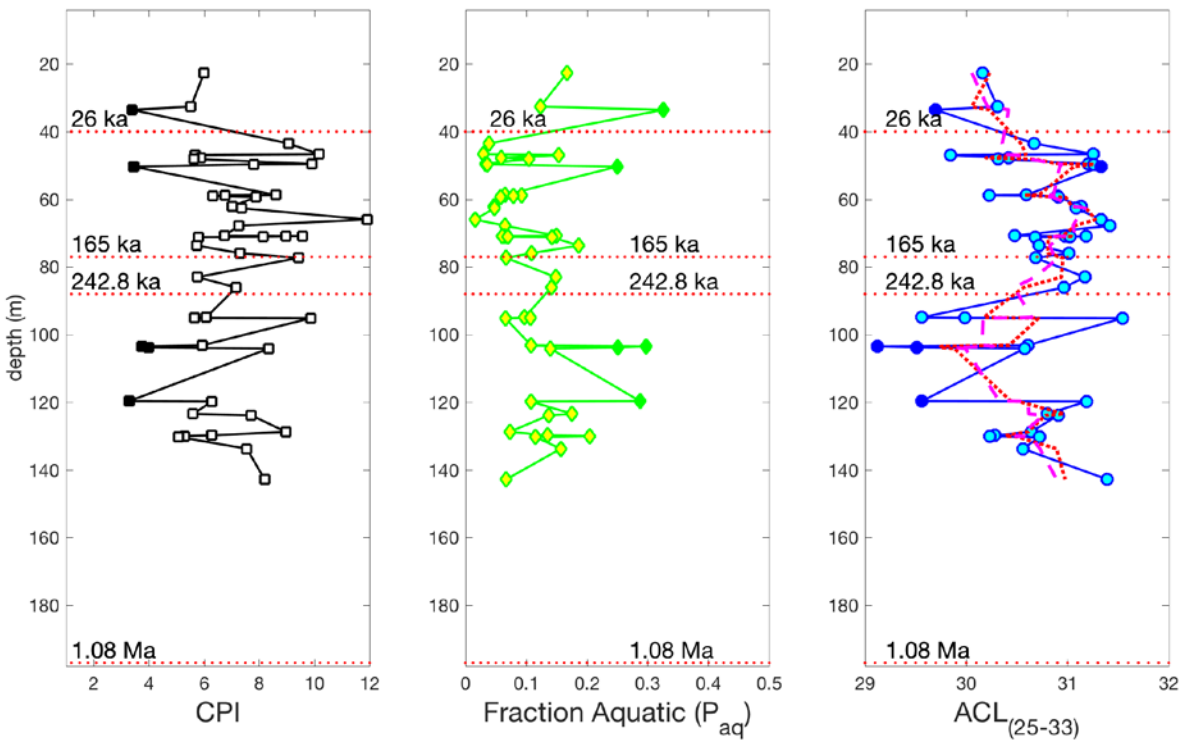

Figure 12 - Of the remaining data points (after removal of the 10 with CPI<3), five have CPI values between 3 and 4, and correspond to the highest remaining values among P_{aq} as well. Though these values are both within an acceptable range to be considered terrestrial signals, they are marked in this figure with a filled-in symbol to denote that they may not record a terrestrial signal with the same fidelity as the rest of the samples.

3.2 TEMPERATURE PROXIES

3.2.1 GDGTs

In total, 64 samples were analyzed for both brGDGTs and isoGDGTs, of which 62 samples had all the isoGDGTs necessary to calculate the TEX_{86} (Appendix C, Equation 8; Appendix H, Table 10 for the raw GDGT data). The full suite of brGDGT compounds (to

calculate MBT/CBT) were not present in any of the samples, though occasionally singular brGDGTs were identified. Sample GDGT chromatograms are shown in Appendix G (Figures 27-29). Seven of the 64 total samples either lacked the isoGDGTs for TEX_{86} (2 samples), or had a poorly resolved chromatogram with many additional peaks (5 samples; all 7 samples were discarded). An additional 26 samples had all the peaks, but included extra peaks as well, and often had a small GDGT-1 peak. The remaining 31 samples with chromatograms resembling "typical" marine isoGDGT distributions are considered potentially suitable for paleotemperature reconstruction.

The TEX_{86} and three temperature calibrations are plotted in Figure 13. The data points representing the 26 questionable samples mentioned previously are marked as filled in points. The temperature calibrations, Kim et al. (2010), Powers et al. (2010), and Tierney et al. (2010) all show similar temperature trends (Figure 13). The Kim et al. (2010) calibration is constructed with marine samples, whereas the Powers et al. (2010) and Tierney et al. (2010) calibrations are both lacustrine. Though Magadi is a lake, it was often very saline (McNulty et al., 2016; Cohen et al., 2016), making the Kim et al. (2010) marine calibration potentially a better fit for the site.

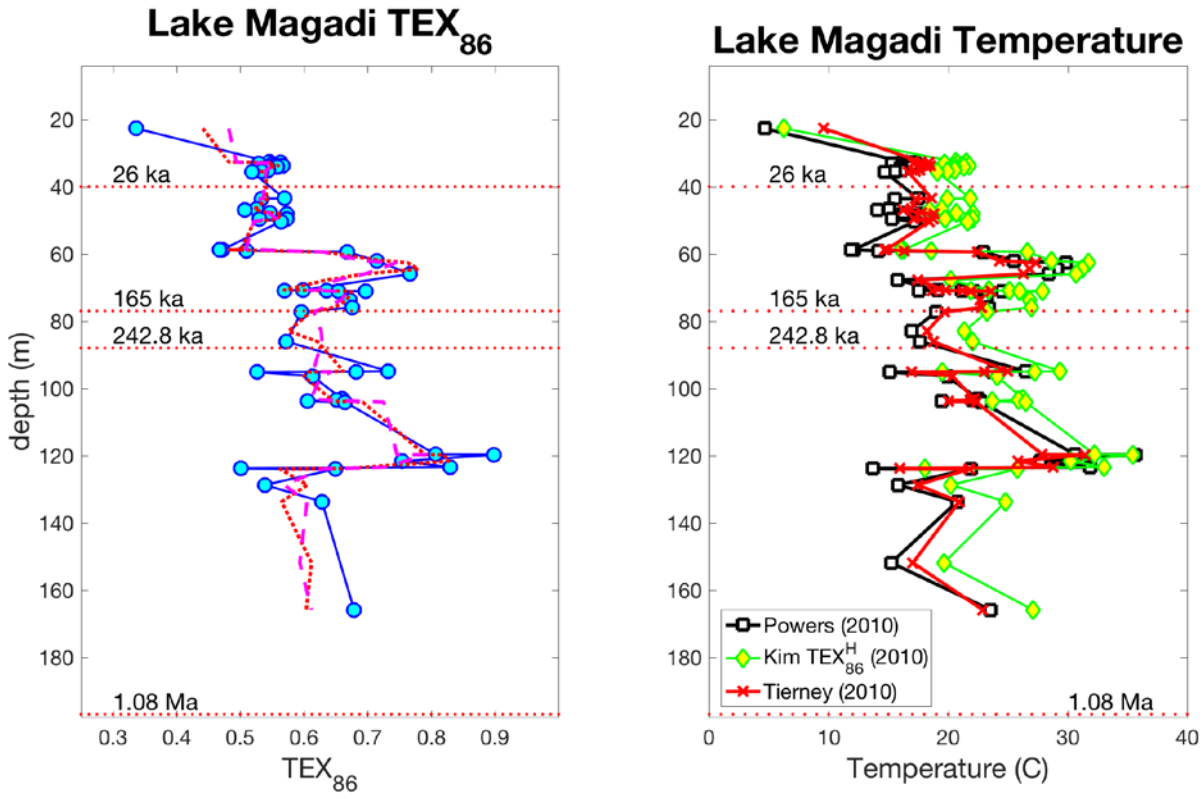

Figure 13 – This figure shows the TEX_{86} (Appendix C, Equation 8) plotted vs. depth, and the three TEX_{86} temperature calibrations (note that the Kim et al., [2010] TEX^{H}_{86} calibration relies on a different TEX_{86} calculation, which is not represented in the plot; Appendix C, Equation 13). The three temperature reconstructions generally agree with each other, but in several intervals where temperatures decrease (e.g. ~120-130 m, or ~60 m depth), the Kim et al. (2010) calibration gives warmer (and more realistic) temperatures. On those grounds, the Kim et al. (2010) temperature calibration was chosen to apply to Lake Magadi.

4.0 DISCUSSION

4.1 EVALUATION OF LEAF WAXES

4.1.1 n-alkane CPI, TAR_{HC}, and P_{aq}

The n-alkane indices are plotted together in Figures 10, 11, and 12. The TAR_{HC} for the first set of pilot samples shows that throughout the core n-alkane distributions from Lake Magadi indicate high terrestrial input relative to aquatic (algal) input. However, TAR_{HC} was difficult to construct in the second set of samples due to the presence of a UCM hump in the beginning of many samples (see Figure 14). The CPI and P_{aq} corroborate this, as 82.5% of samples with n-alkanes present had a CPI greater than 3, and all samples had a P_{aq} less than 0.5. An additional 5 samples had a combined lower CPI (~4) and higher P_{aq} (>0.2). Though these samples fall within an acceptable range for both proxies (Freeman and Pancost, 2014), they are close to the threshold, and therefore potentially not the most robust recorders of terrestrial n-alkanes. From the 68 total samples analyzed for n-alkanes, 42 of them (61.8%) robustly recorded a terrestrial signal, while another 5 samples (7.4%) also suggest a terrestrial origin. Approximately 70% of all samples analyzed for n-alkanes record a viable terrestrial signal with the potential to yield the paleoclimate data desired by the HSPDP.

Though ~70% of total analyzed samples yielded n-alkanes, evaluating the pilot samples over intervals of interest will help determine how well biomarker analysis at Lake Magadi can achieve and further the goals of the HSPDP. Outlined in Campisano et al. (2017), there are five hominin evolutionary events that fall within the timespan (~1 Ma to present) represented by sediments at Lake Magadi, including the existence of Bodo cranium (~0.60 Ma), the first appearance of Middle Stone Age technology (0.280-0.272 Ma), the first appearance of *Homo sapiens* (0.198-0.194 Ma), *Homo sapiens* dispersal out of Africa (0.08-0.05 Ma), and the first appearance of Late Stone Age technology (0.0617-0.0521 Ma). Four of these evolutionary events occur from ~0.280 Ma to present. Based on the four preliminary dates on the Magadi 2A core (26 kyr at 40 m, 165 kyr at 77 m, 242.8 kyr at 88 m, and 1.08 Ma at 197 m depth), the four hominin evolutionary events that occur from 280 kyr to present likely all occur in the top 100 m of Magadi core 2A. Of the 46 samples analyzed between 0-100 m depth, 38 (82.6%) of the samples yielded n-alkanes and 32 (69.6%) of the samples had an odd over even predominance suggesting little to no degradation (CPI>3). It should be noted that 100 m depth was arbitrarily selected to represent core material encompassing the past 300 kyr. When examining samples from 0-88 m (the depth corresponding to 242.8 kyr), 80.5% of samples yield n-alkanes, and 70.7% of samples have a CPI>3. Over intervals of interest to the HSPDP, ~70% of samples analyzed yield robust paleoclimate data and are promising for future analysis.

4.1.2 Unresolved complex mixtures (UCM)

Of the 68 samples analyzed for leaf waxes, 11 of them (16.2%) did not yield quantifiable data for n-alkanes. This was due to either none of the n-alkanes being present (or in too low abundance to measure) or due to baseline disruption (a “hump”, see Figure 14) resulting from an

unresolved complex mixture (UCM) that obscured the desired peaks in the chromatogram. Due to interference from the UCM, the C_{15}-C_{22} n-alkanes were unable to be quantified, making calculation of the TAR_{HC} ratio impossible for UCM-containing samples.

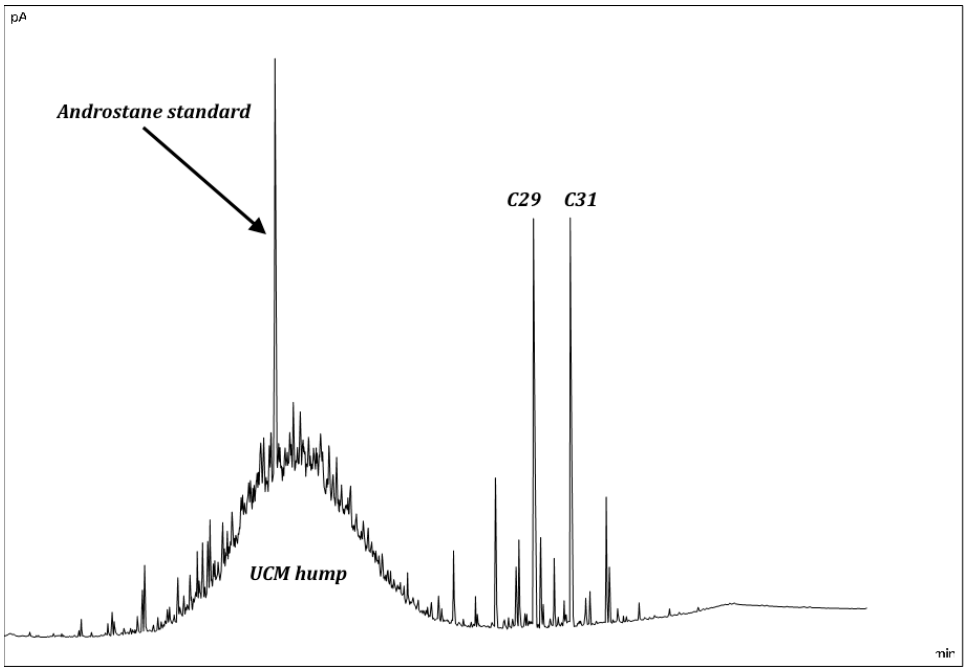

Figure 14 – A sample chromatogram from Magadi core section 2A-17Y-2 showing a pronounced baseline disruption (UCM hump).

None of the samples from the first set (21 samples) contained a UCM hump – all samples containing the UCM hump were from the second set of samples (47 samples). This suggests that the presence of the UCM baseline disruption may be related to differences in the extraction scheme between two samples (e.g. due to the lack of aminopropyl SPE in the second set of samples). It may be the case that the UCM consists of compounds that would have been separated into the free fatty acid fraction during aminopropyl SPE. However, this is unlikely, as compounds that have an affinity for the free fatty acid fraction (a solvent mixture of 4% glacial acetic acid in ethyl ether) would have been too polar to elute in the alumina column

chromatography apolar 1 fraction of the second set of samples (9:1 hexane/DCM solvent) and more likely would have eluted in the apolar 2 (1:1 hexane/DCM solvent) or polar 1 (1:1 DCM/MeOH solvent) fractions.

More likely is that the presence of the UCM hump is related to the effectiveness of the silver silica columns in the second set of samples. Several samples in the n-alkane (apolar) fraction in the first set had many extraneous peaks (though nothing resembling the UCM present in many samples in the second set) and caused the silver silica column chromatography to be added to the chemical work up method. However, silver silica must be activated prior to use (via dehydration in an oven at 90°C for 16 hours) and can slowly become deactivated if exposed to light (silver nitrate silica MSDS). If the silver silica chromatography was less effective at removing unsaturated compounds (e.g. n-alkenes) for the second set of samples due to reagent deactivation, it could have resulted in the UCM not being separated from the saturated fraction containing the n-alkanes. In this scenario, the compounds comprising the UCM are of the correct polarity to be present in the n-alkane (apolar 1) fraction after alumina column chromatography. As such it is more likely that the UCM resulted deactivated silver silica, than skipping the aminopropyl SPE in the second set of samples. In the future, rerunning a subset of samples through a second round of silver silica column chromatography could determine whether ineffective reagent was the source of the UCM hump.

The UCM hump is predominantly present in the top of the core, sections 2A-17Y-1 through 2A-24Y-1, though found throughout the core and as deep as 2A-60Y-2 (Table 3). The presence of a UCM hump could also imply oxic degradation of the sample from exposure to either oxygenated pore water or atmospheric oxygen, suggesting Lake Magadi n-alkanes are recording the drying of the paleolake. As Magadi progressively dried out, perhaps due to

increasing aridity (see section 4.3.2 below), deposited sediments would become increasingly exposed to oxygen. The presence of the UCM humps, under this interpretation, could shed light on the dynamic between precipitation and lake level with future study. However, due to general presence of the UCM from the second set of samples and lack of UCM from the first set of samples it seems most likely that the UCM is an analytical artifact.

4.2 EVALUATION OF TEMPERATURE PROXIES

4.2.1 TEX_{86} validation and calibrations

As discussed in the Results, brGDGTs were generally absent from samples. While there were a few exceptions, they contained only singular brGDGTs, rather than the full suite needed to calculate the MBT or CBT proxies. The isoGDGTs were present in 62 of 64 samples (96.9%) analyzed for GDGTs. Five of these samples were either missing one of the isoGDGTs (usually the crenarchaeol isomer, GDGT-4') needed to construct the TEX_{86} or had a chromatogram with many extra peaks, resulting in seven total samples being discarded. This resulted in 57 of 64 samples (89.1%) yielding a TEX_{86} value.

Initial validation of isoGDGT data and the TEX_{86} was qualitative. During data collection, samples were separated into three categories based on the distribution of isoGDGTs in their chromatogram. The first category consisted of the seven discarded samples that either had missing isoGDGTs or had a very abnormal chromatogram, or both. The second category was comprised of questionable samples (26 in total), defined as samples that had all the isoGDGTs needed to calculate the TEX_{86} but had extra peaks. Finally, the third category (31

samples) consisted of samples that appeared to be typical marine samples where the isoGDGTs used in the TEX_{86} were by far the most prominent compounds (Appendix G, Figures 27, 28 and 29 for sample chromatograms from each category). Both the second and third categories' samples were used in the preliminary temperature reconstruction in Figure 13, though the questionable samples are designated by filled-in markers.

SAMPLE	DEPTH (M)	UCM PRESENCE (Y/N)	RING INDEX (ΔRI)	METHANE INDEX
2A-11Y-1	22.65	N	1.343	0.983
2A-17Y-1	32.61	N	-0.185	0.191
2A-17Y-2	32.791	Y	-0.367	0.222
2A-17Y-2	33.031	Y	0.322	0.414
2A-17Y-2	33.281	Y	0.253	0.374
2A-17Y-2	33.551	Y	-0.182	0.239
2A-17Y-2	33.761	Y	-0.343	0.215
2A-17Y-2	34.061	Y	-0.377	0.226
2A-18Y-1	34.15	Y	-0.261	0.250
2A-18Y-2	35.068	Y	-0.583	0.202
2A-18Y-2	35.418	Y	-0.602	0.197
2A-18Y-2	35.668	N	-0.609	0.196
2A-22Y-1	43.51	N	1.857	0.952
2A-22Y-1	43.545	Y	1.802	0.941
2A-23Y-1	46.68	N	1.850	0.943
2A-23Y-1	46.96	Y	1.734	0.937
2A-23Y-2	47.747	N	1.838	0.948
2A-23Y-2	48.077	Y	1.920	0.956
2A-24Y-1	49.545	N	1.965	0.968
2A-24Y-1	49.675	Y	1.830	0.956
2A-24Y-2	50.355	N	1.869	0.983
2A-28Y-1	58.735	N	1.714	0.928
2A-28Y-1	58.795	N	1.773	0.961
2A-28Y-1	59.055	Y	1.913	0.978
2A-28Y-1	59.395	N	2.424	0.945
2A-29Y-1	62.055	N	2.495	0.949
2A-29Y-1	62.645	Y	2.732	0.978
2A-30Y-1	64.515	Y	2.591	0.984
2A-30Y-2	65.98	N	2.656	0.979
2A-31Y-1	67.815	Y	1.987	1.000

SAMPLE	DEPTH (M)	UCM PRESENCE (Y/N)	RING INDEX (ΔRI)	METHANE INDEX
2A-32Y-1	70.775	Y	-0.148	0.195
2A-32Y-1	70.86	N	-0.402	0.248
2A-32Y-1	70.965	N	1.947	0.373
2A-32Y-1	71.075	N	1.853	0.353
2A-32Y-1	71.185	N	0.336	0.235
2A-33Y-1	73.695	Y	-0.119	0.218
2A-33Y-2	75.925	Y	0.064	0.213
2A-35Y-2	77.317	N	2.142	0.959
2A-39Y-1	83.005	Y	1.900	0.920
2A-40Y-1	86.065	Y	-0.102	0.215
2A-45Y-1	94.915	Y	2.719	0.952
2A-45Y-1	95.045	Y	2.528	0.926
2A-45Y-1	95.145	N	1.978	0.957
2A-45Y-2	96.382	N	1.669	0.864
2A-48Y-2	103.157	N	1.015	0.209
2A-48Y-2	103.487	Y	0.474	0.172
2A-48Y-2	103.787	Y	-0.594	0.198
2A-48Y-2	104.095	N	-0.224	0.308
2A-56Y-1	119.64	Y	1.925	0.888
2A-56Y-1	119.75	N	1.840	0.982
2A-57Y-2	121.662	Y	1.964	0.983
2A-58Y-2	123.431	Y	2.001	0.967
2A-58Y-2	123.82	N	1.914	0.956
2A-58Y-2	124.021	N	1.896	0.987
2A-60Y-1	128.74	N	2.067	0.835
2A-60Y-2	129.77	Y	1.363	0.975
2A-60Y-2	129.835	Y	1.364	0.981
2A-60Y-2	129.955	Y	1.345	0.973
2A-60Y-2	130.21	Y	1.919	0.978
2A-61Y-2	133.72	N	-0.287	0.289
2A-69Y-1	151.905	N	2.070	1.000
2A-81Q-2	165.935	N	2.262	0.428
TOTAL GOOD			25	10
TOTAL DISCARDED			40	55

Table 3 – A table showing the presence of the UCM hump in Magadi samples as well as values for the Methane Index (Zhang et al., 2011) and the Ring Index (Zhang et al., 2016). The number of good samples (<0.5 for MI, <|0.3| for ΔRI) and bad samples for both MI and ΔRI are also shown.

Calculated MI and ΔRI values from the Magadi pilot samples were much more discriminating than the visual assessment of the chromatograms during data collection. Table 3 shows the number of good samples and discarded samples from both indices. Based on the MI 25 of 65 samples (38.5%) can be used for TEX_{86} and based on the ΔRI with a 95%-confidence value of |0.3|, only 10 of 55 samples (18.2%). Only 58% of samples determined visually to be good for TEX_{86} had predominantly *Thaumarchaeota* input based on MI values. Samples validated by MI and ΔRI are not interspersed amongst the core but occur in several groups from 32-35, 70-76, and 103-104 m depth (Table 3). Both MI and ΔRI were plotted against the TEX_{86} values and neither show correlation (Figure 15), with r^2 values of 0.0059 for MI and 0.0803 for ΔRI. Together the MI and ΔRI indicate that TEX_{86} is only valid for temperature reconstruction through limited sections of the core.

Both the MI and ΔRI validate TEX_{86} through comparison to typical marine samples. Though differentiation from typical marine TEX_{86} values indicates TEX_{86} should not be used for temperature reconstruction in many Magadi samples, the variable distributions of isoGDGTs does indicate shifting microbial communities. Intervals where MI values are >0.5 imply a significant presence of methanotrophic *Euryarchaeota* and similarly, ΔRI values of >|0.3| indicate an abnormal community compared to modern marine environments (Zhang et al., 2011; Zhang et al., 2016). The TEX_{86} does not provide continuous, robust temperature data throughout core 2A at Lake Magadi but the GDGT data still shows changes in microbial community that may be environmentally influenced. Only a combined 34 of 62 samples (54.8%) have either a UCM hump and an MI value of >0.5, or no UCM hump and an MI value <0.5 throughout the core. This suggests no relationship between drying of the paleolake (if the UCM hump is a proxy for lake drying) and changing microbial communities. However, surface sediments from

the modern Lake Nasikie Engida (see Figure 4) have been obtained from collaborator Gijs De Cort at Ghent University. The modern samples may provide insight into the present-day microbial community and associated GDGT distributions that could then be used to better understand past changes in microbial communities from isoGDGTs at Lake Magadi.

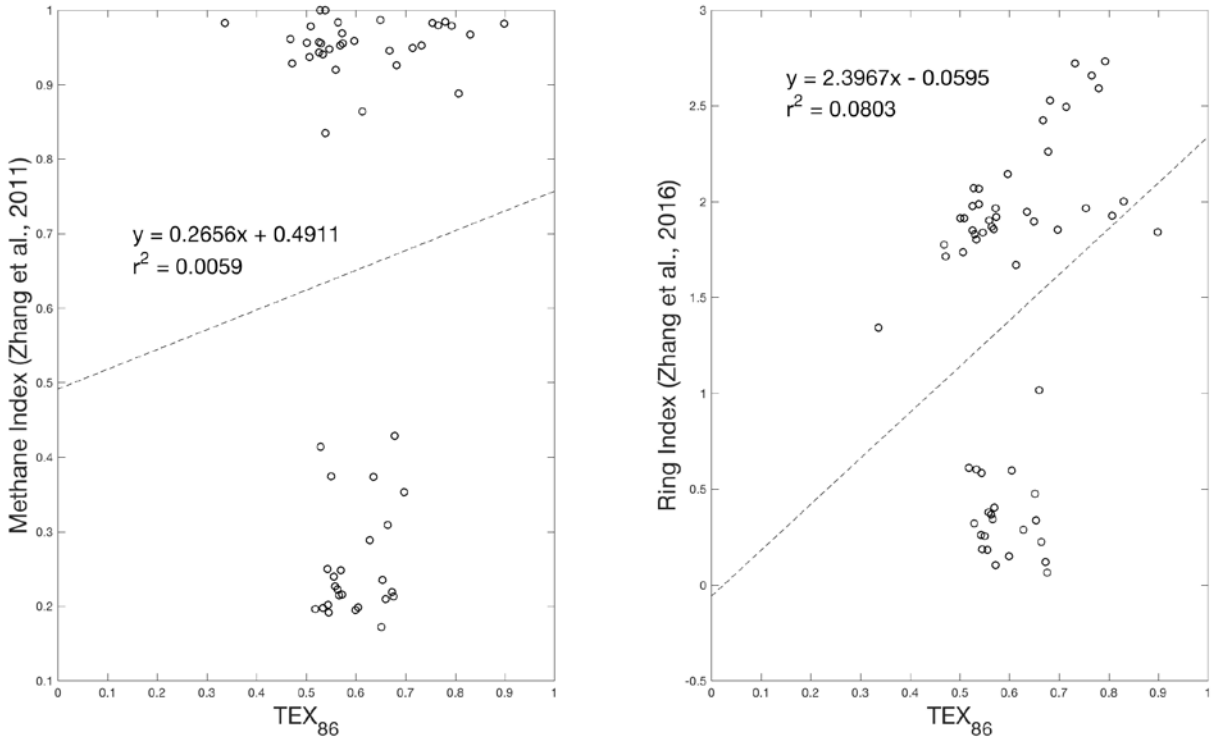

Figure 15 – Magadi TEX_{86} plotted versus the Methane Index (Zhang et al., 2011) and the Ring Index (Zhang et al., 2016), showing no correlation with either. This suggests that shifts in microbial community shown by both the MI and RI are not reflected in recorded TEX_{86} values. Both the MI and RI indices indicate that TEX_{86} shouldn't be used for temperature reconstruction at Lake Magadi, however TEX_{86} shows apparent agreement with other climate parameters and records (see Figures 18 and 19).

Three different temperature calibrations were applied to the TEX_{86} data (Appendix C, Equations 14, 15 and 16). Both the Powers et al. (2010) and the Tierney et al. (2010) calibrations are based on lacustrine samples, whereas the Kim et al. (2010) calibration is established from marine samples. All three calibrations are plotted with the TEX_{86} in Figure 13

and show similar temperature trends. However, the Kim et al. (2010) calibration tends to yield warmer temperatures (~2°C warmer) than the two lacustrine calibrations. This is particularly true in "cooler" sections of the core where the Powers et al. (2010) and Tierney et al. (2010) calibrations produce temperatures as low as 12.1 and 14.8°C, respectively, compared to 16.3°C by Kim et al. (2010). A notable exception is at the top of the core (sample 2A-11Y-1 at a depth of 22.65 m). This sample presents an anomalously cold temperature relative to all three calibrations. For this sample, the Tierney et al. (2010) calibration produces a warmer temperature than Kim et al. (2010) (4.6°C from Powers et al. [2010], 6.3°C from Kim et al. [2010] and 9.6°C from Tierney et al. [2010]). TEX_{86}-produced temperatures are not absolute measurements of MAAT, however the relative temperature trends through time are still interesting and useful data for paleoclimate studies. However, at tropical sites like Lake Magadi, the temperature calibration yielding the warmest (or least cool, in this case) temperatures may be the most appropriate to use. As mentioned previously, the Kim et al. (2010) calibration, though based on marine core top samples, may be a good fit for Lake Magadi due to Magadi's saline nature (Cohen et al. 2016).

4.3 PRELIMINARY ASSESSMENT OF MID-PLEISTOCENE PALEOENVIRONMENTAL HISTORY IN THE MAGADI-NATRON BASIN

4.3.1 n-alkane ACL and vegetation regime

The ACL was calculated for n-alkane chain lengths C_{27} to C_{33} (even chain lengths omitted, modified from Eglinton and Hamilton, 1967), and is plotted alongside the other n-alkane indices in Figures 10, 11, and 12. Though Diefendorf et al. (2011) showed that there is significant phylogenetic variability in the leaf wax distributions produced by vascular plants, multiple studies (e.g. Schefuß et al. 2003; Krull et al., 2006) have shown ACL correlates with changes in vegetation regime (i.e. C_4 grass-dominated versus C_3 tree-dominated ecosystem). Carbon isotope analysis of the n-alkanes will provide further insight into the vegetative history at Lake Magadi, though it remains likely that variations in ACL record changing vegetation.

Figure 16 shows ACL plotted versus depth in the core, with its three-point (red) and five-point (magenta) moving average. In modern East Africa, vegetation (woody cover) varies strongly with precipitation (i.e. aridity), resulting in predominantly C_3 (e.g. trees) vegetation in wetter environments, and C_4 (e.g. grasses) vegetation in more arid environments (Sankaran et al., 2005) due to higher water-use efficiency in C_4 plants (Raven et al., 1999). Schefuß et al. (2003) suggest that ACL (as a proxy for vegetation regime) and aridity are also strongly related, though other studies (e.g. Castañeda et al., 2009a) find no correlation between the two. Future analysis of the H isotope composition of the n-alkane samples will help determine whether ACL varies with precipitation at this site.

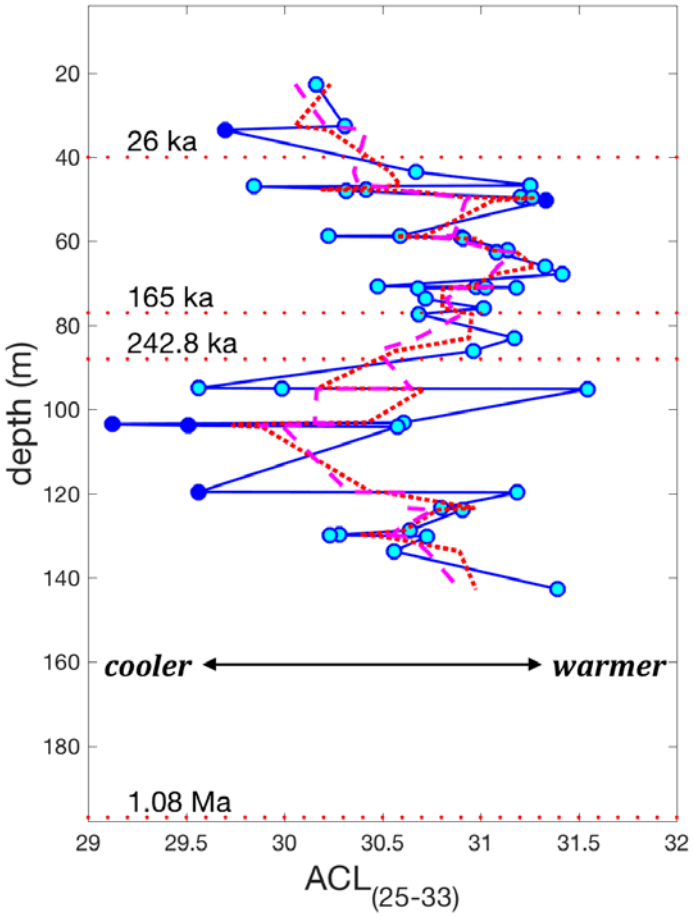

Figure 16 – Average chain length from Lake Magadi pilot samples plotted over depth. Longer chain lengths can either be indicative of a warmer climate (Rommerskirchen et al., 2003), or greater C_3 plant input. However in East Africa, warmer climate is associated with wetter, C_4 plant-dominated environments.

4.3.2 Comparison of n-alkane ACL and TEX_{86}

Castañeda et al. (2009a) suggest that average chain length correlates well with GDGT-constructed temperature in Lake Malawi. Figure 17 (data from the present study) shows n-alkane ACL plotted alongside a TEX^{H}_{86} temperature reconstruction (Kim et al., 2010) where there appear to be two different relationships between ACL and temperature throughout the core.

From the core bottom to ~90 m depth, ACL and temperature are not correlated, but from ~90 m to core top, temperature tracks ACL well (Figure 17). The relationship between vegetation regime and temperature is dependent on precipitation in East Africa as well, where higher temperatures cause greater evaporation (leading to more precipitation), and lower temperatures lead to lower levels of precipitation. A higher ACL value can indicate either a warmer or drier climate (or both; indication of warmth as suggested by Rommerskirchen et al., 2003) and lower ACL values should represent cooler, wetter climates. However, the predominant trend in East Africa is increased aridity in cooler climates (drier and cooler), and wetter periods with increased temperatures (wetter and warmer). Periods where a disagreement between ACL and temperature exists (i.e. 1.08-0.2428 Ma) implies an interesting local climate story, where either precipitation or vegetation (or both) is controlled by some other parameter in addition to temperature.

The transition from no correlation to weak, positive correlation between the ACL and temperature records at ~90 m depth is interesting but doesn't have an immediate climate explanation. The emergence and spread of the C_4-dominated biome had already occurred ~7 Ma (Maslin and Christensen, 2007). The onset of northern hemisphere glaciation (~2.5 Ma) and intensification of Walker Circulation (~1.9 Ma) also happened before the time period represented by sedimentary record at Lake Magadi. However, glacial-interglacial climate may play a role in this transition, as it roughly aligns with glacial termination III (Lisiecki and Raymo, 2005), a rapid deglaciation of the northern hemisphere. Additionally, there could be more local climate parameters affecting the relationship between temperature and vegetation regime, such as changes in local weather patterns (e.g. similar mean annual precipitation, but a more pronounced wet-dry seasonality).

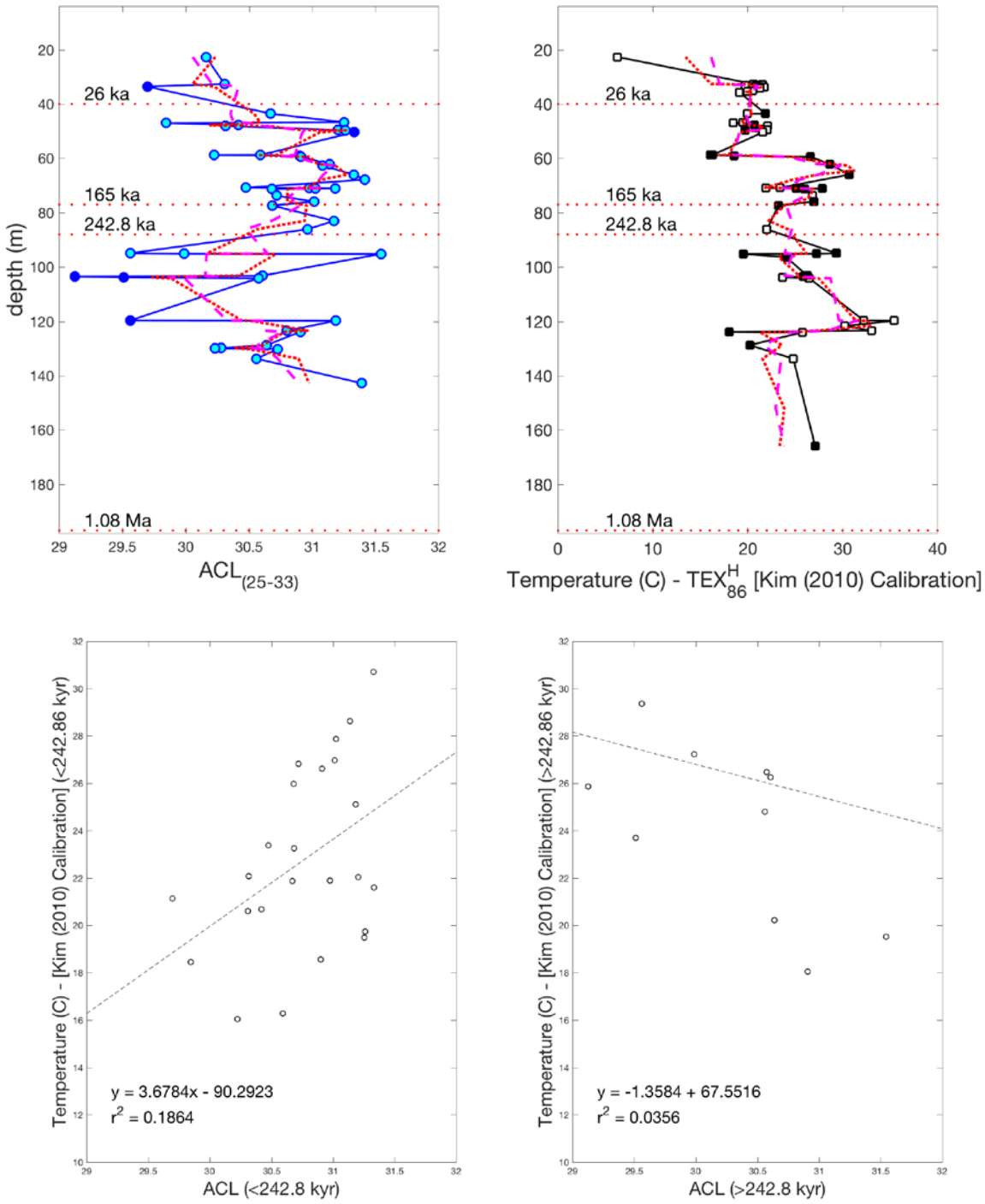

Figure 17 – The upper plots show Magadi core 2A ACL next to the Kim et al. (2010) TEX^{H}_{86} temperature reconstruction. The lower plots show Magadi core 2A ACL plotted against the Kim et al. (2010) TEX^{H}_{86} temperature reconstruction, showing no correlation below 90 m depth, and a (non-significant) weak, positive correlation above 90 m depth.

It is possible that climate dynamics at tropical Lake Magadi could be influenced by northern hemisphere glaciation (and deglaciation). In Figures 18 and 19, n-alkane ACL and temperature from Lake Magadi are plotted next to $\delta^{18}O$ data from the second Greenland Ice Core Project (GRIP-2) to compare trends between climate parameters at Lake Magadi and the Arctic (Figure 18 displays data from 26-242.8 kyr, Figure 19 from 26-165 kyr). Figure 19 suggests that temperature and vegetation at Lake Magadi were potentially affected by global climate (e.g. glacial-interglacial cycles). There is apparent agreement between the $\delta^{18}O$ record and temperature/vegetation at Magadi – as ACL and temperature sharply increase (~70 m depth), GRIP-2 $\delta^{18}O$ increases as well, recording northern hemisphere deglaciation. Due to the lack of age model from Lake Magadi, the connection between northern hemisphere deglaciation and climate at Lake Magadi is not clear. However, these results provide a strong indication that Lake Magadi has the potential to elucidate the relationship between local/regional East African and global climate.

In Figure 16, the ACL oscillates through time, lacking a long-term directionality, showing that this pilot data supports climate-evolution hypotheses centered around an oscillating, variable climate (e.g. the *pulsed climate variability hypothesis*, see section 1.1). However, the temporal resolution of the data is still be too low to provide definite support in favor of oscillating climate. The GDGT-based temperature reconstruction (e.g. Figure 17) appears to have a directionality (again, with low temporal resolution) and suggests a cooling trend and increasing aridity at Lake Magadi over the past ~500 kyr based on the depths of the four age points established for core 2A thus far. This temperature trend, with internal variability amongst the directionality, provides some support for the hypotheses of climate variability underlain by

increasing aridity impacting hominin evolution in East Africa (deMenocal et al., 2004; Maslin and Trauth, 2009; Maslin et al., 2014).

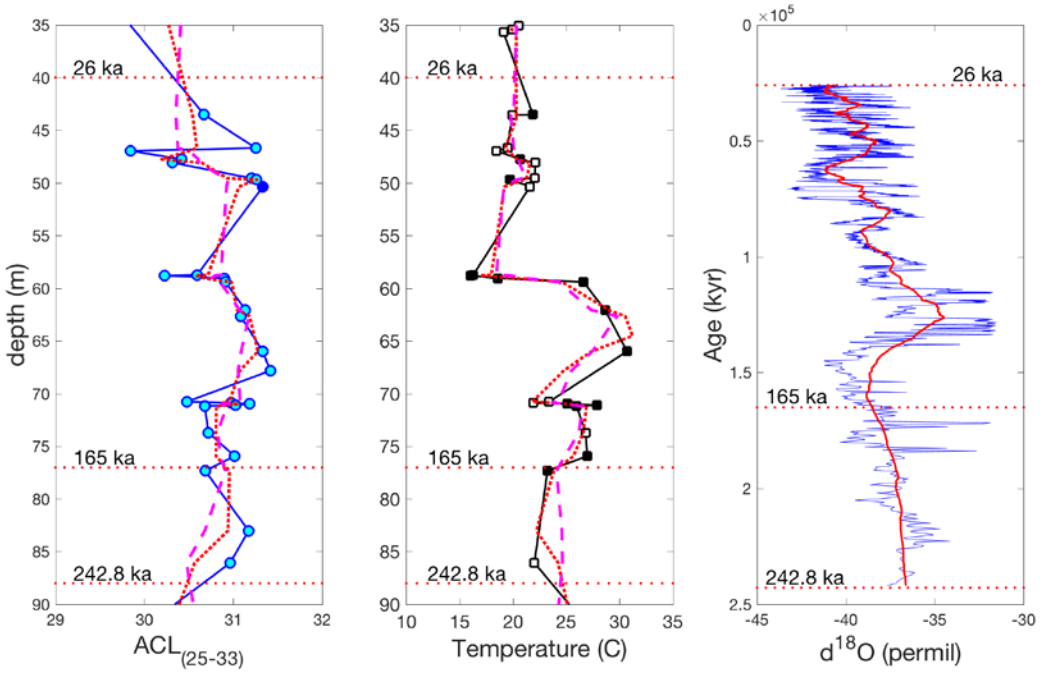

Figure 18 – Magadi core 2A n-alkane ACL and Kim et al. (2010) TEX^{H}_{86} temperature plotted alongside the GRIP-2 ice $\delta^{18}O$ data from 242.8-26 kyr. There are apparent similarities between ACL, the TEX_{86} temperature reconstruction by Kim et al. (2010) and the GRIP-2 ice core isotope data, specifically the positive excursion after 165 kyr showing northern hemisphere deglaciation and simultaneous warming at tropical Lake Magadi.

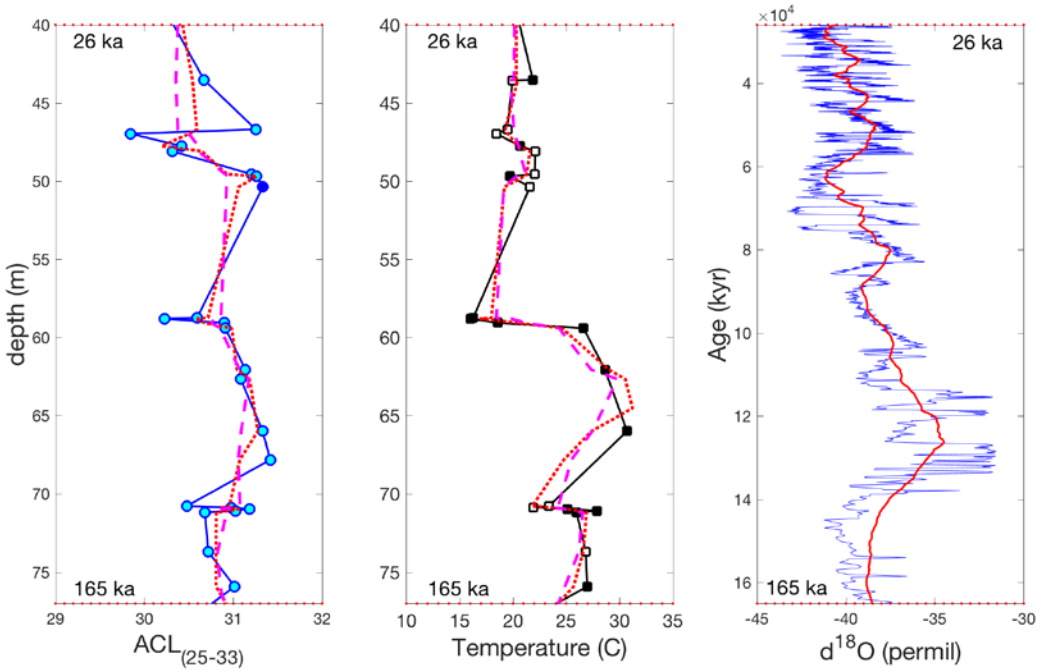

Figure 19 – Magadi core 2A n-alkane ACL and Kim et al. (2010) TEX^{H}_{86} temperature plotted alongside the GRIP-2 ice $\delta^{18}O$ data from 165-26 kyr. Similar to Figure 18, this figure shows an apparent relationship between climate at Magadi and arctic glaciation/deglaciation. A more robust age model for the Magadi cores will better elucidate the nature of this relationship.

4.4 FUTURE DIRECTIONS

4.4.1 n-alkane $\delta^{13}C$ and vegetation shifts

The n-alkane samples are in the process of being analyzed for compound-specific carbon and hydrogen isotope composition in the Werne Organic Geochemistry Lab at the University of Pittsburgh. When complete this data will clarify historical vegetation and precipitation changes at Lake Magadi. Previous studies (Magill et al., 2013b) at nearby Olduvai Gorge (Figure 5) used

sedimentary n-alkane $\delta^{13}C$ to reconstruct vegetation-biome changes by establishing the apparent carbon-isotope fractionation between leaf tissue, soil organic matter (SOM), and leaf lipids. Magill et al. (2013b) found that in modern C_3 and C_4 plant soil systems, there is an apparent carbon-isotope fractionation of 9‰ between SOM and the C_{31} alkane, allowing reconstruction of the carbon isotope composition of SOM from sedimentary n-alkanes (Figure 20). As SOM carbon isotope data has been established as a proxy for woody cover (Cerling et al., 2011), this link between sedimentary n-alkanes and SOM allows for estimation of woody cover from n-alkanes. The relationship between leaf lipids and SOM is based on data from xeric woodlands, scrublands, tropical deciduous forests, and C_4 grasslands, but because Lake Magadi is so geographically close to paleolake Olduvai, local vegetation should be similar, allowing application of the same relationship between sedimentary n-alkanes and SOM.

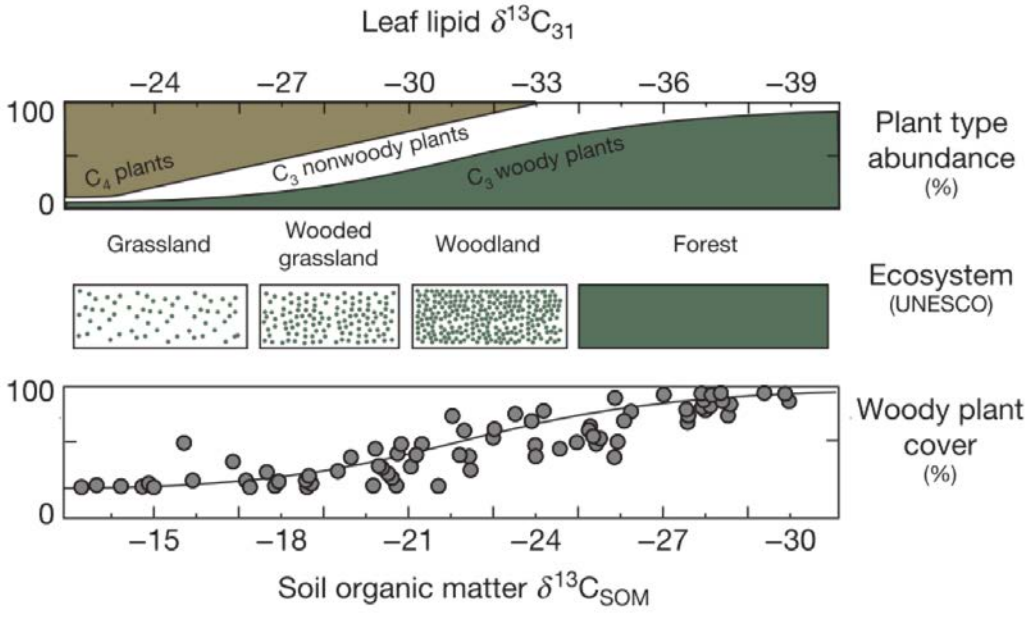

Figure 20 – A figure from Magill et al. (2013b) showing the methodology for reconstruction of vegetation regime from sedimentary leaf wax $\delta^{13}C$ due to its average 9‰ isotopic offset from soil organic matter $\delta^{13}C$ (based on the C_{31} alkane).

4.4.2 n-alkane δD record of past precipitation

As mentioned above, the n-alkane samples from Lake Magadi are being analyzed for their compound-specific hydrogen isotope composition. Upon analysis, there are several methods to calculate precipitation from n-alkane H isotope composition (Magill et al., 2013a; Tierney et al., 2017), that are described below.

Tierney et al. (2017) combined C- and H-isotope analysis on fatty acids (C_{30}) to attempt to quantitatively reconstruct precipitation in the western Sahara through the Holocene. Tierney et al. (2017) use end member values for the C isotope composition of C_3 and C_4 plants (-33.4 and -19.8‰, respectively; Garcin et al., 2014) to estimate the C_3 and C_4 plant isotopic offset between leaf wax (δD_{wax}) and precipitation ($\delta D_{precipitation}$) (average values of -113‰ for $\varepsilon_{C3,}$ -126‰ for ε_{C4}; Sachse et al., 2012). Data from the Online Isotopes in Precipitation Calculator (OIPC) and core top leaf wax-derived $\delta D_{precipitation}$ estimates were used to establish the non-linear (Rayleigh distribution) relationship between $\delta D_{precipitation}$ and precipitation amount. From this relationship, paleo-precipitation amounts were estimated from δD_{wax}, and Bayesian methods used to estimate uncertainties (there was greater uncertainty at higher precipitation amounts, as the δD_{wax}-precipitation regression was logarithmic).

Magill et al. (2013a) used a different approach to estimate the apparent fractionation between leaf waxes (the C_{31} alkane) and modeled precipitation for the site, termed $\varepsilon_{lipid/model}$ (precipitation isotopes modeled from Bowen and Revenaugh, 2003; International Atomic Energy Agency [2006] Isotope Hydrology Information System [www.iaea.org/water]). Estimations of $\varepsilon_{lipid/model}$ were based on common plant functional types (PFTs) for the site, including C_4 graminoids ($\varepsilon_{lipid/model}$ of -146‰), C_3 herbs ($\varepsilon_{lipid/model}$ of -124‰), and C_3 woody plants ($\varepsilon_{lipid/model}$

of -109‰). Relative PFT abundance was determined by the leaf wax C isotope composition (see Figure 20), and the PFT $\varepsilon_{lipid/models}$ were multiplied by the relative PFT abundance to establish an apparent isotope fraction for the landscape, dubbed $\varepsilon_{landscape}$ (Magill et al., 2013a). The $\varepsilon_{landscape}$ is used to infer the H isotope composition of soil water (δD_{soil}), as no significant fractionation results from root uptake and stem-water tends to have similar H isotope composition to soil water (Ehleringer and Dawson, 1992). Magill et al. (2013a) acknowledge that the importance of stem-water versus leaf-water for leaf wax biosynthesis is unknown (McInerney et al., 2011) and leaf-water H isotope composition can be drastically different from that of soil-water (Farquhar et al., 2007). Magill et al. (2013a) then use a modern regional meteoric water line (RMWL) to estimate the range of δD_{soil}, and determine the percentage of variability in δD_{soil} caused by precipitation amount, calculating mean annual precipitation from reconstructed δD_{soil}.

Though both methods yield quantitative estimates of past precipitation, the Magill et al. (2013a) approach may be better suited to Lake Magadi. Due to their proximity (Figure 5), Magadi and Olduvai not only have similar vegetation (PFT), but also experience similar climate patterns (a bimodal wet season caused by the intersection of the Intertropical Convergence Zone [ITCZ] and the Interoceanic Confluence [IOC]). However, regardless of method chosen, both n-alkane C and H isotopes are needed to quantitatively reconstruct past precipitation.

4.4.3 Future core sampling and promising core sections

Aside from evaluating the potential of leaf waxes and GDGTs to reconstruct past environmental conditions at Lake Magadi, the other objective of this thesis is to determine the feasible temporal resolution achievable for future biomarker analyses. Below, Table 4 shows the

core section, depths, and number of potential samples, as well as any notes on the stratigraphy (Initial Core Description Booklet, LacCore, 2014) for samples that could be analyzed for biomarkers in the future. Table 4 is split into four sections, defined by the dates currently established for the core (0-40 m depth representing 26 kyr to present; 40-77 m depth for 26-165 kyr, 77-88 m depth for 165-242.8 kyr, and 88-197 m for 242.8-1080 kyr). These sections are delineated by a bold cell border.

Previously analyzed samples for biomarkers are omitted from Table 4 and core sections that have been used for other analyses (e.g. phytolith analysis) have not been taken into account, so the number of potential samples remains an estimate. However, this estimate can still provide insight into the temporal resolution achievable through some sections of the core.

The data presented in Table 4 is summarized in Table 5 and suggests that there is marked potential for future biomarker work from Lake Magadi drill core 2A. From the first section, representing 26 kyr to present, there are a potential 214 biomarker samples. Including the 12 pilot samples already run in this section, there is a potential for just over century scale resolution (~115 yr per sample). Of the pilot samples analyzed in this section, only a quarter produced usable n-alkane data, but 92% of samples produced robust GDGT data (according to the MI). This would result in a temporal resolution of ~460 yr/sample for leaf wax data, and ~125 yr/sample for GDGT temperature data. Though none of the hominin evolution event goals for the Magadi site, outlined by Campisano et al. (2017), are represented by this section, the potential for a high-resolution East African Holocene record is still exciting.

Core Section	Depth Range (m)	Number of Potential Samples	Depths in Section (cm; each range represents one sample)	Section Notes
2A-4Y-1	9.54-9.86	6	4-8, 8-12, 12-16, 16-20, 20-24, 29-32	trona crystals abundant
2A-6Y-2	13.341-14.841	18	20-24, 25-29, 30-34, 35-39, 50-54, 55-59, 60-64, 65-69, 70-74, 75-79, 90-94, 95-99, 100-104, 105-109, 110-114, 115-119, 120-124, 125-129	black massive trona-rich mud
2A-7Y-1	15.63-16.81	17	12-16, 16-20, 20-24, 30-34, 35-39, 40-44, 45-49, 50-54, 55-59, 60-64, 65-69, 70-74, 90-94, 95-99, 100-104, 105-109, 110-114	black to dark green mud, trona crystals, appears massive
2A-7Y-2	16-81-18.31	22	20-24, 25-29, 30-34, 35-39, 40-44, 45-49, 50-54, 55-59, 60-64, 65-69, 70-74, 75-79, 80-84, 85-89, 90-94, 95-99, 100-104, 105-109, 110-114, 115-119, 120-124, 125-129	black to green trona-bearing mud (less trona than overlying cores)
2A-8Y-1	18.5-19.23	18	0-4, 5-9, 10-14, 15-19, 20-24, 25-29, 30-34, 35-39, 40-44, 45-49, 50-54, 55-59, 60-64, 65-69, 70-74, 75-79, 80-84, 85-89	black clayey silt, no visible trona
2A-10Y-1	21.62-22.145	4	2-6, 7-11, 12-16, 17-21	dark greenish silty clay
2A-13Y-1	24.78-25.83	11	12-16, 17-21, 22-26, 27-31, 32-36, 37-41, 42-46, 47-51, 52-56, 57-61, 62-66	black mud with trona crystals
2A-14Y-1	26.43-27.043	4	42-46, 47-51, 52-56, 57-61	black clayey silt, scattered trona crystals
2A-16Y-1	29.28-30.779	28	5-9, 10-14, 15-19, 20-24, 25-29, 30-34, 35-39, 40-44, 45-49, 50-54, 55-59, 60-64, 65-69, 70-74, 75-79, 80-84, 85-89, 90-94, 95-99, 100-104, 105-109, 110-114, 115-119, 120-124, 125-129, 130-134, 135-139, 140-144	black clay, appears massive
2A-16Y-2	30.779-32.281	29	5-9, 10-14, 15-19, 20-24, 25-29, 30-34, 35-39, 40-44, 45-49, 50-54, 55-59, 60-64, 65-69, 70-74, 75-79, 80-84, 85-89, 90-94, 95-99, 100-104, 105-109, 110-114, 115-119, 120-124, 125-129, 130-134, 135-139, 140-144, 145-149	black silty clay, no trona, appears homogenous

Core Section	Depth Range (m)	Number of Potential Samples	Depths in Section (cm; each range represents one sample)	Section Notes
2A-17Y-1	32.35-32.696	7	2-6, 7-11, 12-16, 17-21, 29-33, 34-38, 39-43	black silty clay, homogenous
2A-17Y-2	32.696-33.856	21	3-7, 12-16, 17-21, 22-26, 27-31, 36-40, 41-45, 46-50, 52-56, 61-65, 66-70, 71-75, 76-80, 88-92, 93-97, 98-102, 109-113, 114-118, 119-123, 124-128, 129-133	black silty clay, no trona
2A-18Y-1	33.92-34.303	4	1-5, 16-20, 26-30, 31-35	black silty clay
2A-18Y-2	34.303-35.806	25	5-9, 10-14, 15-19, 20-24, 25-29, 30-34, 35-39, 40-44, 45-49, 50-54, 55-59, 60-64, 65-69, 70-74, 80-84, 85-89, 90-94, 95-99, 100-104, 105-109, 115-119, 120-124, 125-129, 130-134, 140-144	black clayey silt, massive, weak bedding towards bottom
2A-22Y-1	43.06-43.623	1	40-44	black laminated silty clay-clay silt
2A-23Y-1	46.11-47.432	12	40-44, 45-49, 50-54, 60-64, 65-69, 70-74, 75-79, 90-94, 95-99, 100-104, 115-119, 120-124	black clay, weak lamination; brown clayey silt after 0.85 m
2A-23Y-2	47.432-48.932	23	0-4, 5-9, 10-14, 15-19, 20-24, 25-29, 35-39, 40-44, 45-49, 50-54, 55-59, 60-63, 66-69, 70-74, 75-79, 80-84, 85-89, 105-109, 115-119, 120-124, 125-129, 130-134, 140-144	moderately well laminated dark greyish brown silt
2A-24Y-1	49.16-50.297	4	27-31, 32-36, 41-44, 45-49	dark grey laminated silty clay
2A-28Y-1	58.3-59.439	11	52-56, 60-64, 66-69, 70-74, 79-83, 84-88, 92-96, 97-100, 101-104, 105-108, 112-114.5	black clay, some fine lamination
2A-29Y-1	61.35-62.728	7	65-69, 70-74, 94-98, 105-109, 110-114, 115-119, 120-124	green and black clay
2A-30Y-1	64.4-65.435	5	40-44, 45-49, 50-54, 55-58*, 70-73	green clay, massive (*avoid underlying disturbed mud)
2A-30Y-2	65.435-66.146	3	34-38, 48-51, 61-64	black laminated clay, light and dark colored bands down core

Core Section	Depth Range (m)	Number of Potential Samples	Depths in Section (cm; each range represents one sample)	Section Notes
2A-32Y-1	70.5-71.373	7	25-29, 30-34, 38-42, 50-54, 61-65, 71-74, 81-85	green and black laminated clay
2A-33Y-1	72.93-74.44	21	40-44, 45-49, 50-54, 55-59, 60-64, 65-69, 70-74, 80-84, 85-89, 90-94, 95-99, 100-104, 105-109, 110-114, 115-119, 120-124, 125-129, 130-134, 135-139, 140-144, 145-149	massive green clay, pyrite more abundant towards bottom
2A-33Y-2	74.44-75.97	28	5-9, 10-14, 15-19, 20-24, 25-29, 30-34, 35-39, 40-44, 45-49, 50-54, 55-59, 60-64, 65-69, 70-74, 75-79, 80-84, 85-89, 90-94, 95-99, 100-104, 105-109, 110-114, 115-119, 120-124, 125-129, 130-134, 135-139, 140-144	green clay, scattered patches of pyrite
2A-35Y-1	76.59-77.282	3	30-34, 34-38, 38-42	green clay, massive
2A-39Y-1	82.79-84.246	8	10-14, 15-19, 25-29, 30-34, 35-39, 40-44, 45-50, 100-104	greenish grey clayey silt
2A-40Y-1	85.74-86.984	11	30-34, 35-39, 40-44, 50-54, 55-59, 60-64, 65-69, 70-74, 75-79, 80-84, 85-89	horizontally laminated clay, greenish clay from 50-90cm
2A-45Y-1	94.5-95.989	5	47-51, 57-61, 67-71, 72-76, 83-87	laminated green and black clays, with chert bands
2A-45Y-2	95.989-97.477	9	5-9, 10-14, 15-19, 20-24, 25-29, 30-34, 35-39, 40-44, 45-49	dark grey silt/siltstone, avoid heavily lithified sections
2A-46Y-1*	97.56-99.026	27	6-10, 11-15, 16-20, 21-25, 31-35, 36-40, 41-45, 46-50, 51-55, 56-60, 61-65, 66-70, 71-75, 76-80, 81-85, 86-90, 91-95, 101-105, 106-110, 111-115, 116-120, 121-125, 126-130, 131-135, 136-140, 141-145, 146-150	dark grey silt/siltstone, avoid heavily lithified sections
2A-46Y-2*	99.026-100.515	11	15-19, 30-34, 35-39, 40-44, 45-49, 50-54, 90-94, 95-99, 100-104, 105-109, 110-114	dark grey silt/siltstone, avoid heavily lithified sections

Core Section	Depth Range (m)	Number of Potential Samples	Depths in Section (cm; each range represents one sample)	Section Notes
2A-48Y-2	102.887-104.02	22	1-4, 5-9, 10-14, 15-19, 20-24, 30-34, 35-39, 45-49, 51-55, 65-69, 70-74, 75-79, 81-85, 94-98, 100-104, 105-109, 110-114, 115-118, 125-129, 130-134, 135-139, 140-144	black clay with pyrite bands
2A-49Y-1	104.02-104.574	4	1-5, 6-10, 11-15, 16-19	black clayey silt with scattered pyrite; avoid underlying drilling breccia
2A-55Y-1	116.22-117.728	7	41-45, 46-50, 51-55, 56-60, 61-65, 66-70, 71-75	medium green silty clay with chert fragments
2A-56Y-1	118.35-119.845	1	132-136	black and green silty clay
2A-57Y-2	120.872-122.219	3	56-60, 60-64, 71-75	black and green silty clay with pyrite
2A-58Y-2	122.821-124.221	4	56-50, 61-65, 124-128, 129-133	banded silty clay with pyrite
2A-59Y-3	126.874-128.311	1	48-52	massive greenish black clayey silt
2A-60Y-1	128.41-129.5	7	40-44, 47-50, 65-69, 70-74, 88-92, 99-103, 104-108	clayey silt bands, lamina of varying color
2A-60Y-2	129.5-130.316	5	10-14, 15-19, 20-24, 36-40, 48-52	dark grey-green clayey silt bands
2A-61Y-1	131.46-132.601	7	80-84, 85-89, 90-94, 95-99, 100-104, 105-109, 110-113	dark grey/black laminated clayey silt
2A-61Y-2**	132.601-134.054	17	16-20, 21-25, 31-35, 36-40, 41-45, 46-50, 51-55, 56-60, 61-65, 66-70, 71-75, 76-80, 81-85, 86-90, 91-95, 101-105, 117-120	black clay, abundant pyrite
2A-61Y-3**	134.054-134.5	5	7-10, 13-15, 16-20, 29-33, 39-42	black clay, abundant pyrite
2A-62Y-2	135.053-136.276	1	116-120	black clay with mm scale pyrite
2A-63Y-2	138.412-139.955	13	86-90, 91-95, 96-100, 101-105, 106-110, 111-115, 116-120, 121-125, 126-130, 131-135, 136-140, 141-145, 146-150	black clay, weak lamination
2A-63Y-3	139.955-140.057	1	3-7	laminated green/brown clay

Core Section	Depth Range (m)	Number of Potential Samples	Depths in Section (cm; each range represents one sample)	Section Notes
2A-64Y-1	140.057-141.416	13	10-14, 15-19, 20-24, 25-29, 30-34, 35-39, 40-44, 45-49, 50-54, 55-59, 60-64, 65-69, 70-74	black clay, weak lamination
2A-64Y-2	141.416-142.876	12	65-69. 70-74, 75-79, 80-84, 86-90, 91-95, 96-100, 101-105, 106-110, 111-115, 116-120, 121-125	black clay, massive
2A-65Y-1	143.65-144.286	2	49-53, 67-71	black clay, weak lamination
2A-65Y-2**	144.286-145.15	9	5-9, 10-14, 15-19, 20-24, 25-29, 30-34, 35-39, 40-44, 45-49	black clay, pyrite laminae
2A-66Y-1	145.15-146.208	11	41-45, 46-50, 51-55, 56-60, 61-65, 66-70, 71-75, 76-80, 81-85, 86-90, 91-95	black clay, crystal (unidentified mineral) veins
***test sample from core to be run soon to determine leaf wax & GDGT potential**				
****abundant pyrite present, sample with caution**				

Table 4 – A table containing the sample depths of every potential sample for biomarker analysis, based on the results of this pilot study. Samples are included if they have the potential to provide robust data for n-alkanes or GDGTs, though not all samples listed here have a high probability of providing both. Core sections are split into four sections, delineated by the initial four dates associated with core 2A (transition between sections marked by a bolded cell border).

The second section, representing 26-165 kyr, there are 125 future samples that look promising for biomarker analysis. Combined with 26 samples that have already been analyzed in this study, there is potential for sub-millennial scale temporal resolution (~920 yr/sample). Through this section, 24 of 25 (96%) of the pilot samples analyzed for n-alkanes produced robust data, and 7 of 26 GDGT samples (26.9%, according to the MI) yielded temperature data. The future temporal resolution of climate data in this section would still be sub-millennial (~965 yr/sample) for n-alkanes, and over millennial (~3,375 yr/sample) for GDGTs. This section (26-165 kyr) is particularly exciting, as two of the four hominin evolution events encompassed by the

Magadi 2A core fall within this time period – the *Homo sapiens* dispersal out of Africa (80-50 kyr) and the first appearance of Late Stone Age technology (61.7-52.1 kyr) (Capisano et al., 2017). Moreover, these events both fall within the span of 30 kyr (80-50 kyr). Better temporal resolution than estimated above may be possible, depending on which core sections represent this 30 kyr interval, but this will only be determinable after an age model is refined for the core. A linear age interpolation between a depth of 40 m (26 kyr) and 77 m (165 kyr) places the 50-80 kyr period between the approximate depths of 46-55 m, represented by core sections 2A-23Y-1, 2A-23Y-2, and 2A-24Y-1, which contain a combined 39 future samples (46 total samples, including the 8 samples already taken from these three sections). Of the pilot samples from these sections, all 7 analyzed produced usable n-alkane but none have produced usable GDGT data. However, if these sections indeed represent the 50-80 kyr period, then the achievable temporal resolution for leaf wax climate data through this interval may be as good as ~650 yr/sample.

The third section (165-242.8 kyr) is the narrowest section of the core, spanning from 77-88 m depth, comprised principally of core sections 2A-39Y-1 and 2A-40Y-1. From this section, there are 19 potential samples for biomarker analysis, plus 2 pilot samples analyzed in this study, for a total of 21 samples. Both pilot samples yielded robust n-alkane data, though only one of the samples produced usable GDGT data. The potential temporal resolution for n-alkane climate data through this section is projected to be ~3,700 yr/sample, while the resolution for temperature data may be only ~7,400 yr/sample. The first appearance of *Homo sapiens* (198-194 kyr) is the only hominin evolution event during this period (Capisano et al., 2017, and references therein). Linear age interpolation over this core section estimates that the interval of interest (194-198 kyr) should fall between 81.1-81.67 m depth, a range that is not represented by any

potential future samples. When an age model is established for the core, the potential for this section may improve, but as of now, it is not recommended as a target of future study.

The final section of the core spans from 88-197 m depth, representing the time interval of 242.8 kyr to 1.08 Ma. A potential 197 future samples have been identified through this section, totaling 226 total samples (including 29 pilot samples, 25 of which were analyzed in this study), resulting in an initial estimated temporal resolution of ~3,700 yr/sample. It should be noted that the future samples are skewed towards the younger sections from this interval – there are no future samples selected from deeper than 146 m depth, due to lack of material to sample as well as pilot samples from below that depth proving unusable for both leaf waxes and GDGTs. For n-alkanes, 17 of the 25 (68%) pilot samples produced robust data, while 6 of the GDGT samples (based on the MI) produced good climate data. In this section, the first appearance of Middle Stone Age technology is estimated to have occurred between 272-280 kyr (Capisano et al., 2017). Linear age interpolation places the interval of 272-280 kyr to fall within 91.8-92.8 m depth. Just as with section three, there are no future samples that fall within this meter of core. As mentioned above, prospects for this section may improve when an age model is produced for the core, however no further analysis in this section with the goal of describing climate during the 272-280 kyr interval is recommended.

The HSPDP's four paleoanthropological goals for Lake Magadi include events such as the transitions between Acheulean and Middle Stone Age technology, the transition between Middle Stone Age and Late Stone Age technology, the appearance of *Homo sapiens*, and the dispersal of *Homo sapiens* out of Africa (Table 6). The potential to establish a high-resolution

SECTION	AGE RANGE (KYR)	# OF POTENTIAL SAMPLES	TOTAL # OF SAMPLES	ALKANE %	ALKANE RESOLUTION (YR/SAMPLE)	GDGT % (V/MI/RI)	GDGT RESOLUTION (YR/SAMPLE)
1	0 – 26	214	226	25	460	92/92/33	125 – 350
2	26 – 165	125	153	96	946	89/27/12	1,027 – 7,875
3	165 – 242.8	19	21	100	3,700	50	7,400
4	242.8 - 1080	197	226	68	--	84/25/8	--

Table 5 - A summary of the data presented in Table 4, describing the potential of organic biomarkers through the four sections of Magadi core 2A.

climate record from organic proxies at Lake Magadi is summarized in Tables 5 and 6. Leaf wax n-alkanes have good potential for sections 1 and 2, poor potential for section 3 and fair potential for section 4. GDGTs have fair potential for section 1 and poor potential for all other sections. Section 2 is the most promising for future study as two of the highlighted paleoanthropological events are in the section.

Paleoanthropological Event	Core Section	Leaf Wax Potential	GDGT Potential
Late Stone Age technology FAD	2	GOOD	POOR
Homo sapiens dispersal out of Africa	2	GOOD	POOR
Homo sapiens FAD	3	POOR*	POOR*
Middle Stone Age technology FAD	4	FAIR*	POOR*
*prospects could improve with better age model			

Table 6 – Summary of paleoanthropological events covered by the Magadi core, and proxy evaluation for each of these events.

5.0 CONCLUSIONS

The objective of this thesis was to evaluate the potential to produce a climate record from the biomarker proxies, leaf waxes and GDGTs, from a lake core recovered from Lake Magadi, Kenya. This site was one of five selected by the Hominin Sites and Paleolakes Drilling Project, with the goal of establishing high resolution, multi-proxy climate reconstructions adjacent to established hominin sites. To that end, 68 pilot samples were selected and analyzed for n-alkanes, fatty acids, and GDGTs. Approximately 70% of samples analyzed for n-alkanes recorded a robust terrestrial signal, and the TEX_{86} was established for nearly 90% of samples analyzed for GDGTs, however the Methane Index and Ring Index suggest that the TEX_{86} is not applicable to temperature reconstruction for large sections of Magadi core 2A. The n-alkanes were determined to have a better potential to yield compound specific carbon and hydrogen isotope data than fatty acids. Additionally, no samples contained the suite of brGDGTs necessary to construct the MBT/CBT temperature proxy.

Initial construction of Lake Magadi paleoclimate using n-alkane average chain length, and the Kim et al. (2010) TEX^{H}_{86} temperature calibration show an oscillating vegetation regime, but a more directional temperature trend towards a cooler and drier climate. There is a transition at ~90 m core depth – older ACL and temperature data are not correlated ($r^2 = 0.0356$), but in younger samples the ACL and temperature data show a non-significant, weak positive correlation ($r^2 = 0.1864$) with one another. Plotted alongside $\delta^{18}O$ data from the GRIP-2 ice

core, our climate data demonstrate a potentially interesting correlation between climate at Lake Magadi and ice volume in the Arctic.

The overall goal of the HSPDP is to provide an environmental and climate context for many of the milestones in hominin adaptation and evolution, spatially adjacent to where hominins lived, and temporally resolved to evolutionary (orbital to sub-millennial) timescales. The core recovered from Lake Magadi is estimated to represent the time interval from 1.08 Ma to present, during which four predominant hominin adaptation and evolutionary events happened. Based on initial chronology efforts by HSPDP collaborators, Magadi core 2A can be separated into four sections: 0-26 kyr, 26-165 kyr, 165-242.8 kyr, and 242.8 kyr to 1.08 Ma. We estimate the future biomarker potential for the four sections and determine Lake Magadi to have particularly exciting promise for the 0-26 kyr and 26-165 kyr sections.

APPENDIX A

LEAF WAX INDICES

$$CPI = \frac{1}{2}\left(\frac{(C_{23} + C_{25} + C_{27} + C_{29} + C_{31}) + (C_{25} + C_{27} + C_{29} + C_{31} + C_{33})}{(C_{24} + C_{26} + C_{28} + C_{30} + C_{32})}\right)$$

Equation 1 – Carbon Preference Index (Marzi et al., 1993).

$$P_{aq} = \frac{C_{23} + C_{25}}{C_{23} + C_{25} + C_{29} + C_{31}}$$

Equation 2 – Fraction Aquatic (Ficken et al., 2000).

$$TAR_{HC} = \frac{(C_{29} + C_{31} + C_{33})}{(C_{15} + C_{17} + C_{19} + C_{29} + C_{31} + C_{33})}$$

Equation 3 – Terrestrial Aquatic Ratio for Hydrocarbons (Meyers et al., 1997).

$$ACL_{(25-33)} = \frac{(25[C_{25}] + 27[C_{27}] + 29[C_{29}] + 31[C_{31}] + 33[C_{33}])}{(C_{25} + C_{27} + C_{29} + C_{31} + C_{33})}$$

Equation 4 – Average Chain Length modified from Freeman and Pancost (2014).

APPENDIX B

PLANT METABOLISM AND LEAF WAX BIOSYNTHESIS

Plant metabolism and leaf wax biosynthesis both impart large isotopic fractionations and are a significant portion of the ε between water and leaf wax δD, as well as carbon dioxide and leaf wax $\delta^{13}C$. Below are figures detailing the C_3 and C_4 photosynthetic pathways (Tipple and Pagani, 2007), as well as the acetyl CoA pathway for leaf wax biosynthesis (Jetter and Kunst, 2008).

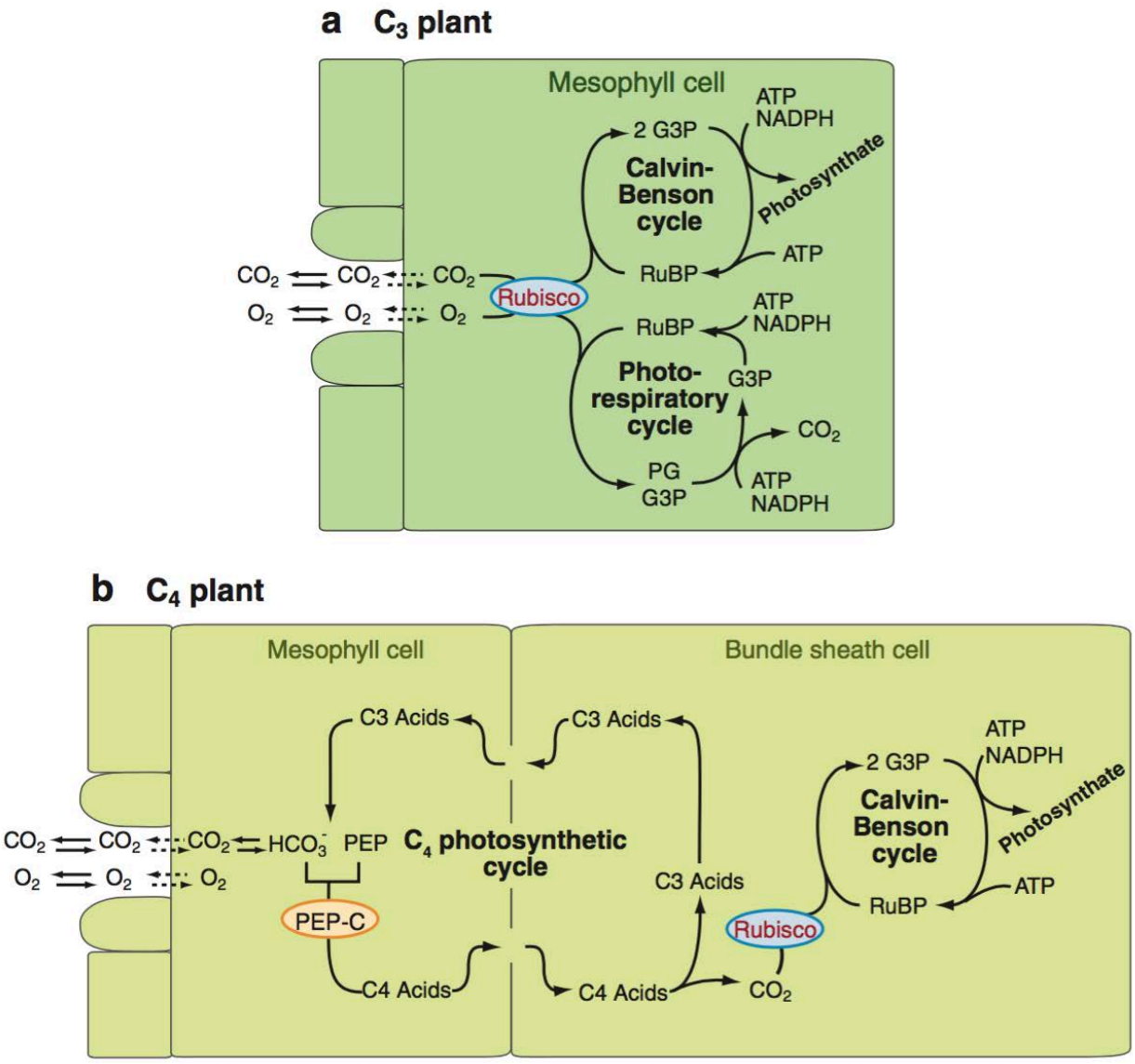

Figure 21 – A comparison between the two major metabolic pathways in higher plants, C_3 and C_4 (Tipple and Pagani, 2007).

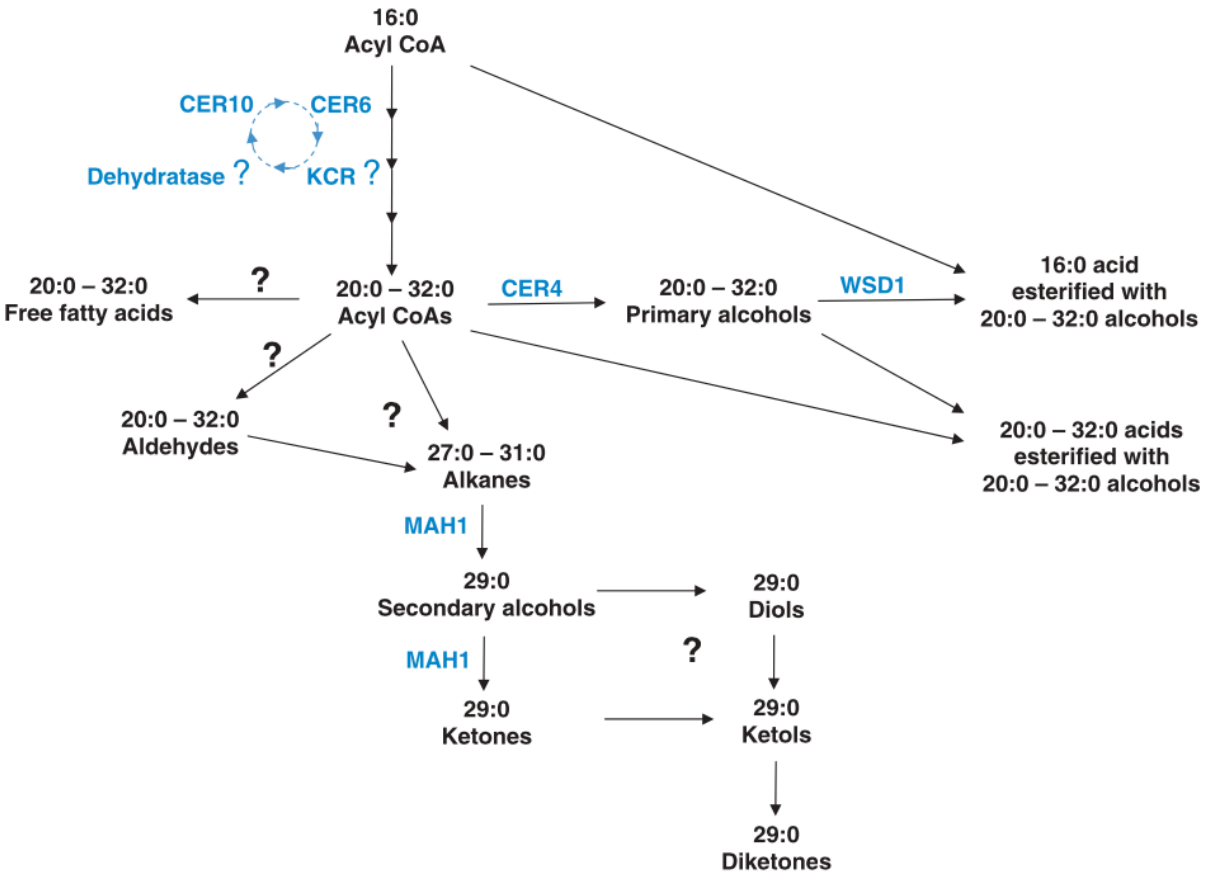

Figure 22 – The proposed biosynthesis of leaf waxes (Jetter and Kunst, 2008).

APPENDIX C

GDGT INDICES

The equations for the various GDGT indices mentioned in section 1.5.2 are listed below here. This includes the BIT, MBT, CBT, MI and RI proxies, as well as TEX_{86}, and the various temperature calibrations used for TEX_{86} (Tierney et al., 2010; Powers et al., 2010; Kim et al., 2010). All references to GDGTs in the MBT and CBT equations are to brGDGTs, and references to GDGTs in MI, RI and TEX_{86} are to isoGDGTs.

$$BIT = \frac{(GDGTI + GDGTII + GDGTIII)}{(crenarchaeol + GDGTI + GDGTII + GDGTIII)}$$

Equation 5 – The Branched to Isoprenoid Tetraethers index.

$$MBT = \frac{(GDGTI + GDGTIb + GDGTIc)}{(\sum all\ branched\ GDGTs)}$$

Equation 6 – The Methylation of Branched Tetraethers index.

$$CBT = \frac{(GDGTIb + GDGTIIb)}{(GDGTI + GDGTII)}$$

Equation 7 – The Cyclisation of Branched Tetraethers index.

$$TEX_{86} = \frac{(GDGT2 + GDGT3 + GDGT4')}{(GDGT1 + GDGT2 + GDGT3 + GDGT4')}$$

Equation 8 – The TetraEther indeX with 86 carbon atoms.

$$MI = \frac{GDGT1 + GDGT2 + GDGT3}{GDGT1 + GDGT2 + GDGT3 + GDGT4 + GDGT4'}$$

Equation 9 – The Methane Index (Zhang et al., 2011).

$$RI = 0\times[GDGT0] + 1\times[GDGT1] + 2\times[GDGT2] + 3\times[GDGT3]$$
$$+4\times[GDGT4] + 4\times[GDGT4']$$

Equation 10 – The Ring Index (Zhang et al., 2016).

$$RI_{TEX} = -0.77\times TEX_{86} + 3.32\times(TEX_{86})^2 + 1.59$$

Equation 11 – The relationship between global core top RI values and TEX_{86}.

$$\Delta RI = RI_{TEX} - RI_{sample}$$

Equation 12 – ΔRI, established from RI (Equation 10) and RI_{TEX} (Equation 11).

The TEX_{86} calibration shown above is used in both the Powers et al. (2010) and Tierney et al. (2010) temperature calibrations from lake surface sediments. The Kim et al. (2010) calibration from marine sediments uses a log equation for TEX_{86} called TEX^{H}_{86} (shown below). There is also TEX^{L}_{86}, but as it is calibrated for polar waters, it is not applied to tropical Lake Magadi.

$$TEX_{86}^{H} = \log\frac{(GDGT2 + GDGT3 + GDGT4')}{(GDGT1 + GDGT2 + GDGT3 + GDGT4')}$$

Equation 13 – The log TEX_{86} function used for the Kim et al. (2010) temperature calibration.

The MBT/CBT temperature calibrations are omitted here, as none of the samples contained all the brGDGTs needed for the proxies. Below are the equations for the temperature calibrations applied to TEX_{86} in Lake Magadi:

$$T = 55.231 \times TEX_{86} - 13.955$$

Equation 14 – The Powers et al. (2010) temperature calibration equation.

$$T = TEX_{86} \times 38.874\text{-}3.4992$$

Equation 15 – The Tierney et al. (2010) temperature calibration equation.

$$T = 68.4 \times TEX_{86}^{H} + 38.6$$

Equation 16 – The Kim et al. (2010) temperature calibration equation.

APPENDIX D

CORE DATA AND STRATIGRAPHY

The core stratigraphy and description was performed by Emma McNulty and Tim Lowenstein at the SUNY – Binghamton. Below is a table showing the Lake Magadi drill core recovery, as well as the color-coded stratigraphy of cores 1A and 2A (the core used in this thesis) Cohen et al. (2016).

DRILL SITE 1A, 1B, AND 1C ON MAGADI CAUSEWAY			
CORE SECTION	**Drill Date**	**Drilled Length (m)**	**Recovery (m, %)**
1A	June 15-21	124	74.5 (59%)
1B	June 24	6.1	2.9 (47%)
1C	June 26-27	26.5	17.0 (64%)
DRILL SITE 2A, NORTH OF MAGADI CAUSEWAY			
2A	June 30-July 4	194.4	109.1 (56%)

Table 7 – Drill core recovery data from the 2014 HSPDP Magadi drilling excursion.

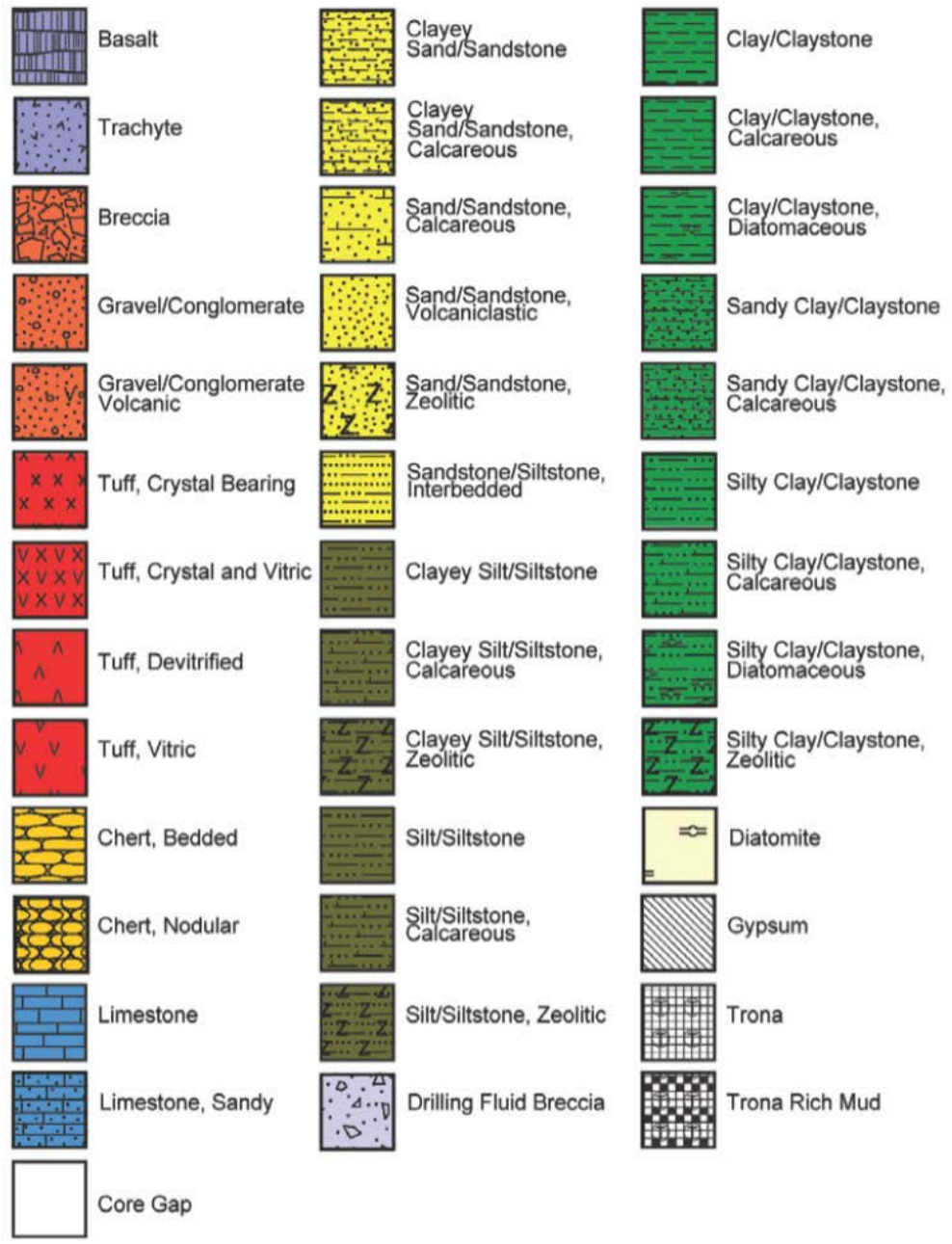

Figure 23 – The lithologic key for the stratigraphy columns presented in Figure 24.

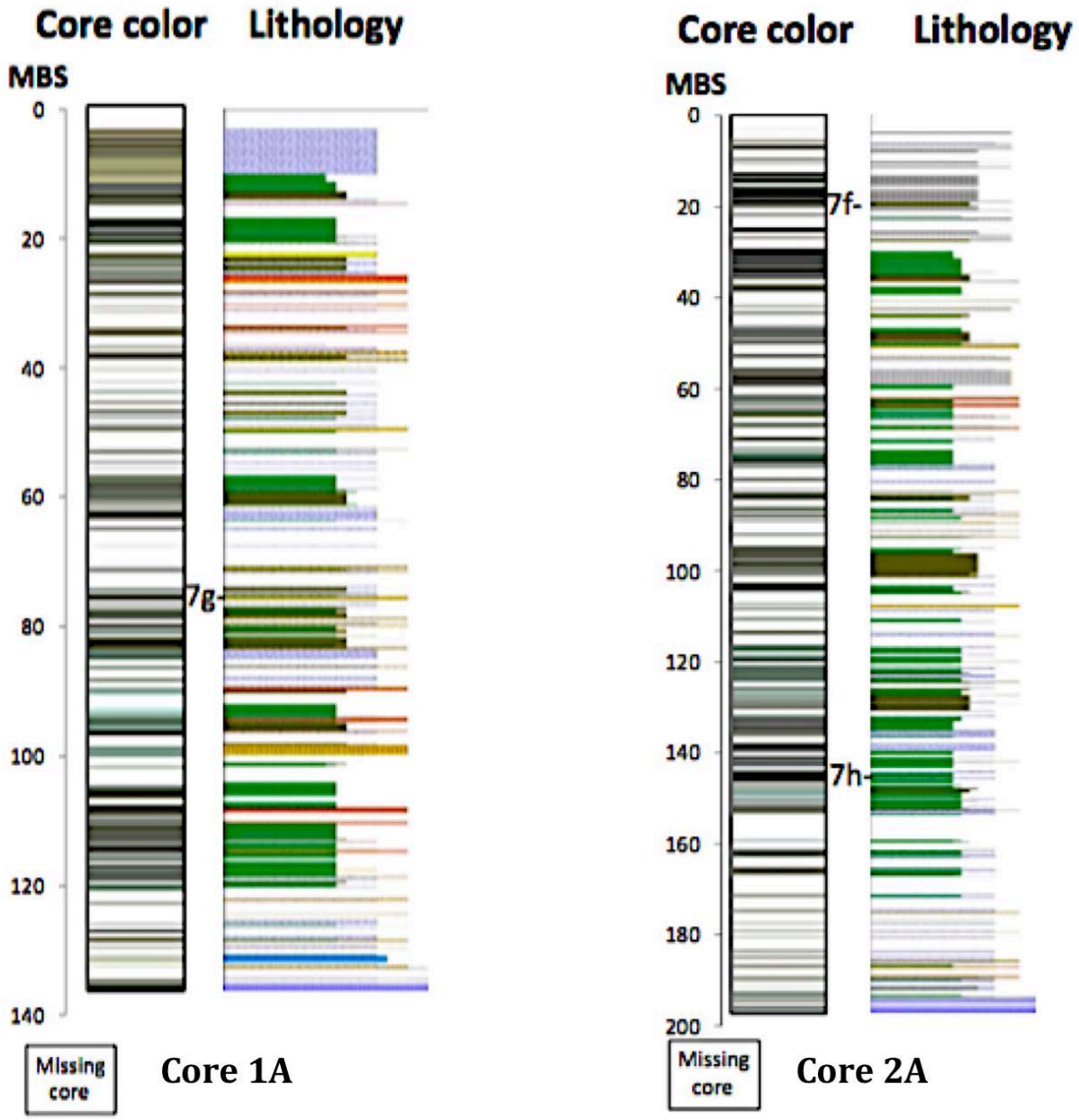

Figure 24 – The stratigraphy column for Lake Magadi cores 1A and 2A. Lithologic key shown in Figure 23. Core 2A was used for all sampling and analyses in this thesis.

APPENDIX E

LEAF WAX CHROMATOGRAMS

Below are sample GC-FID chromatograms of n-alkanes and FAMEs from Lake Magadi. The n-alkane chromatograms generally had fewer extraneous peaks than the FAMEs chromatograms. The chromatograms show intensity on the y-axis, and retention time on the x-axis. The terrestrial leaf wax compounds generally found on the right of the chromatogram.

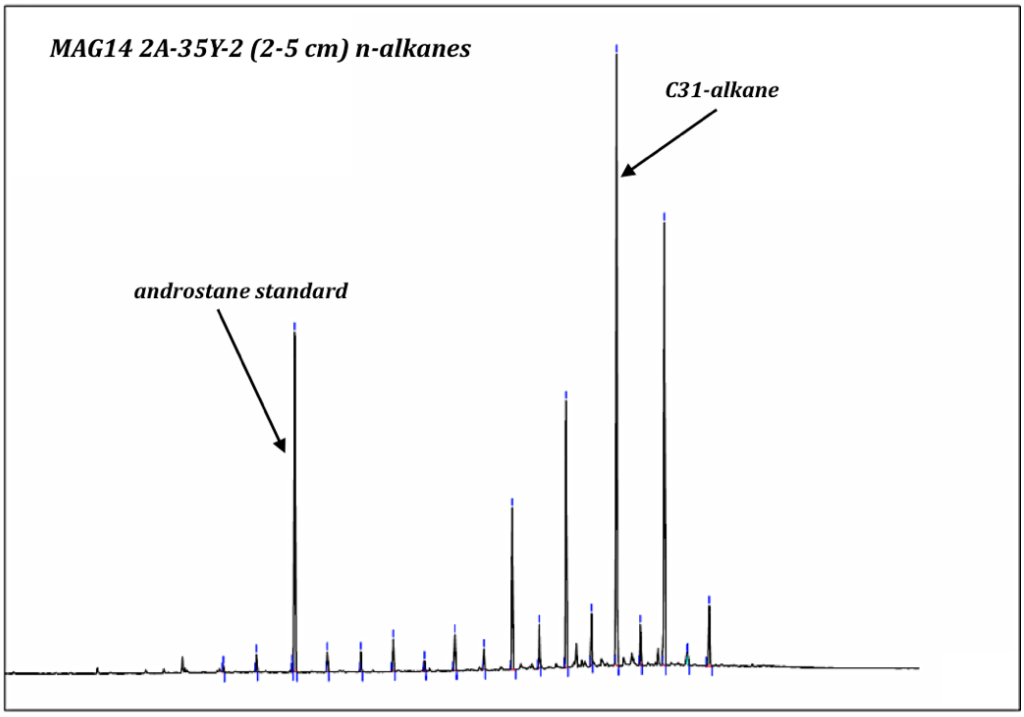

Figure 25 – Sample n-alkane chromatogram.

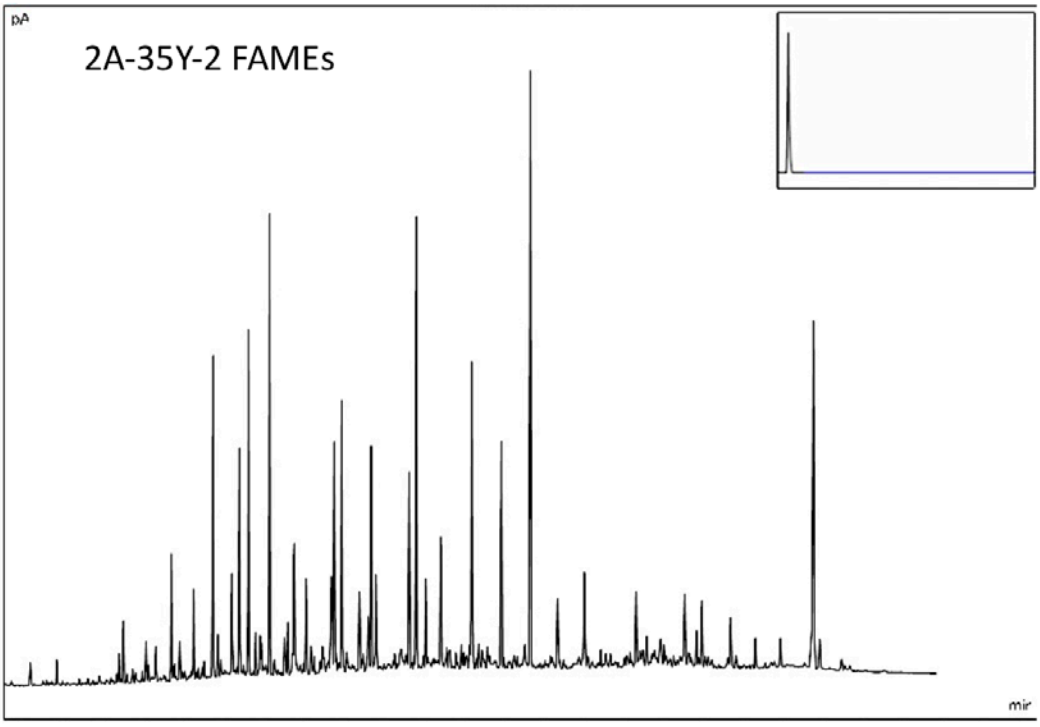

Figure 26 – Sample FAMEs chromatogram.

APPENDIX F

RAW LEAF WAX ABUNDANCE DATA

Below is the raw leaf wax abundance data (Table 8), showing masses of the individual n-alkane compounds used to calculate the n-alkane indices presented in Appendix A (Equations 1 through 4). Also included is a table with the values calculated from the raw data for each index (Table 9).

Sample ID	Depth (m)	n-alkane abundances by chain length (ng/g sediment extracted)													
		C15	C17	C19	C23	C24	C25	C26	C27	C28	C29	C30	C31	C32	C33
2A-6Y-1	--	--	1.35	1.69	3.83	4.66	6.23	3.90	5.78	2.83	7.05	2.88	12.05	1.16	8.11
2A-11Y-1	22.65	0.17	--	1.60	1.93	2.16	3.30	1.63	5.61	1.49	9.32	2.00	16.75	1.62	11.10
2A-17Y-1	32.61	3.81	3.09	4.07	4.90	3.64	7.87	--	16.55	4.69	31.78	13.91	59.05	4.19	36.08
2A-17Y-2	33.281	--	--	--	617.16	614.72	546.78	512.60	379.16	309.60	474.77	367.77	563.05	479.65	497.55
2A-17Y-2	33.551	--	--	--	55.40	37.52	51.26	37.98	80.57	23.86	83.10	16.19	137.58	11.43	101.97
2A-18Y-1	34.15	--	--	--	222.62	258.05	274.65	250.83	299.33	163.46	255.30	125.80	248.42	55.29	147.64
2A-18Y-2	35.068	--	--	--	175.23	125.89	153.24	99.49	156.70	80.78	177.30	53.88	283.00	28.79	231.28
2A-18Y-2	35.418	--	--	--	125.77	246.09	261.21	202.56	303.40	172.26	293.13	122.78	330.06	40.50	248.58
2A-22Y-1	43.51	0.28	0.75	0.51	2.49	2.23	11.70	6.77	55.63	15.39	98.80	22.76	251.99	15.23	151.50
2A-23Y-1	46.68	0.19	1.40	0.79	1.05	0.96	6.05	2.18	17.12	6.03	47.22	14.54	186.89	14.18	151.25
2A-23Y-1	46.96	--	--	--	131.73	64.01	191.52	103.85	627.16	144.20	729.83	141.43	1051.32	74.66	670.09
2A-23Y-2	47.747	--	--	--	144.12	186.47	836.88	415.28	3175.60	944.97	5145.19	1566.31	10583.66	801.49	6397.35
2A-23Y-2	48.077	--	--	--	356.90	393.70	1070.08	541.03	3392.27	771.10	3856.73	1096.51	8398.11	735.29	6066.04
2A-24Y-1	49.545	0.27	1.17	1.06	1.74	1.73	5.15	2.44	15.34	5.73	41.68	11.93	159.27	11.73	123.10
2A-24Y-1	49.675	--	--	--	--	--	187.88	113.13	459.11	157.49	978.41	365.78	4114.45	335.35	3696.24
2A-24Y-2	50.355	10.50	2.86	1.26	7.84	0.93	1.52	7.29	2.56	1.45	5.71	3.74	22.45	2.71	24.89
2A-28Y-1	58.735	0.87	24.97	6.57	14.40	7.08	25.65	14.49	104.60	30.28	191.45	31.91	379.86	28.29	277.86
2A-28Y-1	58.795	--	--	--	1000.59	507.82	1781.11	1000.01	7406.12	1751.90	10449.54	1875.97	17004.29	1238.88	11811.04
2A-28Y-1	59.055	--	--	--	591.45	656.08	982.10	580.49	2819.94	785.34	4650.27	1457.00	13824.45	1009.80	11550.96
2A-28Y-1	59.395	--	--	--	956.81	396.06	1917.54	1125.42	7176.05	2113.60	12407.12	2921.40	34527.41	2427.31	28712.06
2A-29Y-1	62.055	--	--	--	150.33	116.69	420.84	236.60	1180.56	484.11	2492.40	855.02	9138.83	741.38	7532.77
2A-29Y-1	62.645	--	--	--	95.01	60.66	196.96	108.53	520.43	215.45	1242.35	395.97	4553.56	333.19	3278.98
2A-30Y-2	65.98	0.30	0.19	0.42	1.97	1.17	4.45	3.01	30.09	10.85	81.99	22.71	325.05	21.98	273.56
2A-31Y-1	67.815	--	--	--	56.29	34.90	74.13	39.82	145.94	69.50	292.06	122.12	1574.32	132.49	1565.73
2A-32Y-1	70.775	--	--	--	346.91	148.95	431.25	189.65	1083.33	255.81	1390.58	287.68	3017.92	215.97	2612.64
2A-32Y-1	70.86	6.13	5.51	7.82	33.51	11.01	46.28	20.51	169.38	43.71	329.63	57.77	840.17	58.22	780.93
2A-32Y-1	70.965	--	--	--	1286.26	661.29	2493.97	1142.68	8278.34	2196.69	14012.03	3240.56	45087.47	3343.60	48845.74
2A-32Y-1	71.075	--	--	--	592.16	440.69	1302.53	665.52	4157.23	1095.65	6459.88	1412.83	18776.40	1380.11	19312.61
2A-32Y-1	71.185	--	--	--	1617.81	900.33	1779.82	1110.94	4073.45	1175.75	5971.31	1425.71	14520.93	1212.78	13171.60
2A-33Y-1	73.695	--	--	--	67.77	30.67	76.88	33.31	121.99	37.64	167.74	47.11	463.29	41.68	461.07
2A-33Y-2	75.925	--	--	--	92.41	44.67	126.77	59.97	261.79	76.40	439.99	109.06	1362.19	109.80	1368.99
2A-35Y-2	77.317	1.07	18.29	10.57	20.02	6.62	23.10	12.79	106.36	27.24	177.60	33.86	424.55	27.82	297.03
2A-39Y-1	83.005	--	--	--	144.27	43.90	81.62	42.66	170.42	86.10	313.77	106.54	981.34	99.83	1129.39
2A-40Y-1	86.065	--	--	--	91.27	19.75	30.47	25.84	67.74	24.22	143.11	37.96	596.20	39.73	349.17
2A-45Y-1	94.84	0.34	--	0.67	1.85	2.61	3.04	1.99	3.76	16.81	5.58	1.65	11.96	0.93	7.13
2A-45Y-1	94.915	--	--	--	273.34	1005.27	3821.82	1869.12	14436.53	3453.60	18090.28	2670.62	19995.54	1158.88	10421.79
2A-45Y-1	95.045	--	--	--	205.06	223.88	771.20	354.64	2312.62	674.12	3281.94	711.27	4873.38	306.60	3002.09
2A-45Y-1	95.145	--	--	--	499.69	406.18	963.35	365.01	1911.25	574.75	3919.43	979.22	16890.71	1291.47	23458.27
2A-45Y-1	95.295	--	--	--	387.29	319.27	360.71	207.13	382.47	166.28	414.96	153.28	941.46	80.53	895.58
2A-48Y-2	103.157	--	--	--	1567.97	1581.52	3073.10	1440.65	7870.76	2512.88	11557.18	2610.40	26718.96	2147.16	22445.23
2A-48Y-2	103.487	--	--	--	256.31	196.18	419.10	171.21	773.36	201.09	680.49	207.65	915.80	62.06	448.60
2A-48Y-2	103.787	--	--	--	1091.05	702.00	1121.01	474.07	1736.77	736.00	2827.41	539.65	3776.77	245.33	1504.80
2A-48Y-2	104.095	0.20	3.27	9.10	30.47	12.23	32.40	12.06	70.13	15.90	114.81	20.72	273.19	17.96	204.61

Sample ID	Depth (m)	n-alkane abundances by chain length (ng/g sediment extracted)												
		C15	C17	C19	C23	C24	C25	C26	C27	C28	C29	C30	C31	C32	C33
2A-56Y-1	119.64	--	--	--	69.09	44.23	82.36	49.10	124.30	41.05	88.11	54.23	287.70	13.27	95.99
2A-56Y-1	119.75	0.89	--	--	6.55	1.33	3.08	2.73	9.04	4.63	15.66	7.76	64.30	6.33	56.83
2A-57Y-2	121.662	--	--	--	804.30	835.73	1181.26	684.01	1078.01	463.36	798.76	283.73	1582.29	159.50	1431.32
2A-58Y-2	123.431	--	--	--	207.81	105.86	247.23	113.68	428.26	140.84	562.14	168.53	1573.84	143.78	1707.45
2A-58Y-2	123.82	2.52	3.83	8.69	60.90	36.27	129.63	43.11	176.69	50.85	247.17	80.74	952.44	82.94	879.75
2A-60Y-2	128.74	2.49	214.62	16.43	25.77	12.22	46.74	21.76	179.50	52.65	282.07	49.01	640.54	45.72	486.73
2A-60Y-2	129.77	--	--	--	2125.32	1080.71	3746.38	1579.13	11510.37	2754.32	12842.68	3000.08	24823.34	1811.09	20628.44
2A-60Y-2	129.835	--	--	--	1874.69	923.49	2511.90	1089.72	7230.95	18285.17	8930.18	1699.23	14572.72	1034.31	8948.65
2A-60Y-2	129.955	--	--	--	651.85	309.05	885.50	348.50	1916.53	437.93	1873.13	636.07	4118.44	330.97	3606.87
2A-60Y-2	130.21	--	--	--	229.81	144.64	258.20	125.35	661.58	219.10	761.21	477.83	2989.14	168.21	1948.84
2A-61Y-2	133.72	0.23	1.48	4.71	17.22	8.17	18.49	6.94	33.97	7.50	59.24	11.26	132.69	8.63	105.52
2A-64Y-2	142.77	0.70	0.32	--	1.44	0.98	2.16	1.13	5.83	2.17	9.57	3.90	40.45	5.07	48.68
2A-69Y-1	151.905	15.14	12.57	15.75	53.37	42.92	50.84	37.89	33.85	22.19	72.32	93.72	250.28	23.42	292.47
2A-81Q-2	165.935	5.48	52.21	46.98	206.58	91.29	119.34	45.26	149.01	198.92	212.28	328.66	456.74	43.31	364.46

Table 8 – Raw leaf wax abundance data.

Sample ID	Depth (m)	Total Abundance (ug/g)	$ACL_{(27-35)}$	P_{aq}	$TAR_{(HC)\ (29-33)}$	$CPI_{(25-33)}$
2A-6Y-1	--	0.01	29.512	0.345	0.899	3.093
2A-11Y-1	22.65	0.01	30.161	0.167	0.954	6.004
2A-17Y-1	32.61	0.04	30.307	0.123	0.920	5.528
2A-17Y-2	33.281	5.36	29.069	0.529	--	1.104
2A-17Y-2	33.551	0.68	29.697	0.326	--	3.395
2A-18Y-1	34.15	2.30	28.502	0.497	--	1.480
2A-18Y-2	35.068	1.67	29.564	0.416	--	2.504
2A-18Y-2	35.418	2.35	29.002	0.383	--	1.753
2A-22Y-1	43.51	0.15	30.671	0.039	0.997	9.061
2A-23Y-1	46.68	0.15	31.253	0.029	0.994	10.167
2A-23Y-1	46.96	4.08	29.845	0.154	--	5.682
2A-23Y-2	47.747	33.67	30.418	0.059	--	5.879
2A-23Y-2	48.077	28.09	30.317	0.104	--	5.633
2A-24Y-1	49.545	0.12	31.205	0.033	0.992	9.904
2A-24Y-1	49.675	11.25	31.262	0.036	--	7.809
2A-24Y-2	50.355	0.02	31.333	0.250	0.784	3.463
2A-28Y-1	58.735	0.28	30.592	0.066	0.963	8.605
2A-28Y-1	58.795	58.39	30.224	0.092	--	6.753
2A-28Y-1	59.055	41.48	30.900	0.078	--	6.315
2A-28Y-1	59.395	100.32	30.910	0.058	--	7.888
2A-29Y-1	62.055	24.97	31.136	0.047	--	7.015
2A-29Y-1	62.645	11.61	31.083	0.048	--	7.362
2A-30Y-2	65.98	0.27	31.330	0.016	0.999	11.911
2A-31Y-1	67.815	4.46	31.416	0.065	--	7.265
2A-32Y-1	70.775	10.68	30.476	0.150	--	6.742
2A-32Y-1	70.86	0.78	30.976	0.064	0.990	9.575
2A-32Y-1	70.965	143.46	31.182	0.060	--	8.969
2A-32Y-1	71.075	60.40	31.025	0.070	--	8.138
2A-32Y-1	71.185	50.53	30.682	0.142	--	5.792
2A-33Y-1	73.695	1.68	30.719	0.186	--	5.748
2A-33Y-2	75.925	4.42	31.014	0.108	--	7.305
2A-35Y-2	77.317	0.30	30.684	0.067	0.968	9.425
2A-39Y-1	83.005	3.47	31.172	0.149	--	5.762
2A-40Y-1	86.065	1.50	30.965	0.141	--	7.171
2A-45Y-1	94.84	0.01	30.042	0.218	0.961	1.392
2A-45Y-1	94.915	78.86	29.562	0.097	--	6.074
2A-45Y-1	95.045	17.35	29.986	0.107	--	5.656
2A-45Y-1	95.145	59.19	31.544	0.066	--	9.861
2A-45Y-1	95.295	4.56	30.088	0.355	--	2.959
2A-48Y-2	103.157	87.94	30.607	0.108	--	5.949
2A-48Y-2	103.487	4.43	29.124	0.297	--	3.748
2A-48Y-2	103.787	15.08	29.512	0.251	--	3.989
2A-48Y-2	104.095	0.20	30.575	0.139	0.979	8.348
2A-56Y-1	119.64	0.98	29.562	0.287	--	3.294
2A-56Y-1	119.75	0.06	31.186	0.108	0.994	6.290
2A-57Y-2	121.662	9.84	29.331	0.455	--	2.373
2A-58Y-2	123.431	5.93	30.800	0.176	--	5.603

Sample ID	Depth (m)	Total Abundance (ug/g)	$ACL_{(27-35)}$	P_{aq}	$TAR_{(HC)\ (29-33)}$	$CPI_{(25-33)}$
2A-58Y-2	123.82	0.88	30.908	0.137	0.993	7.712
2A-60Y-2	128.74	0.49	30.640	0.073	0.858	8.969
2A-60Y-2	129.77	91.11	30.280	0.135	--	6.288
2A-60Y-2	129.835	69.48	29.958	0.157	--	1.678
2A-60Y-2	129.955	16.21	30.233	0.204	--	5.296
2A-60Y-2	130.21	8.50	30.725	0.115	--	5.074
2A-61Y-2	133.72	0.11	30.559	0.157	0.979	7.551
2A-64Y-2	142.77	0.05	31.393	0.067	0.990	8.195
2A-69Y-1	151.905	0.29	31.000	0.244	0.934	2.845
2A-81Q-2	165.935	0.36	30.226	0.328	0.908	1.717

Table 9 – Calculated leaf wax indices (Equations 1-4 found in Appendix A).

APPENDIX G

GDGT SAMPLE CHROMATOGRAMS

Below are three chromatograms of isoGDGT samples – one with a isoGDGT distribution like a "normal" marine sample, and shows high promise for temperature reconstructions in Lake Magadi, and two others, from the "questionable" and "discard" categories (see Results).

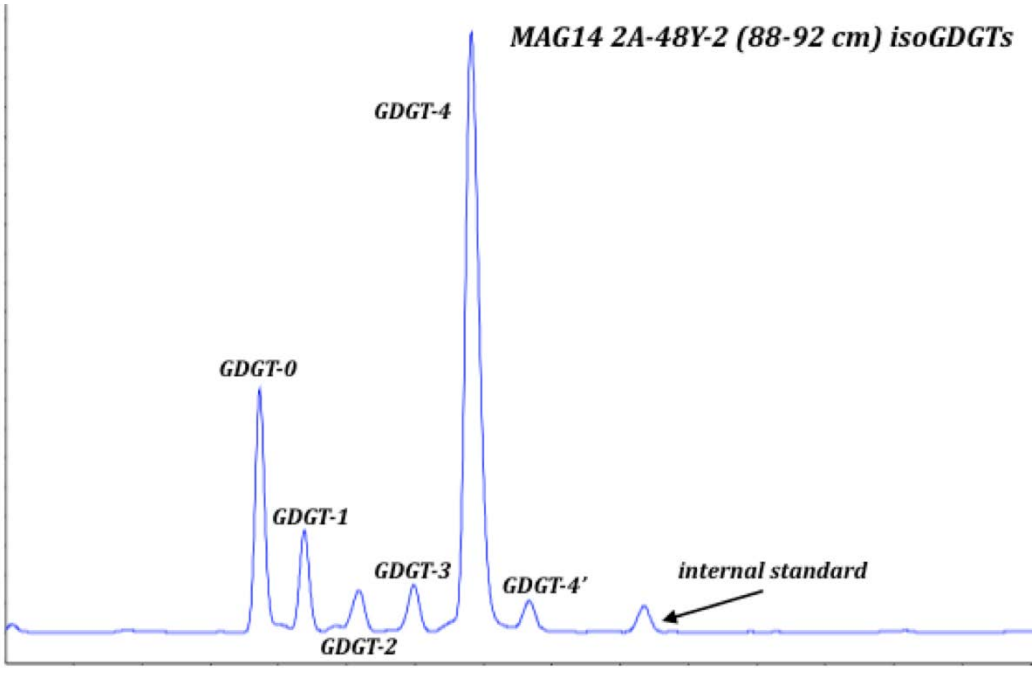

Figure 27 – Sample GDGT chromatogram with the isoGDGTs used in indices (Appendix C) labeled.

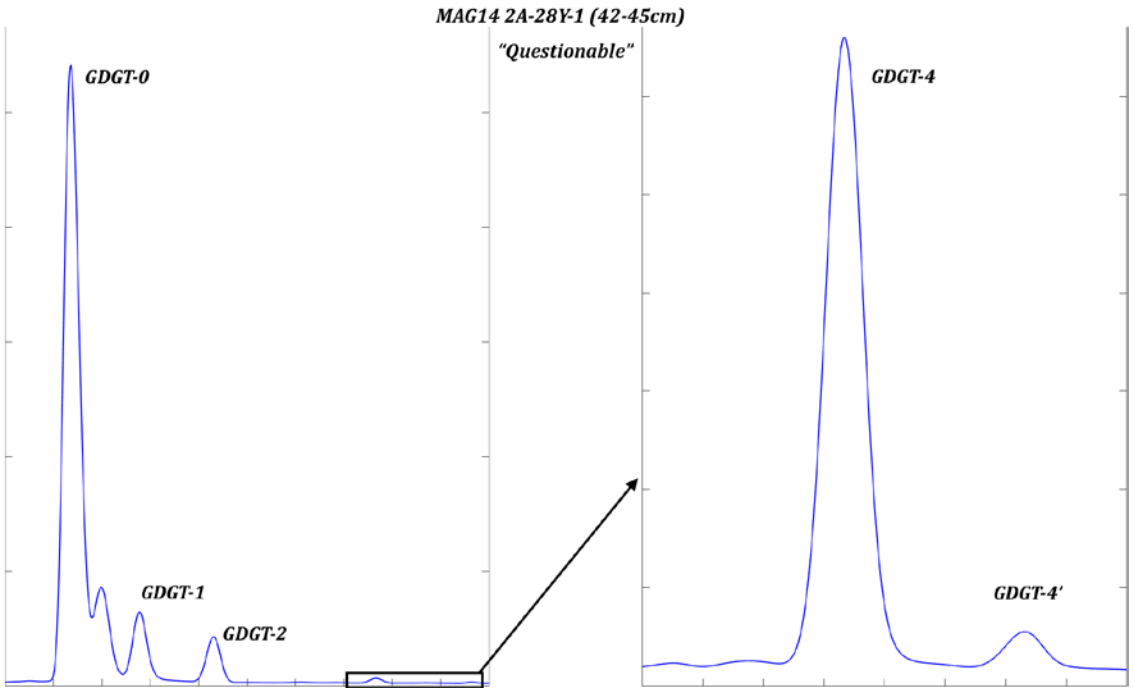

Figure 28 – A visually "questionable" isoGDGT sample characterized by extraneous peaks and small crenarchaeol peaks.

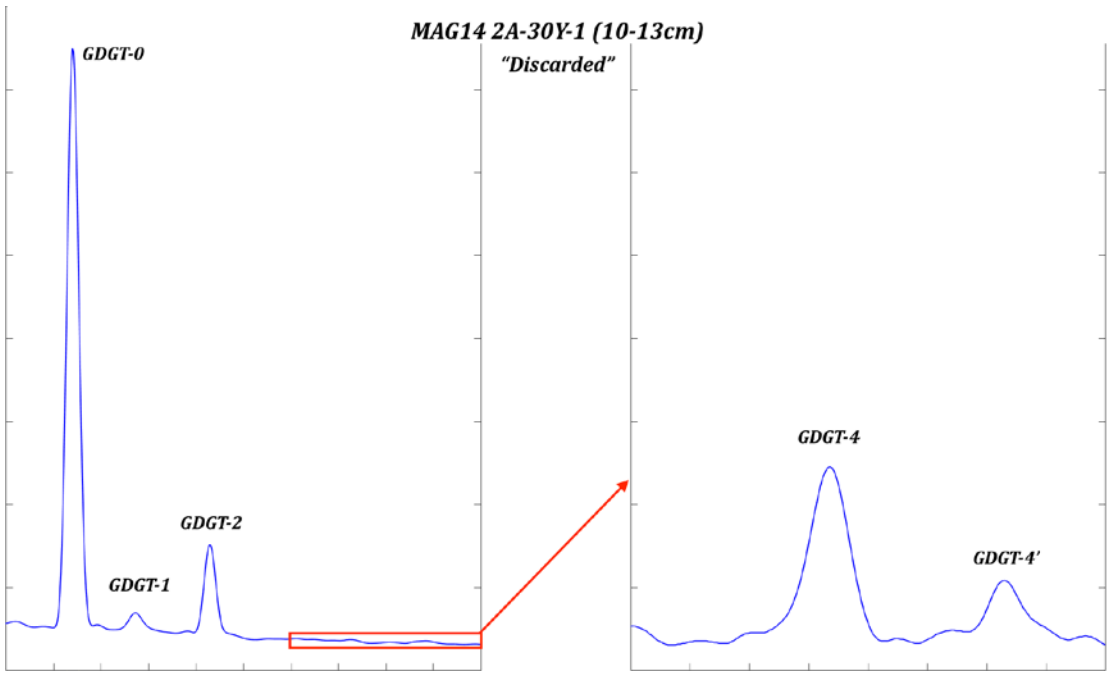

Figure 29 – A visually "discarded" sample characterized by small peaks, and almost undetectable crenarchaeol regioisomer.

APPENDIX H

RAW GDGT ABUNDANCE DATA

Sample ID	Depth (m)	isoGDGT peak areas (pA)						TEX_{86}	GDGT Index1 (TEX_{86}-L)	GDGT Index2 (TEX_{86}-H)
		GDGT-0	GDGT-1	GDGT-2	GDGT-3	GDGT-4	GDGT-4'			
2A-6Y-1	–	4.18E+06	1.37E+06	6.98E+05	1.04E+04	1.02E+04	1885.353	0.341	-0.474	-0.467
2A-11Y-1	22.65	4.52E+05	1.05E+05	5.33E+04	--	2792.249	--	0.337	-0.473	-0.473
2A-17Y-1	32.61	3.82E+06	7.32E+05	3.81E+05	2.94E+05	5.75E+06	2.04E+05	0.546	-0.567	-0.263
2A-17Y-2	32.791	3.45E+05	1.03E+05	7.04E+04	4.23E+04	7.34E+05	2.00E+04	0.563	-0.486	-0.081
2A-17Y-2	33.031	7.45E+05	2.22E+05	1.91E+05	4.12E+04	6.26E+05	1.78E+04	0.530	-0.376	-0.276
2A-17Y-2	33.281	2.49E+05	6.96E+04	6.24E+04	1.67E+04	2.43E+05	6010.718	0.550	-0.377	-0.260
2A-17Y-2	33.551	2.85E+05	7.18E+04	4.90E+04	2.86E+04	4.63E+05	1.22E+04	0.556	-0.484	-0.255
2A-17Y-2	33.761	2.89E+05	8.01E+04	5.38E+04	3.42E+04	5.97E+05	1.69E+04	0.567	-0.495	-0.247
2A-17Y-2	34.061	2.88E+05	8.79E+04	6.00E+04	3.60E+04	6.14E+05	1.52E+04	0.558	-0.487	-0.253
2A-18Y-1	34.15	1.83E+04	5403.745	3556.406	1950.883	3.19E+04	920.8510	0.543	-0.487	-0.265
2A-18Y-2	35.068	1.67E+05	5.77E+04	3.60E+04	2.21E+04	4.48E+05	1.08E+04	0.544	-0.508	-0.264
2A-18Y-2	35.418	3.34E+05	1.14E+05	6.72E+04	4.01E+04	8.77E+05	2.28E+04	0.534	-0.517	-0.273
2A-18Y-2	35.668	6.87E+05	2.27E+05	1.18E+05	8.22E+04	1.71E+06	4.51E+04	0.519	-0.560	-0.285
2A-22Y-1	43.51	2.74E+06	3.10E+05	3.81E+05	2.70E+04	3.35E+04	2426.831	0.569	-0.275	-0.245
2A-22Y-1	43.545	2.05E+06	2.11E+05	2.25E+05	1.45E+04	2.63E+04	2053.796	0.534	-0.301	-0.249
2A-23Y-1	46.68	5.60E+06	4.38E+05	4.49E+05	3.17E+04	5.07E+04	4947.309	0.525	-0.311	-0.280
2A-23Y-1	46.96	3.30E+06	3.58E+05	3.45E+05	2.03E+04	4.56E+04	3209.341	0.507	-0.321	-0.295
2A-23Y-2	47.747	4.16E+06	4.22E+05	4.76E+05	2.91E+04	4.72E+04	4065.708	0.547	-0.289	-0.273
2A-23Y-2	48.077	1.51E+06	1.41E+05	1.76E+05	1.28E+04	1.40E+04	1342.264	0.573	-0.273	-0.262
2A-24Y-1	49.545	2.76E+06	2.23E+05	2.78E+05	1.76E+04	1.37E+04	3165.840	0.573	-0.271	-0.242
2A-24Y-1	49.675	2.01E+06	1.88E+05	2.00E+05	9146.896	1.58E+04	2670.149	0.530	-0.298	-0.242
2A-24Y-2	50.355	6.43E+05	7.33E+04	8.83E+04	5901.126	2159.734	680.6398	0.564	-0.278	-0.249
2A-28Y-1	58.735	2.53E+07	2.22E+06	1.89E+06	6.50E+04	3.00E+05	2.56E+04	0.472	-0.344	-0.326
2A-28Y-1	58.795	1.39E+07	9.42E+05	8.03E+05	2.12E+04	6.67E+04	4728.887	0.468	-0.342	-0.276
2A-28Y-1	59.055	1.28E+07	6.35E+05	6.44E+05	1.26E+04	2.60E+04	3491.753	0.510	-0.302	-0.330
2A-28Y-1	59.395	4.45E+06	1.12E+05	2.16E+05	7155.434	1.63E+04	3069.500	0.668	-0.191	-0.175
2A-29Y-1	62.055	1.34E+06	5.51E+04	1.33E+05	2926.482	8297.982	1946.479	0.715	-0.157	-0.146
2A-29Y-1	62.645	2.60E+06	1.16E+05	4.27E+05	1.60E+04	8058.071	4291.804	0.793	-0.117	-0.101
2A-30Y-1	64.515	1.44E+06	9.26E+04	3.19E+05	6912.608	5264.823	1563.478	0.780	-0.118	-0.293
2A-30Y-2	65.98	3.36E+06	1.45E+05	4.48E+05	2.84E+04	1.17E+04	1519.601	0.767	-0.143	-0.115
2A-31Y-1	67.815	9.17E+05	4.46E+04	4.76E+04	4364.120	–	–	0.538	-0.307	-0.269
2A-32Y-1	70.775	9.33E+05	1.81E+05	1.25E+05	9.94E+04	1.63E+06	4.63E+04	0.599	-0.511	-0.223
2A-32Y-1	70.86	1.23E+07	4.83E+06	2.63E+06	2.42E+06	2.86E+07	1.35E+06	0.570	-0.575	-0.244
2A-32Y-1	70.965	9.98E+05	2.66E+04	3.28E+04	9430.587	1.12E+05	4061.459	0.635	-0.322	-0.197
2A-32Y-1	71.075	7.15E+05	2.62E+04	2.81E+04	2.81E+04	1.47E+05	3943.063	0.697	-0.467	-0.157
2A-32Y-1	71.185	7.93E+05	1.13E+05	9.94E+04	8.86E+04	9.56E+05	2.51E+04	0.654	-0.481	-0.185

Sample ID	Depth (m)	isoGDGT peak areas (pA)						TEX_{86}	GDGT Index1 (TEX_{86}-L)	GDGT Index2 (TEX_{86}-H)
		GDGT-0	GDGT-1	GDGT-2	GDGT-3	GDGT-4	GDGT-4'			
2A-33Y-1	73.695	5.15E+05	1.25E+05	1.17E+05	1.10E+05	1.23E+06	2.95E+04	0.673	-0.478	-0.172
2A-33Y-2	75.925	4.44E+05	8.08E+04	7.43E+04	7.39E+04	8.24E+05	2.03E+04	0.676	-0.489	-0.170
2A-35Y-2	77.317	1.30E+07	5.58E+05	7.95E+05	2.21E+04	5.22E+04	7010.667	0.596	-0.238	-0.224
2A-39Y-1	83.005	5.78E+05	4.67E+04	5.54E+04	3944.872	9248.753	--	0.559	-0.282	-0.252
2A-40Y-1	86.065	1.15E+05	2.32E+04	1.73E+04	9106.664	1.76E+05	4554.245	0.572	-0.457	-0.242
2A-45Y-1	94.84	--	--	--	--	--	--	--	--	--
2A-45Y-1	94.915	4.43E+06	5.55E+04	1.40E+05	1.13E+04	9.48E+03	8.42E+02	0.733	-0.170	-0.135
2A-45Y-1	95.045	7.17E+06	9.52E+04	1.93E+05	8542.412	2.16E+04	2183.025	0.682	-0.187	-0.108
2A-45Y-1	95.145	9.45E+06	3.54E+05	3.74E+05	1.65E+04	3.07E+04	2895.269	0.526	-0.299	-0.166
2A-45Y-2	96.382	3.25E+04	5731.297	7738.161	1353.760	2343.197	--	0.613	-0.282	-0.212
2A-48Y-2	103.157	2.09E+06	1.24E+05	1.38E+05	6.34E+04	1.19E+06	3.90E+04	0.660	-0.372	-0.180
2A-48Y-2	103.487	6.40E+06	5.66E+05	4.78E+05	3.41E+05	6.45E+06	2.40E+05	0.652	-0.462	-0.186
2A-48Y-2	103.787	8.18E+06	3.59E+06	1.98E+06	2.03E+06	2.92E+07	1.50E+06	0.605	-0.584	-0.218
2A-48Y-2	104.095	4.98E+07	3.02E+07	2.18E+07	2.16E+07	1.49E+08	1.64E+07	0.665	-0.528	-0.177
2A-56Y-1	119.64	1.72E+05	3.64E+04	1.20E+05	3.03E+04	2.17E+04	1885.761	0.807	-0.192	-0.212
2A-56Y-1	119.75	1.51E+04	6316.277	4.23E+04	1.37E+04	1136.852	--	0.899	-0.169	-0.046
2A-57Y-2	121.662	1.38E+06	3.08E+05	7.49E+05	1.96E+05	2.00E+04	1882.826	0.755	-0.224	-0.093
2A-58Y-2	123.431	5.30E+05	1.32E+05	5.14E+05	1.25E+05	2.40E+04	2551.758	0.830	-0.176	-0.122
2A-58Y-2	123.82	2.04E+07	7.96E+05	7.41E+05	4.37E+04	5.92E+04	1.32E+04	0.501	-0.329	-0.300
2A-58Y-2	124.021	1.46E+06	2.72E+05	4.84E+05	1.64E+04	8064.053	2413.083	0.649	-0.203	-0.279
2A-60Y-2	128.74	1.16E+07	1.75E+05	1.77E+05	1.27E+04	5.70E+04	1.51E+04	0.539	-0.314	-0.269
2A-60Y-2	129.77	5.12E+06	8.93E+05	6.72E+04	3994.271	1.97E+04	5400.759	0.079	-1.157	-0.187
2A-60Y-2	129.835	7.56E+06	1.33E+06	9.99E+04	11331.00	2.25E+04	5678.958	0.081	-1.159	-1.103
2A-60Y-2	129.955	6.73E+06	1.10E+06	1.84E+05	1.89E+04	2.95E+04	7057.400	0.160	-0.850	-1.092
2A-60Y-2	130.21	1.32E+06	1.13E+05	1.17E+05	7228.438	3758.910	1486.432	0.526	-0.307	-0.795
2A-61Y-2	133.72	1.67E+07	8.46E+06	5.34E+06	5.52E+06	4.42E+07	3.45E+06	0.628	-0.558	-0.202
2A-69Y-1	151.905	8.09E+05	1.03E+04	1.15E+04	–	–	–	0.528	-0.277	-0.277
2A-79Q-1	163.25	--	--	--	--	--	--	--	--	--
2A-81Q-2	165.935	7.91E+05	1.70E+04	2.26E+04	3190.131	4.69E+04	1.01E+04	0.679	-0.277	-0.168

Table 10 – Raw abundance data from isoGDGTs.

BIBLIOGRAPHY

Armitage, Simon J., et al. "The southern route “out of Africa”: evidence for an early expansion of modern humans into Arabia." *Science* 331.6016 (2011): 453-456.

Baldocchi, Dennis D. "Scaling water vapor and carbon dioxide exchange from leaves to a canopy: rules and tools." *Scaling physiological processes: leaf to globe. Academic Press, San Diego* (1993): 77-114.

Behrensmeyer, Anna K., et al. "Geology and geochronology of the middle Miocene Kipsaramon site complex, Muruyur beds, Tugen Hills, Kenya." *Journal of Human Evolution* 42.1-2 (2002): 11-38.

Berger, Wolfgang H., and Eystein Jansen. "Mid-pleistocene climate shift-the Nansen connection." *The polar oceans and their role in shaping the global environment* (1994): 295-311.

Bowen, Gabriel J., and Justin Revenaugh. "Interpolating the isotopic composition of modern meteoric precipitation." *Water Resources Research*39.10 (2003).

Bowling, David R., Pieter P. Tans, and Russell K. Monson. "Partitioning net ecosystem carbon exchange with isotopic fluxes of CO2." *Global Change Biology* 7.2 (2001): 127-145.

Brachert, Thomas Christian, et al. "Stable isotope variation in tooth enamel from Neogene hippopotamids: monitor of meso and global climate and rift dynamics on the Albertine Rift, Uganda." *International Journal of Earth Sciences* 99.7 (2010): 1663-1675.

Campisano, Christopher J., et al. "The Hominin Sites and Paleolakes Drilling Project: High-Resolution Paleoclimate Records from the East African Rift System and Their Implications for Understanding the Environmental Context of Hominin Evolution." *PaleoAnthropology* 1 (2017): 43.

Cane, Mark A., and Peter Molnar. "Closing of the Indonesian seaway as a precursor to east African aridification around 3–4 million years ago." *Nature*411.6834 (2001): 157-162.

Castañeda, Isla S., et al. "Late Quaternary vegetation history of southeast Africa: the molecular isotopic record from Lake Malawi." *Palaeogeography, Palaeoclimatology, Palaeoecology* 275.1 (2009a): 100-112.

Castañeda, Isla S., et al. "Wet phases in the Sahara/Sahel region and human migration patterns in North Africa." *Proceedings of the National Academy of Sciences* 106.48 (2009b): 20159-20163.

Castañeda, Isla S., and Stefan Schouten. "A review of molecular organic proxies for examining modern and ancient lacustrine environments." *Quaternary Science Reviews* 30.21 (2011): 2851-2891.

Cerling, Thure E., et al. "Woody cover and hominin environments in the past 6 [thinsp] million years." *Nature* 476.7358 (2011): 51-56.

Cohen, A., et al. "The Hominin Sites and Paleolakes Drilling Project: inferring the environmental context of human evolution from eastern African rift lake deposits." *Scientific Drilling* 21 (2016): 1.

Couvreur, Thomas LP, et al. "Molecular phylogenetics reveal multiple tertiary vicariance origins of the African rain forest trees." *Bmc Biology* 6.1 (2008): 54.

Cranwell, P. A. "Diagenesis of free and bound lipids in terrestrial detritus deposited in a lacustrine sediment." *Organic Geochemistry* 3.3 (1981): 79-89.

Cranwell, P. A., G. Eglinton, and N. Robinson. "Lipids of aquatic organisms as potential contributors to lacustrine sediments—II." *Organic Geochemistry*11.6 (1987): 513-527.

D'Andrea, William J., and Yongsong Huang. "Long chain alkenones in Greenland lake sediments: Low δ 13 C values and exceptional abundance." *Organic Geochemistry* 36.9 (2005): 1234-1241.

DeLong, Edward F. "Archaea in coastal marine environments." *Proceedings of the National Academy of Sciences* 89.12 (1992): 5685-5689.

deMenocal, Peter B. "Plio-Pleistocene African climate." *Science (New York, NY)* 270.5233 (1995): 53-59.

deMenocal, Peter B., et al. "Abrupt onset and termination of the African Humid Period: rapid climate responses to gradual insolation forcing." *Quaternary science reviews* 19.1 (2000): 347-361.

deMenocal, Peter B. "African climate change and faunal evolution during the Pliocene–Pleistocene." *Earth and Planetary Science Letters* 220.1-2 (2004): 3-24.

Diefendorf, Aaron F., et al. "Production of n-alkyl lipids in living plants and implications for the geologic past." *Geochimica et Cosmochimica Acta* 75.23 (2011): 7472-7485.

Ebinger, C. J., et al. "Rift deflection, migration, and propagation: Linkage of the Ethiopian and Eastern rifts, Africa." *Geological Society of America Bulletin* 112.2 (2000): 163-176.

Eglinton, Geoffrey, et al. "Hydrocarbon constituents of the wax coatings of plant leaves: a taxonomic survey." *Phytochemistry* 1.2 (1962): 89-102.

Ehleringer, J. R., and T. E. Dawson. "Water uptake by plants: perspectives from stable isotope composition." *Plant, Cell & Environment* 15.9 (1992): 1073-1082.

Farquhar, Graham D., James R. Ehleringer, and Kerry T. Hubick. "Carbon isotope discrimination and photosynthesis." *Annual review of plant biology*40.1 (1989): 503-537.

Farquhar, Graham D., Lucas A. Cernusak, and Belinda Barnes. "Heavy water fractionation during transpiration." *Plant Physiology* 143.1 (2007): 11-18.

Feakins, Sarah J., et al. "Northeast African vegetation change over 12 my." *Geology* 41.3 (2013): 295-298.

Ficken, Katherine J., et al. "An n-alkane proxy for the sedimentary input of submerged/floating freshwater aquatic macrophytes." *Organic geochemistry*31.7 (2000): 745-749.

Freeman, K. H., and R. D. Pancost. "Biomarkers for terrestrial plants and climate." *Falkowski, P. and Freeman, K., Treatise on Geochemistry, Elsevier, Amsterdam* 12 (2014): 395-416.

Garcin, Yannick, et al. "Reconstructing C 3 and C 4 vegetation cover using n-alkane carbon isotope ratios in recent lake sediments from Cameroon, Western Central Africa." *Geochimica et Cosmochimica Acta* 142 (2014): 482-500.

George, Rhiannon, Nick Rogers, and Simon Kelley. "Earliest magmatism in Ethiopia: evidence for two mantle plumes in one flood basalt province." *Geology* 26.10 (1998): 923-926.

Haug, Gerald H., and Ralf Tiedemann. "Effect of the formation of the Isthmus of Panama on Atlantic Ocean thermohaline circulation." *Nature* 393.6686 (1998): 673-676.

Hayes, J. M., et al. "Compound-specific isotopic analyses: a novel tool for reconstruction of ancient biogeochemical processes." *Organic Geochemistry*16.4-6 (1990): 1115-1128.

Hopmans, Ellen C., et al. "A novel proxy for terrestrial organic matter in sediments based on branched and isoprenoid tetraether lipids." *Earth and Planetary Science Letters* 224.1 (2004): 107-116.

Hopmans, Ellen C., Stefan Schouten, and Jaap S. Sinninghe Damsté. "The effect of improved chromatography on GDGT-based palaeoproxies." *Organic Geochemistry* 93 (2016): 1-6.

Jetter, Reinhard, and Ljerka Kunst. "Plant surface lipid biosynthetic pathways and their utility for metabolic engineering of waxes and hydrocarbon biofuels." *The Plant Journal* 54.4 (2008): 670-683.

Johnson, T. C., et al. "A progressively wetter climate in southern East Africa over the past 1.3 million years." *Nature* 537.7619 (2016): 220-224.

Joordens, Josephine CA, et al. "An astronomically-tuned climate framework for hominins in the Turkana Basin." *Earth and Planetary Science Letters*307.1 (2011): 1-8.

Karner, Markus B., Edward F. DeLong, and David M. Karl. "Archaeal dominance in the mesopelagic zone of the Pacific Ocean." *Nature* 409.6819 (2001): 507-510.

Keough, B. P., T. M. Schmidt, and R. E. Hicks. "Archaeal nucleic acids in picoplankton from great lakes on three continents." *Microbial Ecology* 46.2 (2003): 238-248.

Kim, Jung-Hyun, et al. "New indices and calibrations derived from the distribution of crenarchaeal isoprenoid tetraether lipids: Implications for past sea surface temperature reconstructions." *Geochimica et Cosmochimica Acta* 74.16 (2010): 4639-4654.

Kingston, John D., et al. "Astronomically forced climate change in the Kenyan Rift Valley 2.7–2.55 Ma: implications for the evolution of early hominin ecosystems." *Journal of Human Evolution* 53.5 (2007): 487-503.

Kroon, Dick, et al. "Oxygen isotope and sapropel stratigraphy in the eastern Mediterranean during the last 3.2 million years." *Proceedings of the Ocean Drilling Program, Scientific Results, Vol. 160; Chapter 14* (1998).

Krull, Evelyn, et al. "Compound-specific δ 13 C and δ 2 H analyses of plant and soil organic matter: a preliminary assessment of the effects of vegetation change on ecosystem hydrology." *Soil Biology and Biochemistry* 38.11 (2006): 3211-3221.

Levin, Naomi E., et al. "Isotopic evidence for Plio–Pleistocene environmental change at Gona, Ethiopia." *Earth and Planetary Science Letters* 219.1 (2004): 93-110.

Levin, N. E. "Compilation of East Africa soil carbonate stable isotope data." *Integrated Earth Data Applications* (2013).

Lipp, Julius S., et al. "Significant contribution of Archaea to extant biomass in marine subsurface sediments." *Nature* 454.7207 (2008): 991-994.

Lisiecki, Lorraine E., and Maureen E. Raymo. "A Pliocene-Pleistocene stack of 57 globally distributed benthic δ18O records." *Paleoceanography* 20.1 (2005).

Loomis, Shannon E., et al. "Calibration and application of the branched GDGT temperature proxy on East African lake sediments." *Earth and Planetary Science Letters* 357 (2012): 277-288.

Magill, Clayton R., Gail M. Ashley, and Katherine H. Freeman. "Water, plants, and early human habitats in eastern Africa." *Proceedings of the National Academy of Sciences* 110.4 (2013a): 1175-1180.

Magill, Clayton R., Gail M. Ashley, and Katherine H. Freeman. "Ecosystem variability and early human habitats in eastern Africa." *Proceedings of the National Academy of Sciences* 110.4 (2013b): 1167-1174.

Marzi, R., B. E. Torkelson, and R. K. Olson. "A revised carbon preference index." *Organic Geochemistry* 20.8 (1993): 1303-1306.

Maslin, Mark A., and Beth Christensen. "Tectonics, orbital forcing, global climate change, and human evolution in Africa: introduction to the African paleoclimate special volume." *Journal of human evolution* 53.5 (2007): 443-464.

Maslin, Mark A., and Martin H. Trauth. "Plio-Pleistocene East African pulsed climate variability and its influence on early human evolution." *The First Humans–Origin and Early Evolution of the Genus Homo* (2009): 151-158.

Maslin, Mark A., et al. "Three and half million year history of moisture availability of South West Africa: evidence from ODP site 1085 biomarker records." *Palaeogeography, Palaeoclimatology, Palaeoecology* 317 (2012): 41-47.

Maslin, Mark A., et al. "East African climate pulses and early human evolution." *Quaternary Science Reviews* 101 (2014): 1-17.

McDougall, Ian, et al. "New single crystal 40Ar/39Ar ages improve time scale for deposition of the Omo Group, Omo–Turkana Basin, East Africa." *Journal of the Geological Society* 169.2 (2012): 213-226.

McInerney, Francesca A., Brent R. Helliker, and Katherine H. Freeman. "Hydrogen isotope ratios of leaf wax n-alkanes in grasses are insensitive to transpiration." *Geochimica et Cosmochimica Acta* 75.2 (2011): 541-554.

McNulty, E.P., Lowenstein, T.K., Owen, R.B., Renaut, R.W., Deocampo, D., Cohen, A.S., Muiruri, V.M., Leet, K., Rabideaux, N.M., Billingsley, A.L., and Mbuthia, A. (2016) The sedimentary record of the Lake Magadi Basin: Core analysis from HSPDP-MAG14 Cores 1A, 1C and 2A. Geo. Soc. Amer. Ann. Mtg., Denver, CO 26-29 Sept., 2016

Meyers, Philip A. "Organic geochemical proxies of paleoceanographic, paleolimnologic, and paleoclimatic processes." *Organic geochemistry* 27.5 (1997): 213-250.

Molnar, Peter, and Mark A. Cane. "Early Pliocene (pre–Ice Age) El Niño–like global climate: Which El Niño?." *Geosphere* 3.5 (2007): 337-365.

Pancost, Richard D., and Christopher S. Boot. "The palaeoclimatic utility of terrestrial biomarkers in marine sediments." *Marine Chemistry* 92.1 (2004): 239-261.

Pearson, Emma J., Steve Juggins, and Paul Farrimond. "Distribution and significance of long-chain alkenones as salinity and temperature indicators in Spanish saline lake sediments." *Geochimica et Cosmochimica Acta* 72.16 (2008): 4035-4046.

Petsch, S. T., R. A. Berner, and T. I. Eglinton. "A field study of the chemical weathering of ancient sedimentary organic matter." *Organic Geochemistry*31.5 (2000): 475-487.

Pitcher, Angela, et al. "Core and intact polar glycerol dibiphytanyl glycerol tetraether lipids of ammonia-oxidizing archaea enriched from marine and estuarine sediments." *Applied and Environmental Microbiology* 77.10 (2011): 3468-3477.

Potts, Richard. "Variability selection in hominid evolution." *Evolutionary Anthropology: Issues, News, and Reviews* 7.3 (1998): 81-96.

Potts, Richard, Anna K. Behrensmeyer, and Peter Ditchfield. "Paleolandscape variation and Early Pleistocene hominid activities: members 1 and 7, Olorgesailie Formation, Kenya." *Journal of human evolution* 37.5 (1999): 747-788.

Potts, Richard. "Hominin evolution in settings of strong environmental variability." *Quaternary Science Reviews* 73 (2013): 1-13.

Powers, Lindsay, et al. "Applicability and calibration of the TEX 86 paleothermometer in lakes." *Organic Geochemistry* 41.4 (2010): 404-413.

Prentice, I. Colin, et al. "Evidence of a universal scaling relationship for leaf CO2 drawdown along an aridity gradient." *New Phytologist* 190.1 (2011): 169-180.

Prömmel, Kerstin, Ulrich Cubasch, and Frank Kaspar. "A regional climate model study of the impact of tectonic and orbital forcing on African precipitation and vegetation." *Palaeogeography, Palaeoclimatology, Palaeoecology* 369 (2013): 154-162.

Ravelo, Ana Christina, et al. "Regional climate shifts caused by gradual global cooling in the Pliocene epoch." *Nature* 429.6989 (2004): 263-267.

Raven, P.H., Event, R.F., Eichnorn, S.E., 1999. Biology of Plants. W.H. Freeman and Company, New York. 875 p.

Reed, Kaye E. "Early hominid evolution and ecological change through the African Plio-Pleistocene." *Journal of human evolution* 32.2-3 (1997): 289-322.

Rommerskirchen, Florian, et al. "A north to south transect of Holocene southeast Atlantic continental margin sediments: Relationship between aerosol transport and compound-specific δ13C land plant biomarker and pollen records." *Geochemistry, Geophysics, Geosystems* 4.12 (2003).

Rossignol-Strick, Martine. "Mediterranean Quaternary sapropels, an immediate response of the African monsoon to variation of insolation." *Palaeogeography, palaeoclimatology, palaeoecology* 49.3 (1985): 237-263.

Sachse, Dirk, Ansgar Kahmen, and Gerd Gleixner. "Significant seasonal variation in the hydrogen isotopic composition of leaf-wax lipids for two deciduous tree ecosystems (Fagus sylvativa and Acerpseudoplatanus)." *Organic Geochemistry* 40.6 (2009): 732-742.

Sachse, Dirk, et al. "Molecular paleohydrology: interpreting the hydrogen-isotopic composition of lipid biomarkers from photosynthesizing organisms." *Annual Review of Earth and Planetary Sciences* 40 (2012).

Sankaran, Mahesh, et al. "Determinants of woody cover in African savannas." *Nature* 438.7069 (2005): 846-849.

Schefuß, Enno, et al. "African vegetation controlled by tropical sea surface temperatures in the mid-Pleistocene period." *Nature* 422.6930 (2003): 418-421.

Schouten, Stefan, et al. "Distributional variations in marine crenarchaeotal membrane lipids: a new tool for reconstructing ancient sea water temperatures?." *Earth and Planetary Science Letters* 204.1 (2002): 265-274.

Schouten, Stefan, et al. "Archaeal and bacterial glycerol dialkyl glycerol tetraether lipids in hot springs of Yellowstone National Park." *Applied and Environmental Microbiology* 73.19 (2007): 6181-6191.

Sepulchre, Pierre, et al. "Tectonic uplift and Eastern Africa aridification." *Science* 313.5792 (2006): 1419-1423.

Shepherd, Tom, and D. Wynne Griffiths. "The effects of stress on plant cuticular waxes." *New Phytologist* 171.3 (2006): 469-499.

Simiyu, Silas M., and G. Randy Keller. "An integrated geophysical analysis of the upper crust of the southern Kenya rift." *Geophysical Journal International*147.3 (2001): 543-561.

Sinninghe-Damsté, Jaap S., et al. "Altitudinal shifts in the branched tetraether lipid distribution in soil from Mt. Kilimanjaro (Tanzania): Implications for the MBT/CBT continental palaeothermometer." *Organic Geochemistry* 39.8 (2008): 1072-1076.

Sinninghe-Damsté, Jaap S., et al. "Fluxes and distribution of tetraether lipids in an equatorial African lake: constraints on the application of the TEX 86 palaeothermometer and BIT index in lacustrine settings." *Geochimica et Cosmochimica Acta* 73.14 (2009): 4232-4249.

Strecker, M. R., P. M. Blisniuk, and G. H. Eisbacher. "Rotation of extension direction in the central Kenya Rift." *Geology* 18.4 (1990): 299-302.

Surdam, Ronald C., and Hans P. Eugster. "Mineral reactions in the sedimentary deposits of the Lake Magadi region, Kenya." *Geological Society of America Bulletin* 87.12 (1976): 1739-1752.

Tierney, Jessica E., et al. "Northern hemisphere controls on tropical southeast African climate during the past 60,000 years." *Science* 322.5899 (2008): 252-255.

Tierney, Jessica E., et al. "Late-twentieth-century warming in Lake Tanganyika unprecedented since AD 500." *Nature Geoscience* 3.6 (2010): 422-425.

Tierney, Jessica E., et al. "Late Quaternary behavior of the East African monsoon and the importance of the Congo Air Boundary." *Quaternary Science Reviews* 30.7 (2011): 798-807.

Tierney, Jessica E., and Francesco SR Pausata. "Rainfall regimes of the Green Sahara." *Science advances* 3.1 (2017): e1601503.

Tipple, Brett J., and Mark Pagani. "The early origins of terrestrial C4 photosynthesis." *Annu. Rev. Earth Planet. Sci.* 35 (2007): 435-461.

Trauth, Martin H., et al. "Late cenozoic moisture history of East Africa." *Science* 309.5743 (2005): 2051-2053.

Trauth, Martin H., et al. "High-and low-latitude forcing of Plio-Pleistocene East African climate and human evolution." *Journal of Human Evolution* 53.5 (2007): 475-486.

Trauth, Martin H., Juan C. Larrasoaña, and Manfred Mudelsee. "Trends, rhythms and events in Plio-Pleistocene African climate." *Quaternary Science Reviews* 28.5 (2009): 399-411.

Underwood, Charlie J., Chris King, and Etienne Steurbaut. "Eocene initiation of Nile drainage due to East African uplift." *Palaeogeography, Palaeoclimatology, Palaeoecology* 392 (2013): 138-145.

Vrba, Elisabeth S. "Late Pliocene climatic events and hominid evolution." *Evolutionary history of the "robust" australopithecines. Aldine de Gruyter, New York* (1988): 405-426.

Washburn, Sherwood L. "Tools and human evolution." *Scientific American*203 (1960): 62-75.

Weijers, Johan WH, et al. "Membrane lipids of mesophilic anaerobic bacteria thriving in peats have typical archaeal traits." *Environmental Microbiology* 8.4 (2006a): 648-657.

Weijers, Johan WH, et al. "Occurrence and distribution of tetraether membrane lipids in soils: implications for the use of the TEX 86 proxy and the BIT index." *Organic Geochemistry* 37.12 (2006b): 1680-1693.

Weijers, Johan WH, et al. "Environmental controls on bacterial tetraether membrane lipid distribution in soils." *Geochimica et Cosmochimica Acta* 71.3 (2007): 703-713.

Wichura, Henry, et al. "Evidence for middle Miocene uplift of the East African Plateau." *Geology* 38.6 (2010): 543-546.

Zhang, Yi Ge, et al. "Methane Index: A tetraether archaeal lipid biomarker indicator for detecting the instability of marine gas hydrates." *Earth and Planetary Science Letters* 307.3 (2011): 525-534.

Zhang, Yi Ge, Mark Pagani, and Zhengrong Wang. "Ring Index: A new strategy to evaluate the integrity of TEX86 paleothermometry." *Paleoceanography* 31.2 (2016): 220-232.